CALIFORNIA INSTITUTE OF TECHNOLOGY

EXPERIMENTAL STUDY OF
THE UPPER HYBRID ECHO IN PLASMAS

by

Luc O. Bauer

Technical Report No. 40

Nonr 220(50)

May 1968

EXPERIMENTAL STUDY OF THE UPPER HYBRID

ECHO IN PLASMAS

by

Luc Olivier Bauer

Technical Report No. 40

May 1968

California Institute of Technology

Pasadena, California

ACKNOWLEDGEMENT

ABSTRACT

The two-pulse stimulated radiation of dense $(10^9/cm^3 < ne \leq 10^{11}/cm^3)$ nonuniform neon and argon afterglow plasma columns longitudinally immersed in a magnetic field is studied. The magnetic field is very homogeneous over the plasma volume ($\Delta B/B \sim .01\%$). If the S-band microwave pulses' center frequency is such that they resonantly excite a narrow band of plasma upper hybrid oscillations close to the maximum upper hybrid frequency of the column, strong two-pulse echoes are observed. This new echo process is called the upper hybrid echo. The echo spectrum, echo power and echo width were studied as a function of the pulse peak power P, pulse separation τ, relative density $(\omega_{po}/\omega)^2$, and relative cyclotron frequency (ω_c/ω). The complex but systematic variations of the echo properties as a function of the above-mentioned parameters are found to be in qualitative agreement with those predicted by a theory of Gould and Blum based upon a simple nonuniform unidimensional cold plasma slab model. The possible effects of electron neutral and electron ion collisions not retained in the theoretical model are discussed.

The existence of a new type of cyclotron echo, different from that of Hill and Kaplan and not predicted by the Blum and Gould model is documented. It is believed to be also of a collective effect nature and can probably be described in terms of a theory retaining some hot plasma effects.

TABLE OF CONTENTS

I.   INTRODUCTION

1.1 Background of the Problem

The state of experimental research in plasma physics has tremendously improved over the last twenty years. This progress is usually attributed to a remarkable development of microwave devices following the discovery and expansion of radar techniques during the second world war. Because of the new instrumentation, old problems such as the Tonks-Dattner resonances found in a cylindrical plasma column have been more thoroughly investigated and finally understood (1). It also became possible to verify important theoretical predictions as to the complicated properties of a plasma in a magnetic field. For instance, by monitoring the absorption by a plasma column of a microwave continuous wave signal fed into the cavity surrounding it, Buchsbaum and Hasegawa (2) showed that fine structure resonances found near the electron cyclotron harmonics could be attributed to interferences of electrostatic waves propagating at right angle with the magnetic fields. Furthermore, they were recognized to be identical with those predicted by Bernstein (3) in the case of an infinite uniform hot plasma in a magnetic field. The continuously advancing technology also produced situations in which the experiment preceded the analysis in the finding of new phenomena. Recently Hill and Kaplan made an important discovery (4) also concerning plasmas in a magnetic field which attracted much attention because of the theoretical problems brought about by the new effect. Their experiment was of a transient nature. Fig. 1.1 presents the sequence of experimental events. Gas, preferably argon or neon, introduced in a glass bottle

RF PULSE
TO PRODUCE
PLASMA

MICROWAVE
PULSES
$(\omega_s \approx \omega_c)$

CYCLOTRON
ECHO

T_a T_p τ τ
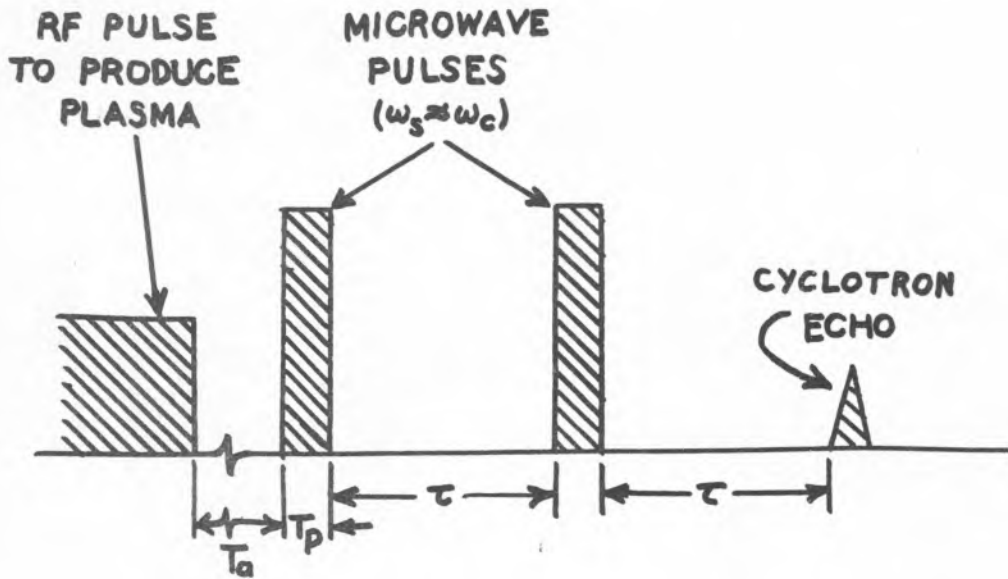
Fig. 1.1 Sequence of pulses in Hill and Kaplan experiment
$(T_a \gg \tau$, $\tau \gg T_p)$.

immersed in a slightly inhomogeneous magnetic field ($\Delta B/B \sim .6\%$ over
the plasma volume), was ionized by a brief, high power 21 MHz pulse.
At a time T_a after the end of the discharge, two short microwave
pulses (~ 10 ns) separated by a time interval τ of the order of
100 ns were sent through waveguides to interact with the plasma. Then,
at times $t = n\tau$ ($n = 1,2,\cdots$) after the end of the second microwave
pulse, bursts of radiation were emitted by the plasma. They were
called echoes or cyclotron echoes because the pulse center frequency
was chosen close to the cyclotron frequency ($\frac{\omega_c}{2\pi}$ was in the X-band
range of frequency).

Although first seen in plasmas by Hill and Kaplan, two-pulse
echoes in gyroresonant systems were by no means a new phenomenon. They
seem to have been originally described by Hahn (5) in 1950 in a paper

concerning studies of nuclear magnetic resonance in liquids. Since then, numerous observations have been reported (6). The first experiment involved nuclear spin resonances in solids and liquids. Then, the resonant excitation of either noninteracting electron spins, as was the case in sodium-ammonia solution and in donor enriched silicon, or of electron spin waves present, for instance, in a YIG (yttrium iron garnet) disc, were used. Furthermore, since it was shown (7) that any two-state quantum-mechanical system, spin or otherwise, can be cast in the same theoretical mold, a recent experiment involving chromium electronic states having their degeneracy removed by the crystal inhomogeneous strains and which were excited by short intense light pulses from a ruby laser, was tried and brought the discovery of a photon-echo.

The great variety of conditions under which these two-pulse echoes can be seen indicates the generality of the phenomenon. It can be shown that two pulses will produce an echo in any material if, in this material, the pulses resonantly excite an ensemble of nondegenerate slightly nonlinear oscillators, the relaxation time of which is not too short compared to the time interval between the exciting pulses. As a result the purpose of echo studies varied depending on each experiment. The first nuclear spin echo measurements had as an objective to measure the relaxation of nuclear spins in solids and liquids. The experiments using standing spin waves in the YIG disc helped to ascertain through echo spectra measurement the density of modes at any particular frequency. The photon echo gave some information as to the amount of degeneracy introduced by the crystal inhomogeneous strains. In their

experiment, Hill and Kaplan, using a low density plasma ($ne < 10^9/cm^3$)
showed that the cyclotron echo comes from the independent electrons
gyrating around the magnetic field lines at the cyclotron frequency;
the nondegeneracy of the "oscillators" being provided by the magnetic
field inhomogeneities and the nonlinearity entering through the energy
dependent electron neutral atom collision frequency. Furthermore,
they pointed out that the echo could be an interesting diagnostic tool
for electron collisions in plasmas.

1.2 Objectives of the Experiment

Because of these interesting implications, an experiment similar
to that of Hill and Kaplan was undertaken with the differences that the
electron density was higher ($10^9/cm^3 < ne < 10^{11}/cm^3$) and the magnetic
field was more homogeneous ($\Delta B/B \sim .01\%$ over the plasma volume). The
first results displayed some fine but systematic discrepancies with the
independent electron theoretical approach. They showed that the
simple theoretical picture which explained the cyclotron echo could not
be carried over to this experiment. It became progressively clearer
that the "oscillators" were not the free electrons gyrating around the
magnetic field lines, but collective oscillations of clusters of elec-
trons in the plasma. The echoes in plasmas therefore showed a similar
evolution to that of the spin echoes. Indeed, the latter were first
discovered and successfully described in terms of independent spins.
Then echoes coming from standing magnetostatic spin waves were found
in a YIG disc. In nonuniform plasma columns immersed in a magnetic
field, Buchsbaum and Hasegawa demonstrated the existence of a band of

closely spaced hot plasma normal modes extending between the cyclotron

frequency ω_c and what is called the maximum upper hybrid frequency

ω_{Ho} where $\omega_{Ho}^2 = \omega_c^2 + \omega_{po}^2$ and where ω_{po} is the plasma frequency

characteristic of the peak electron density on the axis of plasma

column. If a cold plasma picture is adopted, more appropriate to the

low electron temperature found in the afterglow used for echo experi-

ments, it can be shown that there exists similarly a continuum of

normal modes between the cyclotron and the maximum upper hybrid fre-

quency. This band of resonances in the plasma can be excited with a

cold plasma wave propagating across the magnetic field, named the

extraordinary wave. A new experiment was then designed to observe in

better conditions (the pulses' center frequency was lowered from X-band

to S-band) the echo arising from these collective modes of the plasma.

It resulted in the discovery (21) of an echo peaking not at the cyclo-

tron frequency but near the maximum upper hybrid frequency, hence the

name upper hybrid echo (see Fig. 1.2) . Simultaneously with the

experiment, Gould and Blum (18,20) developed a new collective effect

echo theory in terms of a simple nonuniform unidimensional cold plasma

slab. The objectives of the experiment were then to verify the

complex dependences of that new echo on the parameters of interest as

predicted by the new theory.

Chapter II is devoted to the plasma echo theories. The inde-

pendent particle theories are described because of their value for low

density plasma echoes and also for the general frame of understanding

they provide. Consequently, the new cold plasma model of Gould and

microwaves
pulses

1st echo

2nd echo

3rd echo
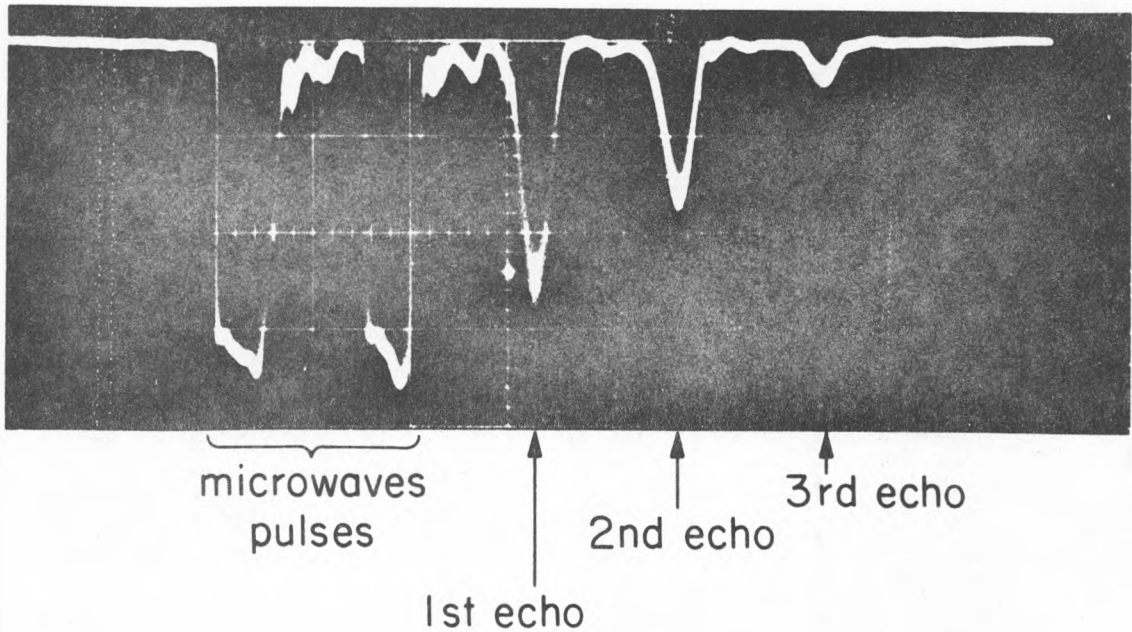
Fig. 1.2 Photograph of upper hybrid echoes and their triggering
pulses for a 5 micron neon afterglow plasma. The first
echo reaches a maximum power when the ratio $(\omega_c/\omega)= .915$
with the maximum upper hybrid frequency defined by
$(\omega_c/\omega) = .91$. The microwave pulses' peak power = 5W,
their center frequency = 3 GHz. (Horizontal scale:
50 nsec per division).

Blum is developed in some detail. The general case is treated first,

followed by the two special cases of the low pulse peak power regime

and high pulse peak power regime or saturation regime. This regime is

studied carefully because of the remarkable complexity of the echo

functional relations to the parameters of interest predicted in that

case. It will offer the best possible test of the theory by comparison

with the experiment. In Chapter III some details on the instrumentation

are given. Special attention is focused on the pulse-producing

electronics and microwave devices, on the magnetic field generation and measurement, and on the receiver system. Some characteristics of the afterglow plasma are presented as well as some techniques used to measure echo properties.

Chapter IV is devoted to the experimental results. They will be compared with those of the theory for each property of the echo. Furthermore, when important, the effects of electron-neutral and ion collisions, not included in the theory, are discussed. In that chapter the last section describes a secondary peak of the echo spectrum at the cyclotron frequency not predicted by the cold plasma theory but believed to be also caused by collective effects and therefore to be different from the Hill and Kaplan cyclotron echo.

The results and conclusions are summarized in Chapter V and some suggestions for further work are given.

II. THEORY

2.1 Introduction

The theory of the plasma echo has been a moving field over the last three years. And a few different points of view have emerged as a consequence of the sometimes contradictory experimental results. Rather than try to find logical reasons for their order of exposition in this chapter, we have developed them in a chronological sequence. Section 2.2 will be concentrated on the independent particle theories and some early experimental results will be injected to illustrate the difficulties encountered in the understanding of that superficially simple phenomenon. In Section 2.3 the new collective-effects model of Blum and Gould will be exposed in some detail. Influence on the echo power and echo width of the power of the exciting pulses will be described and some experimental predictions will be made.

2.2 Independent Particle Theories

The discovery of Hill and Kaplan attracted a great deal of attention because of its phenomenological similarity with the spin echo in solids. It was of particular interest to plasma physicists to know how different the physical mechanisms hiding behind the apparent resemblance of the experiments really were. A number of workers contributed to build a relatively simple picture where these differences were pointed out and also how non-interacting electrons of a plasma can give rise to an echo. In this paragraph a report of Gould (8) on these theories will be closely followed. As did the other workers, Gould started with a plasma consisting of fixed ions and non-

interacting electrons so that one could consider the motion of one of them in a static magnetic field and an oscillating electric field such as those encountered in an echo experiment, and then come back and consider the linear superposition of the motions of each of them. Before entering into any detailed calculations one can try to describe what happens to the electron gas in an echo experiment. It is recalled from the introduction that the plasma is in a relatively homogeneous magnetic field (in most early experiments of the order of 1% over the plasma volume). So before the first microwave pulse hits the plasma, the electrons gyrate around the magnetic field lines with a frequency of rotation called the electron cyclotron frequency $\omega_c = \frac{qB}{m}$, and with a Larmor radius characterized by the temperature of the electrons and the intensity of the magnetic field. The first pulse of microwave whose center frequency is close to the electron cyclotron frequency and whose spectrum width is much larger percentage wise than the magnetic field inhomogeneities will heat up the electrons and synchronize their phases so that right at the end of the pulses they will all be in phase, and will reradiate coherently part of the energy absorbed from the electric field of the microwave pulse. However, because of the weak inhomogeneity in the magnetic field, the electrons gyrate at slightly different frequencies. They will then slowly dephase, causing a rapid drop in the coherent radiation emitted. The observed radiation rate of decrease should not be interpreted as a corresponding loss of energy on the part of each electron, but simply that they have lost their coherence. One recalls from classical electrodynamics that the

intensity of radiation produced by N electrons goes as N^2 if they are in phase, but goes only as N if they are not. So the situation before the second pulse is as follows. The electrons have kept most of their energy acquired during the first pulse, but are out of phase. By the excitation of the second microwave pulse, the electrons will acquire a new amount of energy (equal to that given by the first pulse, since the experimental pulses are chosen to be equal) and coherence again. However, for the same reason the electrons will again lose that coherence and the radiation coming from the ensemble of electrons will drop to a very low level. Why, then, an echo after the second pulse? The answer is evidently not given by the discussion above. It fails because it was based on linear logic which would predict that if there is only an infinitesimal amount of radiation coming from the plasma at a time $t = \tau$ after the end of the first pulse, only an infinitesimal amount of radiation can be expected at a time $t = \tau$ after the end of the second pulse. So the echo has to come from some nonlinear process. However, the first analysis tried by Gould was completely linear. It was hoped that even though such an analysis would not produce an echo, it would point out some particularities in the electron trajectories at times $t = \tau$, $2\tau, \cdots, n\tau$ after the end of the second pulse and then it would be possible to guess at the effects of possible nonlinearities. The motion of a single electron in a magnetic and electric field can be written (neglecting the effects of the spatial variations of $\underline{E}$ and $\underline{B}$ and of the r.f. magnetic field)

$$\dot{\underline{V}} - \underline{\omega}_c \times \underline{V} = -\frac{e}{m}\underline{E} \quad , \quad \omega_c = \frac{qB}{m} \tag{2.1}$$

Now it is convenient to transform to a rotating reference frame of the velocity space in which one of the rotating components of $\underline{E}$ is stationary. In this system the effect of the other rotating component may be neglected, and the cyclotron frequency appears reduced by the frequency ω of the r.f. electric field. Cyclotron resonance corresponds to a "difference cyclotron frequency" ω'_c of zero and near resonance to small ω'_c. So one can write:

$$\dot{\underline{V}}' - \underline{\omega}'_c \times \underline{V}' = -\frac{e}{m}\underline{E}' \quad , \quad \omega'_c = \omega_c - \omega \tag{2.2}$$

Since we shall be concerned only with the components of velocity perpendicular to the static magnetic field (which lies along the axis of rotation) it is also convenient to introduce a complex velocity representation in which the real and imaginary parts of $\overset{\vee}{V}$ are V_x and V_y respectively. So equation 2.2 can be written:

$$\overset{\vee}{V}' - i\omega'_c \overset{\vee}{V}' = -\frac{e}{m}\overset{\vee}{E}' \tag{2.3}$$

with

$$\overset{\vee}{V}' = V'_x + iV'_y$$

Equation 2.3 can be solved using Laplace transform

$$\overset{\vee}{V}'(t) = \overset{\vee}{V}'(0)\, e^{i\omega'_c t} + \int_0^t e^{i\omega'_c(t-s)} \left(-\frac{e}{m}\right) \overset{\vee}{E}'(s)\, ds \tag{2.4}$$

Now the question is to find how the electron velocity has been

perturbed by a short microwave pulse. Since the duration of the pulse is very short and the homogeneity of the magnetic field high, the condition $\omega_c' t_p \ll 1$ is certainly satisfied so that the velocity of one electron at a time $t = t_p$ (end of one pulse) is:

$$\overset{\lor}{V}{}'(t_p) \overset{\sim}{=} \overset{\lor}{V}{}'(0) - \frac{e}{m} \overset{\lor}{E}{}' t_p \qquad (2.5)$$

The effect of the electric field is then simply to translate the velocity vector by an amount proportional to the intensity and duration of the pulse. If the electron has a cyclotron frequency slightly different from the r.f. exciting field frequency ω , the velocity vector will rotate slowly about the axis with the frequency ω_c' . One can then use this result to discuss the behavior of electrons which have a distribution of cyclotron frequencies by virtue of their being located in regions of slightly different magnetic fields. Fig. 2.1 displays Gould's echo diagrams. They describe the behavior in the rotating velocity space of electrons submitted to the two pulses of an echo experiment. If we ignore the thermal velocities of the electrons in comparison with the heating due to the first pulse, the velocity vector of each particle is initially at the origin and is translated by an amount V_1' by the first applied pulse (Figure 2.1a). Following the first pulse, each velocity vector characteristic of one electron rotates about the origin at a rate determined by the "difference cyclotron frequency" ω_c' of that electron, so that after a time all these velocity vectors become distributed around a circle of radius V_1' (Figure 2.1b). One should bear in mind that vectors at B , for
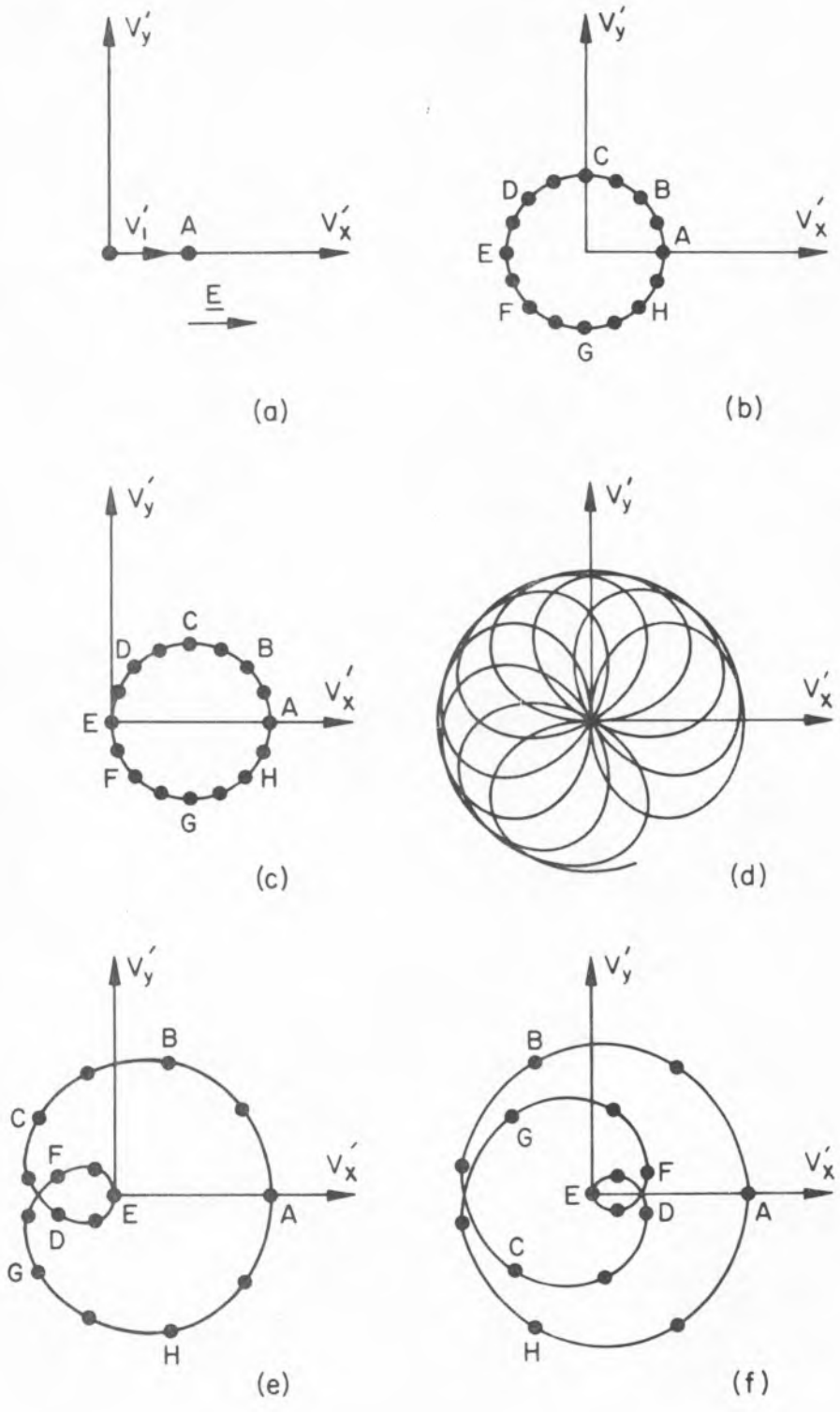
Fig. 2.1 Gould's Diagrams

example, consist of particles which drifted directly to B or encir-
cled the origin once, twice, or more, either clockwise or counter-
clockwise, to reach B . This dispersal represented by Figure 2.1b
shows a situation corresponding to a complete loss of coherence of the
electrons due to the inhomogeneity of the magnetic field. The second
microwave pulse (equal in strength to the first) translates each of
the velocity vectors by the same amount, giving Figure 2.1c. Follow-
ing the second pulse, each velocity vector rotates with its appropriate
rate and the circle in Figure 2.1c breaks into "many circles", since
particles at a given point on the circle have arrived there by rotating
at different rates. However, after a time exactly τ , each vector
will have turned through the same angle as it did during the initial
interval τ between the two pulses and all vectors which were together
at B in Figure 2.1c are together at B in Figure 2.1e. Figure 2.1e
corresponds to the time of the first echo and Figure 2.1f corresponds
to the time of the second echo; Figure 2.1d shows intermediate times.
We see that at special times $n\tau$ (measured from the second pulse),
velocity vectors which are otherwise distributed over the entire plane,
regroup. This regrouping in phase at special times is not sufficient
to produce a macroscopic current in the plasma, since the sums of the
velocity vectors (in diagrams 2.1e and 2.1f) are zero due to an exact
cancellation of positive and negative V_x''s . However, this exact
cancellation at the special times $n\tau$ will be spoiled by any kind of
possible nonlinearities. There seem to be two main classes of possible
nonlinearities for the cyclotron echo; one is the energy-dependent

cyclotron frequency that Gould and Kegel investigated (9), and the
other the energy-dependent relaxation phenomena first introduced by
Gordon, Hill and Kaplan (10). A typical energy-dependent relaxation
phenomenon is the electron-neutral collision frequency which is a
strong function of the electron velocity in most gases (11). What type
of energy-dependent cyclotron frequencies can play a role will be dis-
cussed later. Considering Figures 2.1e and 2.1f, an energy-dependent
cyclotron frequency will spoil the symmetry of the figures with
respect to the V'_x axis. An energy-dependent relaxation phenomenon
such as the energy-dependent electron-neutral collision frequency will
have the effect of selectively removing electrons (or their corres-
ponding velocity vectors) from Figures 2.1e and 2.1f, depending on the
magnitude of their velocity. For instance, if the collision frequency
is a growing function of the velocity, many of the electrons in Figure
2.1e which should have occupied the point A at the time $t = \tau$ will
experience a collision with a neutral before that time and then lose
their phase identification, and so cannot be at A at the time $t = \tau$.
However, among the electrons which should be at point E at $t = \tau$,
very few of them will experience collisions, so that the cancellation
of negative and positive V'_x will again be spoiled. A characteristic,
then, of the cyclotron echo is that the nonlinearities are acting at
all times between the beginning of the first pulse and the time the
echoes appear. This is a main difference with the spin echo, because
one can show that the nonlinearity associated with this phenomenon
comes directly through the pulse excitation. That kind of nonlinear-
ity is called a nonlinear driving force. Coming back to cyclotron

echoes, one can use the hints given by Figure 2.1 to derive a mathematical model. The macroscopic entity we are interested in is the current present in the plasma. To know the current one needs the density of electrons and their velocity. The velocity of an electron at a time t after the second pulse is (using the same notation as in equation 2.5)

$$\overset{v}{V}{}'(t) = (V_1 e^{i\emptyset_1} + V_2) e^{i\emptyset} \qquad (2.6)$$

V_1 is the velocity imparted by the first pulse and is equal to $\frac{e}{m} E_1 t_1$

V_2 is the velocity imparted by the second pulse and is equal to $\frac{e}{m} E_2 t_2$

$\emptyset_1$ is the rotation between the first and second pulses $\overset{\sim}{=} \omega'_c \tau$

$\emptyset_2$ is the rotation after the second pulse $\overset{\sim}{=} \omega'_c t$.

Since the electrons have different cyclotron frequencies depending on their spatial locations, one can define a normalized electron density $G(\omega'_c)$ per increment of "difference cyclotron frequency" ω'_c so that the plasma current can be written

$$\overset{v}{J}{}'(t) = -Ne \int d\omega'_c \; G(\omega'_c) \; \overset{v}{V}{}'(t) \qquad (2.7)$$

N is the number of electrons per cubic centimeter if, for example, one is interested in the plasma current per cubic centimeter. To be more general and also to introduce energy-dependent relaxation type of nonlinearities, one can multiply the integrand of equation 2.7 by a term giving the probability $P(t)$ of no collision between the first pulse and t :

$$P(t) = e^{-\nu(t+\tau)}$$

so that equation 2.7 can be written, using the notation $\overset{\nu}{J'}(t) = J$ to simplify:

$$J = -Ne \int G(\omega_c') \, d\omega_c' \, [V_1 \, e^{i\emptyset_1} + V_2] \, e^{i\emptyset} \, e^{-\nu(t+\tau)} \qquad (2.8)$$

The energy-dependent gyrofrequency nonlinearity is present in the phase. Assuming a weak dependence on V^2, one has:

$$\emptyset = [\omega_c(V^2) - \omega] \, t = [\omega_c' + \frac{\partial \omega_c}{\partial V^2} \, V^2] \, t$$

and

$$\emptyset_1 = [\omega_c' + \frac{\partial \omega_c}{\partial V^2} \, V^2] \, \tau \qquad (2.9)$$

The energy-dependent relaxation can also be written, assuming again a weak dependence on V^2 ,

$$\nu(t+\tau) = [\nu_o + \frac{\partial \nu}{\partial V^2} \, V^2] \, (t+\tau) \qquad (2.10)$$

Now in these early theories the effect of the nonlinear terms in the period of time between the two pulses is neglected, and one considers their effect only starting from $t = 0$, corresponding to the end of the second pulse. The approximation is certainly good when one considers the second or third echo, but seems questionable as far as the first echo is concerned. However, one can show that the qualitative aspect of the results is unchanged. Equations 2.9 and 2.10 will then be written:

$$\emptyset = [\omega'_c + \frac{\partial \omega_c}{\partial v^2} v^2] t \quad , \quad \emptyset_1 = \omega'_c \tau \tag{2.11}$$

$$\nu(t+\tau) = \nu_o \tau + [\nu_o + \frac{\partial \nu}{\partial v^2} v^2] t \tag{2.12}$$

Now

$$v^2 = v_1^2 + v_2^2 + 2V_1 V_2 \cos \emptyset_1 \tag{2.13}$$

and from a well-known Bessel function identity

$$e^{-(\alpha+i\beta)\cos \emptyset_1} = \sum_{-\infty}^{+\infty} I_n(\alpha + i\beta) e^{-in\emptyset_1}$$

with

$$\alpha = \frac{\partial \nu}{\partial v^2} 2V_1 V_2 t \quad , \quad \beta = - \frac{\partial \omega_c}{\partial v^2} 2V_1 V_2 t \tag{2.14}$$

so that finally:

$$|J| = NeV_1 \sum_{-\infty}^{+\infty} A_n(t) \, g(t-n\tau) \tag{2.15}$$

with

$$A_n(t) = \left| (I_{n+1}(\alpha+i\beta) + \frac{V_2}{V_1} I_n(\alpha+i\beta) e^{-[\nu_o(t+\tau)+ \frac{\partial \nu}{\partial v^2} (v_1^2 + v_2^2) t]} \right.$$
$$\left. \times \, e^{i[\frac{\partial \omega_c}{\partial v^2} (v_1^2 + v_2^2) t]} \right| \tag{2.16}$$

and

$$g(t) = \int_{-\infty}^{+\infty} G(\omega'_c) \, e^{i\omega'_c t} \, d\omega'_c \tag{2.17}$$

$A_n(t)$ represents an amplitude factor and $g(t)$ represents the normalized echo shape. One sees that the echo shape is simply the Fourier transform of the distribution of cyclotron frequencies. One

should note that, apart from the assumptions mentioned, the plasma current given by equation 2.15 has been derived in complete generality as far as nonlinearities are concerned. So it is possible to make a choice as to which one is preferred and then to draw some predictions to be confirmed by the experiment. Kegel (12) showed that a possible energy-dependent frequency type of nonlinearity could be the relativistic mass effect. Other workers (13), however, pointed out that the energy-dependent collision frequency type of nonlinearity is much stronger when the energy of the electrons is of the order of 1 eV, which is the energy the electrons are likely to acquire in a typical echo experiment.

For some time the generally accepted picture was an independent particle theory with the energy-dependent collision frequency as the nonlinearity (10). In the first experiment that we tried, an extremely homogeneous magnetic field ($\frac{\Delta B}{B} = 10^{-4}$), at least ten times more homogeneous than was the case in the other experiments, was used. So it was a startling surprise to find that the echo width was ten times narrower than expected by equation 2.17. One recalls that $G(\omega_c')$ in equation 2.17 is expected to be a direct measure of the magnetic field inhomogeneity. Figure 2.2 presents this early experimental result. As the figure makes clear, not only did the echo width appear much narrower than expected, but it shows a systematic variation with the time in the afterglow. The time in afterglow is the time, counted from the end of the 21 MHz pulse creating the plasma at which the echo experiment is done. It is then a measure of the electron density at which the echo experiment is performed. As the density increases
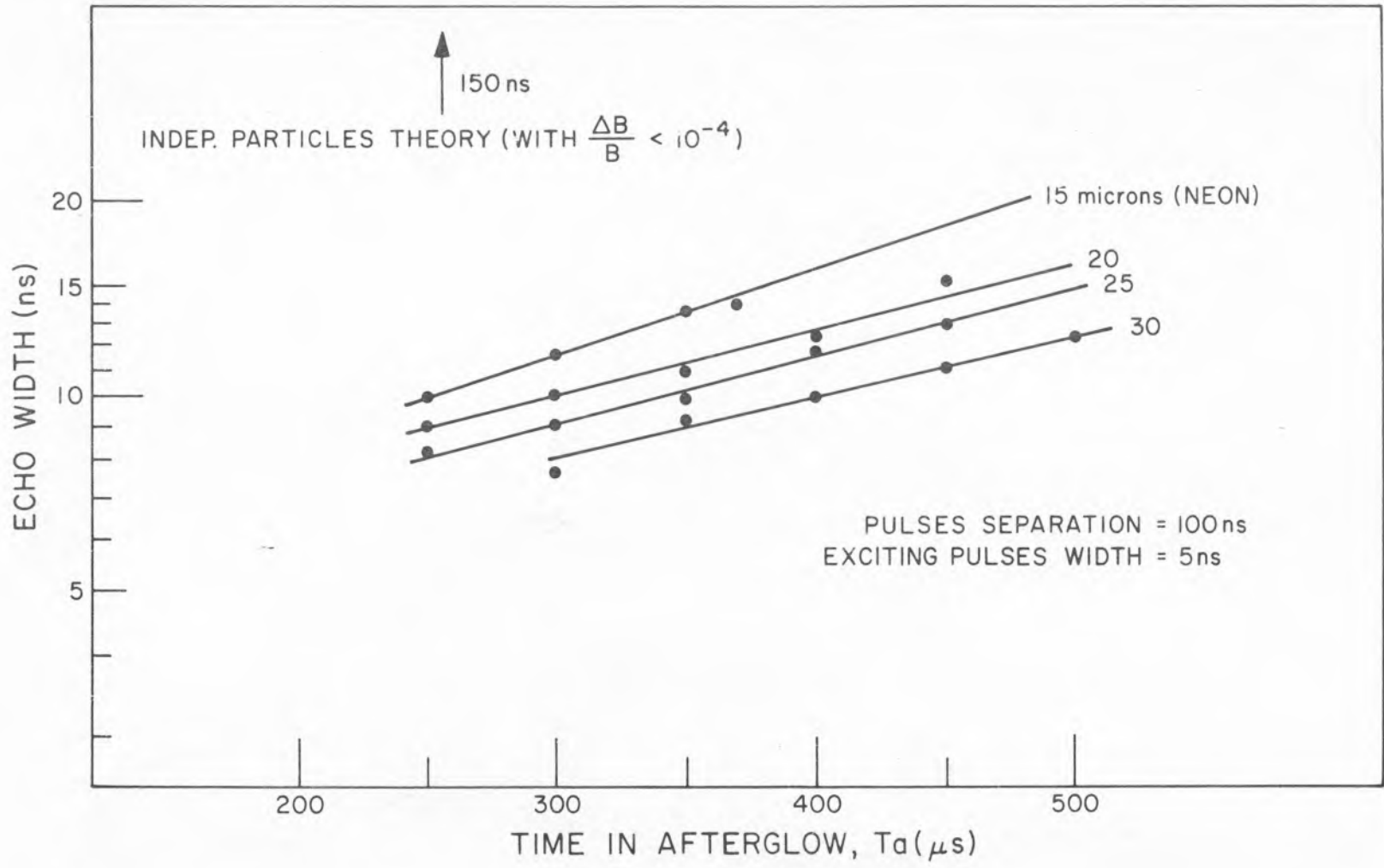
Fig. 2.2   Echo width as a function of the time in the afterglow

the echo gets narrower. As the pressure increases at a fixed time in

the afterglow, the echo gets narrower also. This reflects the fact

that if the pressure is increased at a fixed time in the afterglow the

electron density increases. The same behavior of the echo width was

observed in a cesium plasma by Wong et al (14). A systematic dependence

of the echo width on density was found, a fact not at all predicted by

the model using an energy-dependent collision frequency. Gould and

Kegel (15) then proceeded to resuscitate the energy-dependent cyclotron

frequency model with a new idea. As shown by the calculation of Parker

(16) the radial density profile of a plasma contained in a cylindrical

glass column falls approximately as the Bessel function of order zero

from the axis of the column to a distance of about one Debye length

$(\lambda_D = (\frac{\varepsilon_o kT}{ne^2})^{1/2}$) away from the wall and then drops rapidly to zero.

The zone of plasma situated at one Debye length of the wall is called a

sheath. Large static electric fields are present there as a result of

a steady state diffusion situation. Parker solved the problem for a

plasma not in a magnetic field, but it can be shown that qualitatively

the same type of static electric field exists. It will also be weak in

the center and large in the sheath region. One can take a one-

dimensional model to write the equation of motion of an electron in

such a configuration of fields. The static electric field will be

written $E = E(y)$; the equation of motion of one electron will then be:

$$\ddot{\delta y}(y) + \omega_c^2 \, \delta y(y) + \frac{q}{m} \, E(y + \delta y) = 0 \qquad (2.18)$$

where δy is the displacement of one electron from its equilibrium

position y . Now it is possible to expand $E(y)$ around the position of equilibrium of the electron

$$E(y+\delta y) = E(y) + E'(y) \ \delta y + \frac{1}{2!} E''(y) \ \delta y^2 + \frac{1}{3!} E'''(y) \ \delta y^3 + \cdots$$

$$(2.19)$$

Substitution of equation 2.19 into equation 2.18 gives:

$$\ddot{\delta y}(y) + \left(\omega_c^2 + \frac{q}{m} E'(y)\right) \delta y + \frac{1}{2}\frac{q}{m} E''(y) \ \delta y + \frac{1}{3}\frac{q}{m} E'''(y) \delta y^3 = -\frac{q}{m} E(y)$$

$$(2.20)$$

Equation 2.20 is the equation of an anharmonic oscillator, meaning that its frequency of oscillation is energy-dependent. Through the term $\frac{q}{m} E'(y)$ the electron gyrcfrequencies are seen to depend on the density, since $\frac{qE'(y)}{m} \sim \omega^2 p(y)$ explaining nicely why the echo width is dependent on density. So for a while this new model seemed to hold some serious promise. However, if one investigates the strength of the non-linearity and compares it with the energy-dependent collision frequency, it is found that only the electrons in the sheath experience a nonlinearity equivalent to that due to the collision frequency. Taking into account the small quantity of electrons in the sheath, the echo computed was about two orders of magnitude smaller in the new model than in the collision-frequency type of nonlinearity. The contradictory nature of the experimental and theoretical results brought some understandable confusion and the realization that something was basically wrong in the independent particle theories. One must emphasize, however, that they did serve a useful purpose, shedding some light on what conditions are necessary to obtain an echo from a plasma, or for

that matter, from any physical system. In other words, this system
must possess:

    a) An ensemble of oscillators with a distribution of natural
frequencies, which interact with external forces;

    b) Sufficiently long relaxation times to permit observation;

    c) One of a variety of nonlinear effects to "spoil cancella-
tion":

        1. Energy-dependent driving force

        2. Energy-dependent natural frequency; anharmonic oscilla-
           tors

        3. Energy-dependent relaxation phenomena.

2.3 Collective Effects Model: Echoes from a Cold Nonuniform Magnetoplasma

2.3.1 General Case

The single particle theories considered the independent electrons to be the oscillators required for an echo. This implied that when the plasma interacted with an external RF signal, each electron acted independently. Actually, numerous experiments have shown that a cylindrical nonuniform plasma column in a magnetic field such as we used, exhibits a very complex collection of resonances when excited with a continuous wave signal whose frequency is changed. Among those most successfully explained are the Buchsbaum-Hasegawa resonances (25) caused by standing electrostatic waves in the dense core of the plasma, or the corresponding under-dense modes of Schmitt, Meltz and Freyheit (26) excited in the low density area of the plasma. Both of these phenomena are described in terms of electrostatic waves caused by coherent density fluctuations which propagate through the plasma at a right angle to the magnetic field. In these two cases the collective oscillations are seen to dominate the plasma reaction to the excitation of an external signal. As a rule of thumb, in fact, one can expect that the collective effects of the plasma will prevail as long as the plasma frequency $\omega_p/2\pi$ is not too small compared to the cyclotron frequency $\omega_c/2\pi$ and signal frequency $\omega/2\pi$.

The Buchsbaum-Hasegawa resonances are most easily observed when an active discharge is used, thus requiring a "hot" plasma theory. Our experiment, on the contrary, is done in a late afterglow plasma. The

electrons can then be assumed to be at room temperature so that an
easier cold plasma theory is expected to suffice. Indeed, it is known
that a cold plasma can support two types of waves across the magnetic
field; the ordinary wave and the extraordinary wave. Considering for
the sake of simplicity a uniform, unidimensional slab of plasma, one
can show that the latter type of wave will induce an electrostatic
resonance at what is called the upper hybrid resonance, ω_H^2 :
$\omega_H^2 = \omega_c^2 + \omega_p^2$, where $\omega_c/2\pi$ is the cyclotron frequency and $\omega_p/2\pi$
is the plasma frequency. The idea, then, that these collective
oscillations in the case of a relatively high electron density should
play a role in the echo formation had been present for some time, but
it was difficult to see how a new theory could be developed. Herrmann
and Whittmer (17) were the first to suggest the existence of an echo
associated with the upper hybrid resonance. Later Gould and Blum (18),
Wong and Judd (19) developed that idea. The former showed that a slab
of cold, collisionless plasma with a nonuniform density profile had
all the necessary properties for the formation of an echo. In this
section the theory of Gould and Blum, and new developments of the
theory by Blum (20) will be presented for comparison with the experi-
mental results obtained by the author. For an easier analysis of the
nonuniform plasma slab, see Fig. 2.3, one can approximate it by an
ensemble of thin space charge sheets each carrying a slightly differ-
ent electron density and spaced closely enough to give a "smooth"
variation of density between the center of the slab and its edge. If
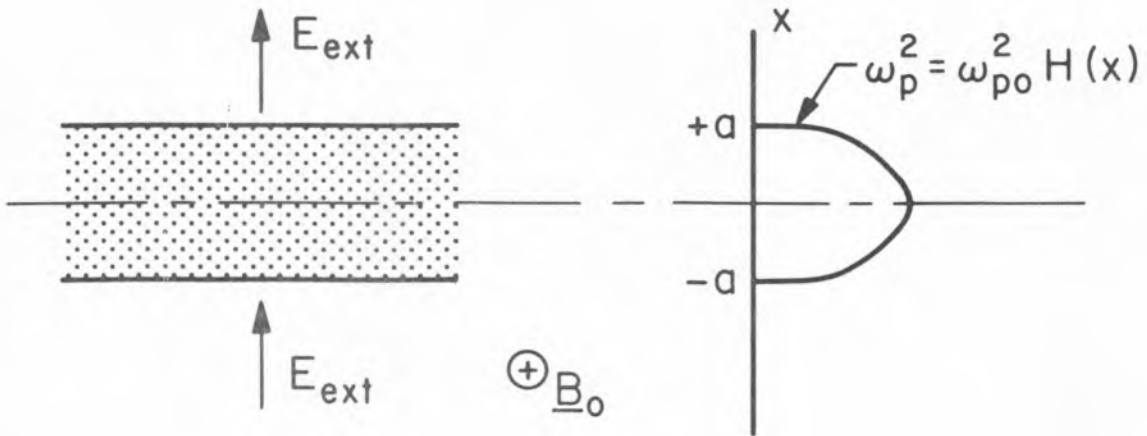the plasma slab is excited by some signal, part or all of the space

Fig. 2.3.   The model's nonuniform plasma slab

charge sheets will be excited and will oscillate at their own upper

hybrid frequencies.   In other words, each sheet is an oscillator and,

depending on their location in the slab, they can have resonant fre-

quencies ranging from the cyclotron frequency--if the sheet is

located at the edge of the slab--to the maximum upper hybrid frequency

$\omega = \omega_{Ho} = (\omega_c^2 + \omega_{po}^2)^{1/2}$ at its center.   (ω_{po} corresponds to the maxi-

mum plasma frequency in the center of the slab.)   Then even though the

magnetic field is very uniform, the spread of the oscillator frequen-

cies could be very wide if the plasma frequency is high enough; even

comparable to or larger than the exciting pulse's spectrum (see Fig.

2.4).   In the independent particle theories the spectrum of the pulse

was always assumed to be much wider than the spectrum of the oscillators.

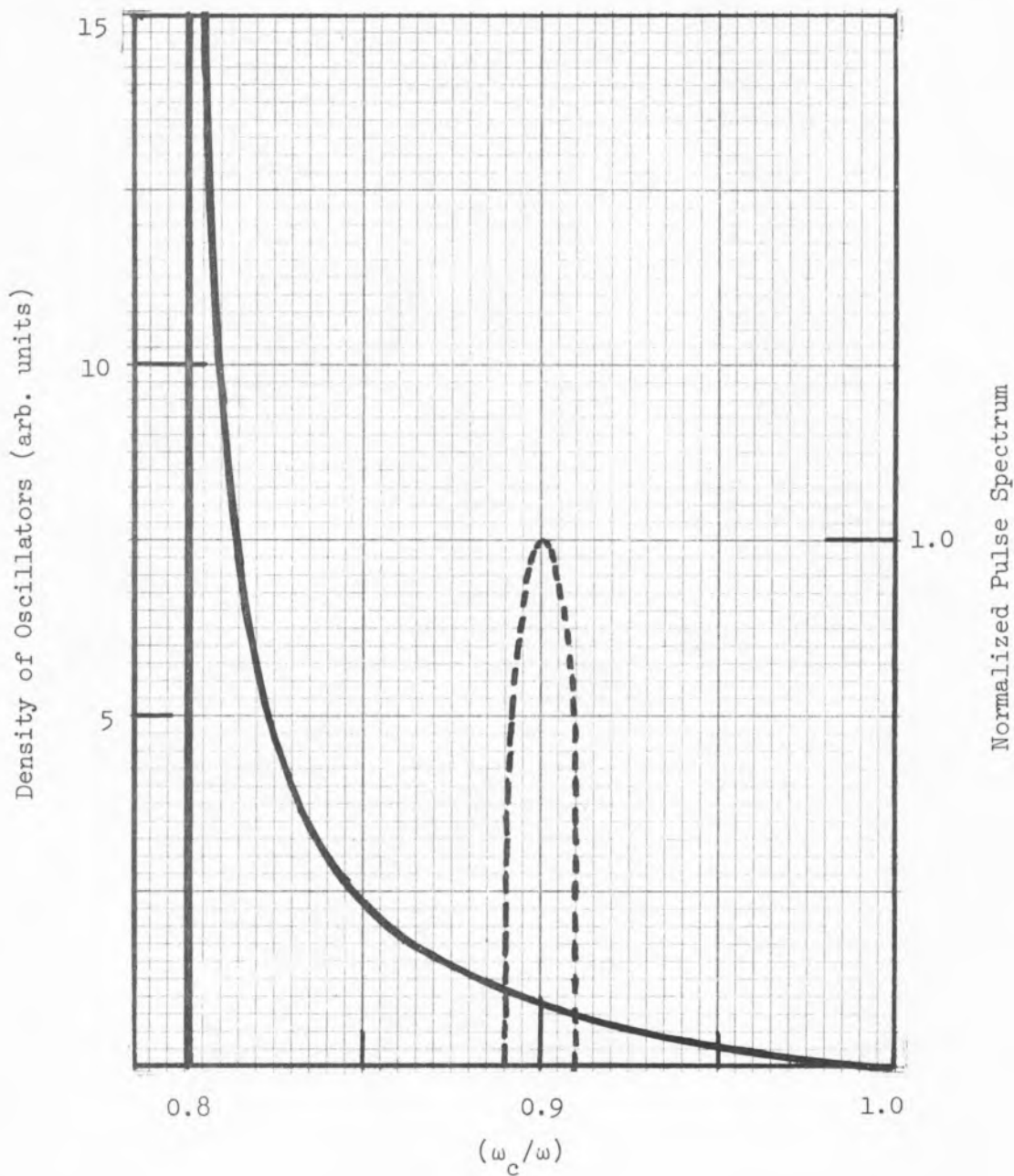This hypothesis will evidently not be adequate here.   After the first

Fig. 2.4 The solid line represents the density of oscillators vs. (ω_c/ω) with $\omega_{po}^2/\omega^2 = .36$. The dashed line represents the spectrum of a typical experimental pulse.

pulse, the sheets will then oscillate and, because of the different
upper hybrid frequencies, slowly dephase in a manner quite similar to
the independent electrons as seen in Section 2.2. It is intuitively
felt, in fact, that when the electron density is small enough the
independent particle theory should be a good approximation. A possible
criterion (21) to fix a density limiting the zones of applicability of
the two theories would be:

$$\frac{(\omega_{Ho}^2 - \omega_c^2)^{1/2}}{\omega_c} = \frac{\Delta\omega_c}{\omega_c} \tag{2.21}$$

where $\Delta\omega_c/\omega_c$ represents the inhomogeneity of the magnetic field and
$(\omega_{Ho}^2 - \omega_c^2)^{1/2}/\omega_c$ represents the spread of upper hybrid frequencies due
to the nonuniformity of the electron density. In our experiment this
fixes the density limit to 10^8 el/cm^3. When compared to the usual
experimental values of 10^9 to 10^{11} el/cm^3, this criterion reinforces
the necessity of a collective effect theory. So far the model of Blum
and Gould has the necessary linear property for an echo. To see where
the nonlinearity comes from, a Lagrangian formulation of the equation
of motion of a sheet perturbed by an external field E_{ext} is used:

$$\ddot{\delta x}(x) + \omega_c^2\, \delta x(x) + \frac{e}{m}\, E(x + \delta x) = 0 \tag{2.22}$$

where $\delta x(x)$ is the sheet displacement from the equilibrium position
x. $E(x+\delta x)$ consists of the external field E_{ext} and the space charge
restoring force of the ions (assumed fixed) which may be expanded in a
Taylor series:

$$\frac{e}{m} E(x + \delta x) = \frac{e}{m} E_{ext} + \omega_p^{2'}(x) \delta x + \omega_p^{2'}(\delta x)^2/2! + \omega_p^{2''}(\delta x)^3/3! + \cdots \quad (2.23)$$

Substituting 2.23 into 2.22:

$$\ddot{\delta x}(x) + (\omega_c^2 + \omega_p^2(x)) \, \delta x(x) \left[1 + \frac{\omega_p^{2'}(x) \, \delta x(x)}{2!(\omega_c^2 + \omega_p^2(x))} + \frac{\omega_p^{2''}(x) \, \delta x^2(x)}{3!(\omega_c^2 + \omega_p^2(x))} + \cdots \right]$$

$$= - \frac{e}{m} E_{ext} \quad (2.24)$$

Equation 2.24 is the equation of an anharmonic oscillator; the nonlinearity required to have an echo comes then simply from the nonuniform density profile of the slab. Equation 2.24 is that of the motion of one sheet only; it is necessary to link its motion to some physically measurable macroscopic quantity. A sheet displaced from its equilibrium position x by δx will generate an electric field $E(x,t)$ such that

$$E(x,t) = \frac{1}{\varepsilon_o} \delta x(x,t) \, \rho_i(x) \quad (2.25)$$

where $\rho_i(x)$ is the fixed ion density.

If all the sheets are considered, they will each generate some electric field which will appear as a voltage $V(t)$ across the slab:

$$V(t) = - \int_{-a}^{+a} E(x,t) dx = - \frac{1}{\varepsilon_o} \int_{-a}^{+a} \delta x(x,t) \, \rho_i(x) \, dx \quad (2.26)$$

This quantity $V(t)$ or the square of it will be compared with the experimentally observed plasma signals. The problem is now defined and one can proceed to look for an approximate solution of 2.24.

However, before that is done some simplifications in 2.24 will be
necessary; first some simplification in writing

$$\delta x(x,t) = \delta x$$

$$\omega_c^2 + \omega_p^2(x) = \omega_H^2$$

$$\frac{\omega_p^{2\prime\prime}}{3! \; \omega_H^2} = \beta$$

$$- \frac{e}{m} E_{ext} = F(t) \qquad\qquad (2.27)$$

Second, the presence of two nonlinear terms will introduce some unnec-
essarily complicated equations. The term in δx^3 only will be kept
throughout the derivations and the results will be adjusted to take
into account the effect of the term in δx^2 so that 2.24 becomes:

$$\ddot{\delta x} + \omega_H^2 \; \delta x[1 + \beta \; \delta x^2] = F(t)$$

$$\text{with} \quad \beta \ll 1 \qquad\qquad (2.28)$$

Using standard small perturbation techniques (22) the time is redefined

$$\theta = \omega t \quad , \qquad \frac{d^2(\delta x)}{d\theta^2} = \delta x^{\prime\prime}$$

where

$$\omega = \omega_o + \beta \omega_1 + \beta^2 \omega_2 + \cdots \quad , \qquad \omega_o = \omega_H$$

$$\delta x = \delta x_o + \beta \delta x_1 + \beta^2 \delta x_2 + \cdots \qquad\qquad (2.29)$$

Using the newly defined variable, equation 2.28 can be written

$$\omega^2 \, \overset{\shortparallel}{\delta x} + \omega_H^2 \, \delta x [1 + \beta \delta x^2] = F(\frac{\theta}{\omega})$$

or

$$(\omega_H + \beta \omega_1 + \cdots)^2 \, (\overset{\shortparallel}{\delta x_o} + \beta \overset{\shortparallel}{\delta x_1} + \cdots) + \omega_H^2 [(\delta x_o + \beta \delta x_1 + \cdots)$$

$$+ \beta (\delta x_o + \beta \delta x_1 + \cdots)^3] = F(\frac{\theta}{\omega}) \tag{2.30}$$

From equation 2.30 one gets different order differential equations by equating the coefficient of β^o, β^1, β^2, $\cdots$

zeroth order:

$$\omega_H^2 \, \overset{\shortparallel}{\delta x_o} + \omega_H^2 \, \delta x_o = F(\frac{\theta}{\omega}) \tag{2.31}$$

first order:

$$\overset{\shortparallel}{\delta x_1} + \delta x_1 = - \delta x_o^3 - \frac{2\omega_1}{\omega_H} \, \overset{\shortparallel}{\delta x_o} \tag{2.32}$$

The zeroth and first order differential equations only will be used here. This will represent a good approximation as long as $\beta \ll 1$.

It can be shown that the solution of 2.31 using Fourier transform is:

$$\delta x_o = \frac{1}{\omega_H^2} \int_{-\infty}^{\theta} \sin(\theta - \theta') \, F(\frac{\theta'}{\omega}) \, d\theta' \tag{2.33}$$

making a transformation of variable from θ to t , equation 2.33 becomes

$$\delta x_o = \frac{\omega}{\omega_H^2} \int_{-\infty}^{\omega t} \sin \omega(t - t') \, F(t') \, dt' \tag{2.34}$$

If one is interested in the value of δx_o for times at which $F(t)$ has become negligible, 2.34 can be written approximately as

$$\delta x_o = \frac{\omega}{\omega_H^2} \int\limits_{-\infty}^{+\infty} \sin \omega(t - t') \, F(t') \, dt' \qquad (2.35)$$

which can be put in the form

$$\delta x_o = \frac{\omega}{\omega_H^2} (f_r(\omega) \sin \omega t - f_i(\omega) \cos \omega t)$$

where

$$f(\omega) = \int\limits_{-\infty}^{+\infty} e^{i\omega t} \, F(t) \, dt = f_r(\omega) + i f_i(\omega) \qquad (2.36)$$

Equation 2.35 or 2.36 would constitute the solution of the problem if ω were known. To achieve that goal, the δx_o just obtained will be substituted into equation 2.32. This will produce "secular" terms from 2.32 unless a condition on ω is satisfied, giving the value of ω to first order (sufficient in this case). Since δx_o is expressed as a function of the variable t , equation 2.32 must be transformed also, giving

$$\ddot{\delta x}_1 + \omega^2 \delta x_1 = - \omega^2 \delta x_o^3 - \frac{2\omega_1}{\omega_H} \ddot{\delta x}_o \qquad (2.37)$$

Now using equation 2.36 one has:

$$\ddot{\delta x}_o = - \omega^2 \, \delta x_o$$

$$\delta x_o^3 = \frac{\omega^3}{\omega_H^6} [f_r(\omega) \sin \omega t - f_i(\omega) \cos \omega t]^3$$

$$= \frac{\omega^3}{\omega_H^6} [f_r^3(\omega) \sin^3 \omega t - 3 \sin^2 \omega t \, f_r^2(\omega) \cos \omega t \, f_i(\omega)$$

$$+ 3 \sin \omega t \, f_r \cos^2 \omega t \, f_i^2(\omega) - \cos^3 \omega t \, f_i^3(\omega)] \qquad (2.38)$$

Among the terms of 2.38 only the terms in $\cos \omega t$ or $\sin \omega t$ will give rise to solutions growing with time or "secular" terms. So, gathering all the secular terms from 2.38 and from the other term of the second member of 2.37, one gets:

Sum of secular terms =

$$- \frac{\omega^5}{\omega_H^6} \left\{ \sin \omega t (\tfrac{3}{4} f_r^3 + \tfrac{3}{4} f_r f_i^2) + \cos \omega t (- \tfrac{3}{4} f_r^2 f_i - \tfrac{3}{4} f_i^3) \right\}$$

$$+ 2\omega_1 \frac{\omega^3}{\omega_H^6} [\sin \omega t \, f_r - \cos \omega t \, f_i] \qquad (2.39)$$

It can be seen that the disappearance of the $\cos \omega t$ and $\sin \omega t$ terms calls for the same condition on $\omega = \omega_H + \beta \omega_1$ which is:

$$\omega_1 = \frac{3}{8\omega_H} (f_r^2(\omega_H) + f_i^2(\omega_H)) \qquad (2.40)$$

which means that

$$\omega = \omega_H + \beta \omega_1 = \omega_H + \frac{3}{8\omega_H} \beta (f_r^2(\omega_H) + f_i^2(\omega_H)) \qquad (2.41)$$

It is then possible to take the value of ω and to substitute it into equation 2.35:

$$\delta x_o(t) = \frac{\omega_H + \beta \omega_1}{\omega_H^2} \int_{-\infty}^{+\infty} \sin(\omega_H + \beta \omega_1)(t - t') \, F(t') \, dt' \qquad (2.42)$$

or since $\beta \omega_1 \ll \omega_H \Rightarrow \frac{\omega_H + \beta \omega_1}{\omega_H^2} \simeq \frac{1}{\omega_H}$, then equation 2.42 can be written:

$$\delta x_o(t) = \frac{1}{\omega_H} \text{Im} \left\{ e^{i(\omega_H + \beta\omega_1)t} \int_{-\infty}^{+\infty} e^{-i\omega_H t'} F(t') dt' \right\}$$

or

$$\delta x_o(t) = \frac{1}{\omega_H} \text{Im} \left\{ e^{i(\omega_H + \beta\omega_1)t} f^*(\omega_H) \right\} \tag{2.43}$$

where

$$f^*(\omega) = \int_{-\infty}^{+\infty} e^{-i\omega_H t} F(t) dt$$

Equation 2.43 is the most general equation of the motion of one plasma sheet in the first approximation analysis used, and subject to the condition that it is good only for a time t for which $F(t)$ has become and stays negligible. Nothing has been said about the exciting external field represented by $F(t)$ to keep the analysis general. Now $F(t)$ will be made to represent an echo experiment. So $F(t)$ will be composed of two pulses F_1 and F_2, one at $t = -\tau$, the other at $t = 0$, so that

$$F(t) = F_1(t+\tau) + F_2(t) \tag{2.44}$$

To adapt 2.43 to this case:

$$f^*(\omega_H) = \int_{-\infty}^{+\infty} e^{-i\omega_H t} (F_1(t + \tau) + F_2(t)) dt$$

$$= f_2^*(\omega_H) + \int_{-\infty}^{+\infty} e^{-i\omega_H(t'-\tau)} F_1(t') dt'$$

or:

$$f^*(\omega_H) = f_1^*(\omega_H) \, e^{i\omega_H \tau} + f_2^*(\omega_H) \tag{2.45}$$

At this point another simplifying assumption can be made by noting that if the exciting pulses are symmetrical in the time domain with respect to their "center line", $f_1(\omega_H)$ and $f_2(\omega_H)$ are real; then:

$$f_1^*(\omega_H) = f_1(\omega_H) \, , \quad f_2^*(\omega_H) = f_2(\omega_H) \tag{2.46}$$

which means that equation 2.45 becomes

$$f^*(\omega_H) = f_1(\omega_H) \, e^{i\omega_H \tau} + f_2(\omega_H) \tag{2.47}$$

The next thing to calculate is ω_1 from equation 2.40:

$$\omega_1 = \frac{3}{8\omega_H} \, (f_r^2 \, (\omega_H) + f_i^2(\omega_H)) \tag{2.40}$$

but

$$f(\omega_H) = f_1(\omega_H) \, e^{-i\omega_H \tau} + f_2(\omega_H)$$

then

$$f_r(\omega_H) = f_1(\omega_H) \, \cos \omega_H \tau + f_2(\omega_H)$$

$$f_i(\omega_H) = - \sin \omega_H \tau \, f_1(\omega_H)$$

which will give

$$\omega_1 = \frac{3}{8\omega_H} \, (f_1^2 + f_2^2 + 2 \, f_1 f_2 \, \cos \omega \tau) \tag{2.48}$$

Using equations 2.43, 2.47, 2.48 the equation of motion of one plasma sheet becomes:

$$\delta x_o(t) = \frac{1}{\omega_H} \text{Im} \left\{ [f_1(\omega_H) \, e^{i\omega_H \tau} + f_2(\omega_H)] \, e^{i(\omega_H + \Delta\omega_2)t} \right\} \qquad (2.49)$$

where $\qquad \Delta\omega_2 = \frac{3}{8} \frac{\beta}{\omega_H} (f_1^2 + f_2^2 + 2f_1 f_2 \cos \omega\tau)$.

Before going on and obtaining a more explicit echo formula, it is interesting to note that with the method employed here there is a correction to the frequency from $t = 0$ to $t = \tau$ which is $\Delta\omega_2$ and which arises from the nonlinearity of the plasma sheet oscillation, but there seems to be no corresponding correction between the times $t = -\tau$ to $t = 0$. This comes about because the solution developed here is only correct for times after which $F(t)$ becomes and stays negligible which is evidently not the case between the two pulses. To correct that difficulty one can consider what would happen if there were only one pulse: the first pulse at $t = -\tau$. The plasma sheet motion can then be obtained from the general equation 2.43:

$$\delta x_o(t) \atop (\text{1 pulse at } t=-\tau) = \frac{1}{\omega_H} \text{Im} \left\{ f_1(\omega_H) \, e^{i(\omega_H + \Delta\omega_1)(t+\tau)} \right\} \qquad (2.50)$$

where $\qquad \Delta\omega_1 = \frac{3}{8\omega_H} \beta \left| f_1(\omega_H) \right|^2$

Then equation 2.49 can be corrected to read:

$$\delta x_o(t) = \frac{1}{\omega_H} \text{Im} \left\{ [f_1(\omega_H) e^{i(\omega_H + \Delta\omega_1)\tau} + f_2(\omega_H)] \, e^{i(\omega_H + \Delta\omega_2)t} \right\} \qquad (2.51)$$

Using a well known Bessel expansion, one can show that

$$e^{i(3/4) \frac{\beta}{\omega_H} f_1 f_2 \cos \omega\tau} = \sum_{n=-\infty}^{n=+\infty} i^n J_n(z) e^{in\omega\tau} \tag{2.52}$$

where
$$z = \frac{3}{4} \frac{\beta}{\omega_H} f_1 f_2$$

Then $\delta x_o(t)$ can be written

$$\delta x_o(t) = \frac{1}{\omega_H} \text{Im} \left\{ \sum_n i^n [f_1 \, iJ_{n+1}(zt) e^{i\Delta\omega_1\tau} + f_2 J_n(zt)] e^{i[\omega_H(t-n\tau)+ \theta t]} \right\} \tag{2.53}$$

where $\theta = \frac{3}{8} \frac{\beta}{\omega_H} (f_1^2 + f_2^2)$

As in the independent particle theories the sum over n means that $\delta x_o(t)$ will comprise the contribution of the first echo: $n = 1$, second echo: $n = 2$ and so on. (The negative values of n do not have any physical meaning; they correspond to echoes which would appear earlier than the exciting pulses). Since one is interested only in one echo at a time, one can consider the equation of motion of the plasma sheet for one value of n only; the displacement of the plasma sheet created by the nth echo will then be:

$$\delta x_{on}(t) = \frac{1}{\omega_H} \text{Im} \left\{ i^n [f_1 iJ_{n+1}(zt) e^{i\Delta\omega_1\tau} + f_2 J_n(zt)] e^{i[\omega_H(t-n\tau)+\theta t]} \right\} \tag{2.54}$$

Calculating the imaginary part of the bracket gives a different result depending on the evenness or oddness of n because of the term i^n.
So n even:

$$\delta x_{on_{even}}(t) = b_{n_{even}} \cos \omega_H(t-n\tau) + a_{n_{even}} \sin \omega_H(t-n\tau) \qquad (2.55)$$

where

$$a_{n_{even}} = \frac{(-1)^{n/2}}{\omega_H} \left\{ \left[-f_1 J_{n+1}(zt)\sin(\Delta\omega_1\tau + \theta t) + f_2 J_n(zt)\cos\theta t \right] \right\}$$
$$(2.56)$$

and

$$b_{n_{even}} = \frac{(-1)^{n/2}}{\omega_H} \left\{ \left[f_1 J_{n+1}(zt)\cos(\Delta\omega_1\tau + \theta t) + f_2 J_n(zt)\sin\theta t \right] \right\}$$
$$(2.57)$$

n odd:

$$\delta x_{on_{odd}}(t) = b_{n_{odd}} \cos \omega_H(t-n\tau) + a_{n_{odd}} \sin \omega_H(t-n\tau) \qquad (2.58)$$

where
$$a_{n_{odd}} = \frac{(-1)^{\frac{n-1}{2}}}{\omega_H} \left\{ \left[-f_1 J_{n+1}(zt) \cos(\Delta\omega_1\tau + \theta t) - f_2 J_n(zt)\sin\theta t \right] \right\}$$
$$(2.59)$$

and
$$b_{n_{odd}} = \frac{(-1)^{\frac{n-1}{2}}}{\omega_H} \left\{ -f_1 J_{n+1}(zt) \sin(\Delta\omega_1\tau + \theta t) + f_2 J_n(zt)\cos\theta t \right] \right\}$$
$$(2.60)$$

Equations 2.55 to 2.60 describe the motion of one plasma sheet triggered by the nth echo. To know the voltage across the slab generated by this echo, one needs equation 2.26

$$V_{on}(t) = -\frac{1}{\epsilon_o} \int_{-a}^{+a} \delta x_{on}(x,t)\, \rho_i(x)\, dx = -\frac{m}{e} \int_{-a}^{+a} \omega_p^2(x)\, \delta x_{on}(x,t)\, dx$$
$$(2.61)$$

Substituting the value of $\delta x_{on}(x,t)$ into equation 2.61

$$V_{on_{(even \atop or \atop odd)}}(t) = -\frac{m}{e} \int_{-a}^{+a} \omega_p^2(x) \, [a_{n_{(even \atop or \atop odd)}} \sin \omega_H(t-n\tau) + b_{n_{(even \atop or \atop odd)}} \cos \omega_H(t-n\tau)] dx$$

(2.62)

Equation 2.62 would be the most general equation for the voltage generated by the nth echo in the first approximation analysis used were it not for the fact that equation 2.24 was solved only for the δx^3 type of nonlinearity. It can be easily shown, however, that the only effect of the δx^2 type of nonlinearity is to add another correcting term to the frequency ω_H , meaning that if one solves

$$\ddot{\delta x} + \omega_H^2 \, \delta x[1 + \alpha \delta x + \beta \delta x^2] = F(t)$$

(2.63)

with

$$\alpha = \frac{1}{2} \frac{\omega_p^{2\prime}}{\omega_H^2}$$

(2.64)

instead of equation 2.28, then ω takes the value:

$$\omega = \omega_H + \left(\frac{3\beta}{8\omega_H} - \frac{5}{12} \frac{\alpha^2}{\omega_H}\right) f^2$$

(2.65)

with the effect that in equations 2.55 to 2.62 z in the argument of the Bessel functions becomes:

$$z = \left(\frac{3}{4} \frac{\beta}{\omega_H} - \frac{5}{6} \frac{\alpha^2}{\omega_H}\right) f_1 f_2$$

(2.66)

θ becomes

$$\theta = \left(\frac{3}{8} \frac{\beta}{\omega_H} - \frac{5}{12} \frac{\alpha^2}{\omega_H}\right)(f_1^2 + f_2^2)$$

(2.67)

$\Delta\omega_1$ becomes:

$$\Delta\omega_1 = (\frac{3}{8\omega_H} - \frac{5\alpha^2}{12\omega_H}) \ f_1^2 \qquad (2.68)$$

Equation 2.62 with the corrections just mentioned represents the microwave signal emitted by the nth echo. However, experimentally, using crystal rectifiers, one just measures the envelope of the microwave signal so that some of the information given by equation 2.62 is superfluous and it is clear that any possible resulting simplifications of that equation will be extremely useful for its later numerical evaluation. An "ideal case" of an equation of type 2.62 can be conceived to show what kind of "theoretical crystal rectification" is possible. Let us suppose that out of some related theoretical echo calculation comes the voltage expression:

$$W_n(t) = \int d\omega \ n(\omega)[c_n(\omega) \sin \omega(t-n\tau) + d_n \cos \omega(t-n\tau)] \qquad (2.69)$$

where it is assumed that:

$$n(\omega) \ c_n(\omega) = F(\omega - \omega_0)$$

$\qquad\qquad\qquad\qquad\qquad\qquad , \ c_n$ and d_n are not functions of time

$$n(\omega) \ d_n(\omega) = G(\omega - \omega_0) \qquad\qquad ((2.70)$$

and where $F(\omega - \omega_0)$ and $G(\omega - \omega_0)$ are symmetrical functions of ω, centered at $\omega = \omega_0$. Then one can write:

$$W_n(t) = \int d\omega \ F(\omega-\omega_0) \sin \omega(t-n\tau) + \int d\omega \ G(\omega-\omega_0) \cos \omega(t-n\tau) \qquad (2.71)$$

Letting $\omega' = \omega - \omega_0$, one gets:

$$W_n(t) = \int d\omega'\ F(\omega')\ \sin[(\omega'+\omega_o)(t-n\tau)] + \int d\omega'G(\omega')\cos[(\omega'+\omega_o)(t-n\tau)]$$

$$(2.72)$$

using the evenness of $F(\omega')$ and $G(\omega')$ and some trigonometric iden-
tities, equation 2.72 can be written

$$W_n(t) = \sin \omega_o(t-n\tau) \int d\omega'\ F(\omega')\ \cos \omega'(t-n\tau)$$

$$+ \cos \omega_o(t-n\tau) \int d\omega'\ G(\omega')\cos \omega'(t-n\tau) \quad (2.73)$$

Calling: $\quad \int d\omega'\ F(\omega')\ \cos \omega'(t-n\tau) = C_n(t-n\tau)$

and $\quad \int d\omega'\ G(\omega')\ \cos \omega'(t-n\tau) = D_n(t-n\tau)$

$$(2.74)$$

the crystal detected output of that signal will be:

$$|W_n(t)|^2 = C_n^2(t-n\tau) + D_n^2(t-n\tau) \tag{2.75}$$

When $t = n\tau$, corresponding to the peak of the "echo" in that simple
case, the detected output is:

$$|W_n(n\tau)|^2 = C_n^2(0) + D_n^2(0)$$

where $\quad C_n(0) = \int d\omega'\ F(\omega') = \int d\omega'\ n(\omega')\ c_n(\omega') \tag{2.76}$

and $\quad D_n(0) = \int d\omega'\ G(\omega') = \int d\omega'\ n(\omega')\ dn(\omega')$

and then, instead of evaluating equation 2.71, one is left with two
simple integrals. To discuss the possibility of applying the same
"detection" technique to equation 2.62, one has to write that equation
with ω_H instead of x as a variable. Using $\omega_p^2(x) = \omega_{po}^2(1 - (x/a)^4)$
then

$$(x/a) = \left(\frac{\omega_{Ho}^2 - \omega_H^2}{\omega_{po}^2} \right)^{1/4} \qquad (2.77)$$

with $\omega_{Ho}^2 = \omega_c^2 + \omega_{po}^2$. The equivalent of equation 2.62 is:

$$V_{on}(t) = \frac{ma}{e\omega_{po}^2} \int_{\omega_{Ho}}^{\omega_c} N(\omega_H) \left[a_n \sin \omega_H(t-n\tau) + b_n \cos \omega_H(t-n\tau) \right] d\omega_H \qquad (2.78)$$

with

$$N(\omega_H) = \frac{(\omega_H^2 - \omega_c^2)\omega_H}{\left\{ (\omega_{Ho}^2 - \omega_H^2)/\omega_{po}^2 \right\}^{3/4}} \qquad (2.79)$$

$N(\omega_H)$ should compare to $n(\omega)$ from equation 2.69 in the ideal case. The former is certainly not a symmetrical function of ω_H . In fact this density of oscillators per increment $\Delta\omega_H$ of upper hybrid frequencies starts at zero when $\omega_H = \omega_c$, goes to ∞ when $\omega_H = \omega_{Ho}$, and drops back to zero when $\omega_H > \omega_{Ho}$. However, both a_n and b_n (equation 2.56 to 2.60) contain the Fourier transform of the incident pulses which are not only symmetrical about their center frequency but have spectra so narrow that the density of oscillators does not change much over the pulses' spectral widths, as long as the density is not too low, see Fig. 2.4. The multiplication of the two types of spectra is then going to be more or less symmetrical about the pulses' center frequency. Another difficulty in applying the simplfications of the "ideal case" to the present one comes from the fact that in

equation 2.62 a_n and b_n are functions of time (not the case for c_n and d_n) through $J_n(zt)$, $J_{n+1}(zt)$, $\frac{\sin}{\cos}(\Delta\omega_1\tau + \theta t)$, $\frac{\sin}{\cos}(\theta t)$. However, their time dependence is very weak compared to that of $\frac{\sin}{\cos}(\omega_H(t-n\tau))$ since it is coming from the very small nonlinear frequency shifts. In view of these arguments it was felt that the simplification previously given could be applied to equation 2.62. Returning to the more familiar variable x , the "theoretical detected output" at $t = n\tau$ due to the nth echo is then:

$$\left|V_{on \binom{even}{odd}}(n\tau)\right|^2 = A^2_{n\binom{even}{odd}} + B^2_{n\binom{even}{odd}} \tag{2.80}$$

where

$$A_{n\binom{even}{odd}} = -\frac{m}{e}\int_{-a}^{+a}\omega_p^2(x)\, a_{n\binom{even}{odd}}\, dx \tag{2.81}$$

$$B_{n\binom{even}{odd}} = -\frac{m}{e}\int_{-a}^{+a}\omega_p^2(x)\, b_{n\binom{even}{odd}}\, dx \tag{2.82}$$

It is interesting to note that in the "ideal case" considered before, the nth echo had a symmetrical shape peaked at $t = n\tau$. However, in our case due to the time dependence of a_n and b_n (as defined by equations 2.56 to 2.60) and the asymmetry of the oscillators in the upper hybrid frequency domain, the echo will probably not peak exactly at $t = n\tau$, and also the echo shape in the time domain could be asymmetrical with respect to its peak. But it is the echo amplitude at $t = n\tau$ as defined by equation 2.80 with the properly chosen

density profile which is the quantity computed and compared with the experimental echo signal amplitude. Finally, there are basic limitations to this plasma sheet model which have not yet been exposed. Because of the density nonuniformity, adjacent sheets of plasma which started to move in phase after the exciting pulses, will slowly dephase and eventually "collide", making a mathematical description much more difficult than the present one. The phenomenon of the collision of the sheets is also called cross-over. Blum (20) showed that the theory, because of that phenomenon, breaks down if zt , the argument of the Bessel, sine and cosine functions, present in a_n and b_n , are too large. For a fixed input power, peak density and pulse separation this happens most easily near the boundary of the plasma. In spite of that basic limitation, the calculations were pursued and fortunately showed that the central area of the slab is by far the most important in the formation of the upper hybrid echo. The problem of the sheet cross-over was, therefore, not considered any further.

2.3.2 Special Cases: Low Input Power Echo Description and Large Input Power Echo Description or Saturation Phenomena

Before any special case is studied it will be useful to express the parameters z, θ, $\Delta\omega_1$ as functions of a general density profile $\omega_p^2(x)$ so that they will be easily evaluated when the proper profile is chosen.

First z will be obtained from equations 2.66, 2.27, 2.64

$$z = \frac{1}{8\omega_H^3} [\omega_p^{2''} - \frac{5}{3} (\frac{\omega_p^{2'}}{\omega_H})^2] \, f_1 f_2 \qquad (2.83)$$

θ is obtained from equations 2.67, 2.27, 2.64

$$\theta = \frac{1}{16\omega_H^3} [\omega_p^{2''} - \frac{5}{3} (\frac{\omega_p^{2'}}{\omega_H})^2] \, (f_1^2 + f_2^2) \qquad (2.84)$$

and $\Delta\omega_1$ from equations 2.68, 2.27, 2.64

$$\Delta\omega_1 = \frac{1}{16\omega_H^2} [\omega_p^{2''} - \frac{5}{3} (\frac{\omega_p^{2'}}{\omega_H})^2] \, f_1^2 \qquad (2.85)$$

where $\omega_p^{2''}$ and $\omega_p^{2'}$ mean $\dfrac{d^2(\omega_p^2)}{dx^2}$ and $\dfrac{d(\omega_p^2)}{dx}$ respectively.

Anticipating the experimental results, it is observed that the density profile giving the closest agreement between theory and experiment is the following one:

$$\omega_p^2(x) = \omega_{po}^2 (1 - (\frac{x}{a})^4) \qquad (2.86)$$

No other attempt to justify the choice of that profile will be given, because it was not possible in our experiment to measure it.

Low input power echo description. A considerable simplification in the mathematical formulation of the echo will be obtained by allowing the input power to be low which means that $\theta\tau$, $\Delta\omega_1\tau$, $z\tau$ will be $<< 1$. Then if this is the case, one can expand the Bessel functions, sine and cosine expressions, in a_n and b_n (equations 2.56 to 2.60) in series and retain only the first term. Another simplification can be achieved by equating f_1 and f_2 since experimentally

only equal pulses were used. In that case:

$$z = \theta = 2\Delta\omega_1 = \frac{1}{8\omega_H^3} [\omega_p^{2''} - \frac{5}{3}(\frac{\omega_p^{2'}}{\omega_H})^2] f^2 \tag{2.87}$$

Using equation 2.87 and the first term of the small argument Bessel function expansion:

$$J_n(x) \sim \frac{x^n}{2^n n!} \tag{2.88}$$

it can be shown that for

<u>n even</u>:

$$a_n = \frac{(-1)^{n/2}}{\omega_H 2^n n!} f \{\frac{1}{8\omega_H^3}[\omega_p^{2''} - \frac{5}{3}(\frac{\omega_p^{2'}}{\omega_H})^2] f^2 t\}^n + 0(\epsilon^{n+1}) \tag{2.89}$$

$$b_n = 0(\epsilon^{n+1}) \tag{2.90}$$

and

<u>n odd</u>:

$$a_n = 0(\epsilon^{n+1}) \tag{2.91}$$

$$b_n = \frac{(-1)^{\frac{n-1}{2}}}{\omega_H 2^n n!} f \{\frac{1}{8\omega_H^3} [\omega_p^{2''} - \frac{5}{3}(\frac{\omega_p^{2''}}{\omega_H})^2 f^2 t\}^n + 0(\epsilon^{n+1}) \tag{2.92}$$

As an example the signal due to the first echo at $t = \tau$ when one uses very low power can be computed:

$$b_1 = \frac{1}{16\omega_H^4} f^3 \tau [\omega_p^{2''} - \frac{5}{3}(\frac{\omega_p^{2'}}{\omega_H})^2] \tag{2.93}$$

So that the echo peak voltage is given by

$$V_o(\tau) \sim \int\limits_{-a}^{+a} \frac{\omega_p^2(x)}{\omega_H^4} f^3(\omega_H)\tau \; [\omega_p^{2''} - \frac{5}{3} (\frac{\omega_p^{2'}}{\omega_H})^2]dx \qquad (2.94)$$

Fig. 2.5a shows a numerical computation of the echo's peak power $V_{01}^2(\tau)$ by Blum as a function of (ω_c/ω) with $\omega_p^2(x) = \omega_{po}^2(1 - (x/a)^4)$. The density was chosen so that the maximum upper hybrid frequency is located at $(\omega_c/\omega) = .85$. This figure presents an important result of the cold plasma model. That is to say, the echo peaks at a frequency very close to the maximum upper hybrid frequency. Fig. 2.5b is a qualitative plot of the three fastest varying functions of $(x/a):\omega_p^2(x)$, $f^3(\omega_H)$ and $[\omega_p^{2''} - \frac{5}{3}(\omega_p^{2'}/\omega_H)^2]$ present in equation 2.94 which will help to understand the results of Fig. 2.5a. The horizontal axis of Fig. 2.5a is labelled as a function of (ω_c/ω) and that of Fig. 2.5b as a function of (x/a) so that a clarification is needed. (ω_c/ω) and (x/a) are physically independent parameters. However, through the local upper hybrid resonances the following mathematical relation exists between them:

$$\omega^2 = \omega_c^2 + \omega_{po}^2(1 - (x/a)^4)$$

so that:
$$\omega_c/\omega = (1 - \frac{\omega_{po}^2}{\omega^2}(1 - (x/a)^4)^{1/2} \qquad (2.95)$$

Fig. 2.5c is a computation of equation 2.95 for the density corresponding to Fig. 2.5a. Through Fig. 2.5c one can then make a correlation between Fig. 2.5a and 2.5b. For instance the maximum upper hybrid frequency corresponds to $(x/a) = 0$ in Fig. 2.5b and $(\omega_c/\omega) = .85$ in
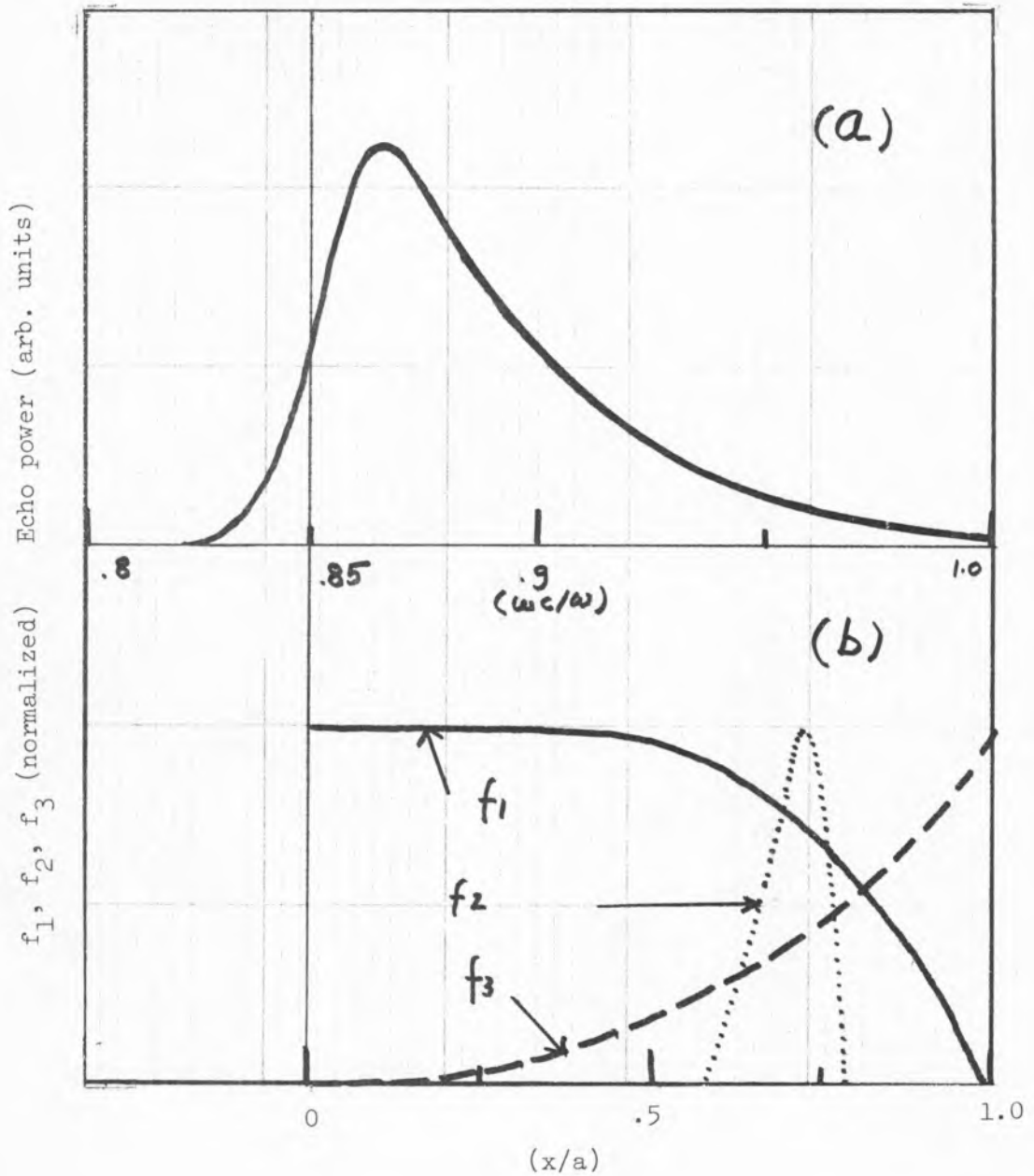
Fig. 2.5a Echo power as a function of (ω_c/ω) for $(\omega_{po}/\omega)^2 = .28$ computed by Blum (low power approximation.)

Fig. 2.5b Diagram showing variation vs. (x/a) of three functions involved in the echo's formation (low power approx.)

$$f_1 = \omega_p^2(x), \quad f_2 = f^3(\omega_H), \quad f_3 = [\omega_p^{2''} - \frac{5}{3}(\omega_p^2/\omega_H)^2]$$

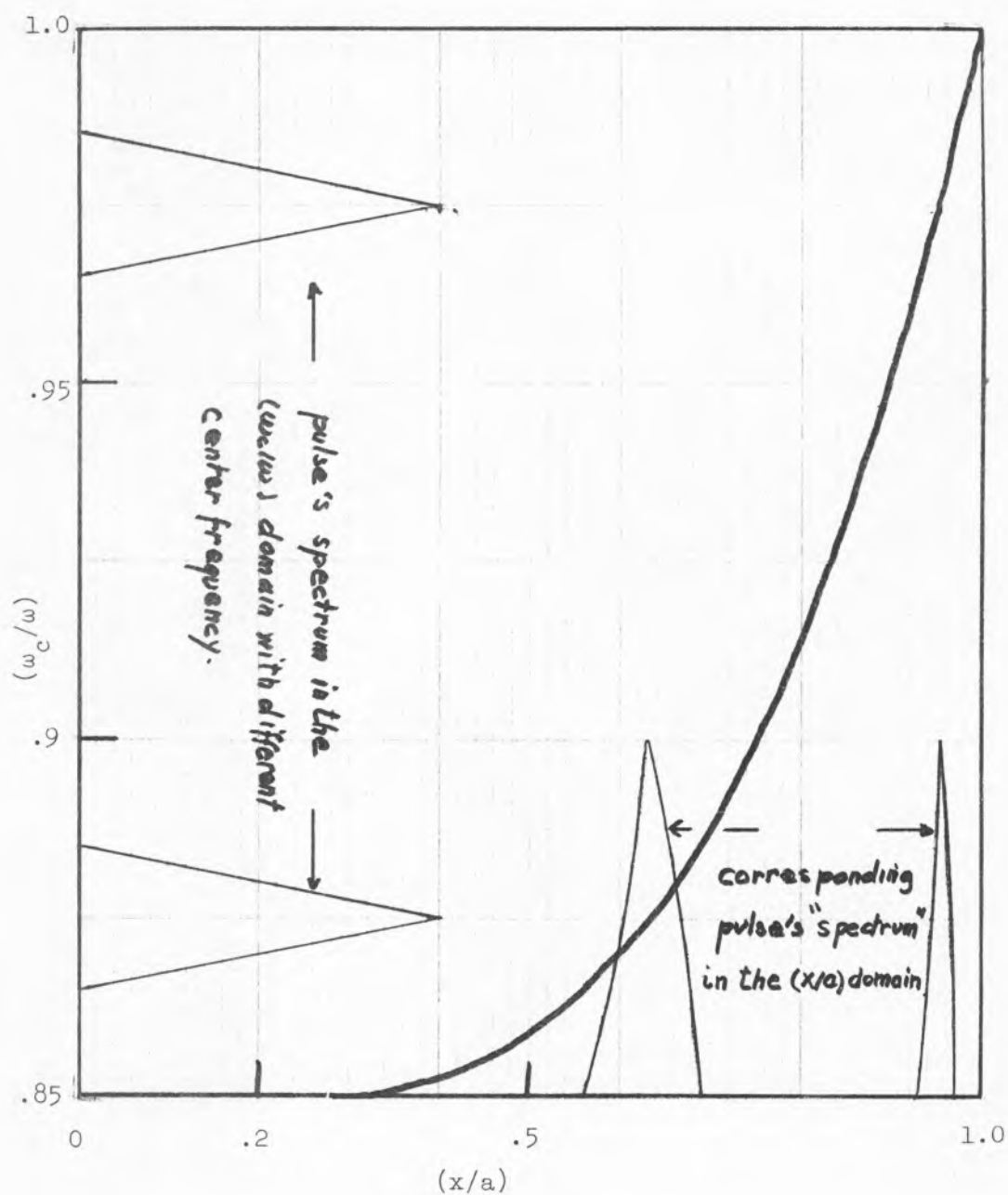Fig. 2.5c   The solid curve shows the relation between the parameters (ω_c/ω) and (x/a). Also shown is the difference between a pulse's spectrum in the (ω_c/ω) and (x/a) domains. $((\omega_{po}/\omega)^2 = .28)$.

Fig. 2.5a. The cyclotron frequency which in Fig. 2.5a is characterized by $\omega_c/\omega = 1.0$, will be assigned to $(x/a) = 1$ in Fig. 2.5b. Now that the relation between the two parameters is clear, one can look at Fig. 2.5b. The solid curve represents the first term: the density profile expressed by $\omega_p^2(x)$. The two other terms: $f^3(\omega_H)$ and $[\omega_p^{2''} - \frac{5}{3}(\frac{\omega_p^{2'}}{\omega_H})^2]$ can be traced back to the frequency shift caused by the nonlinearity of the model. The square bracketed term represented by the dashed line is zero at the center of the slab and grows uniformly to the edge of it. Depending on the center frequency of the pulses, the dotted line displaying the $f^3(\omega_H)$ term* can be anywhere between $(x/a) = 0$ and $(x/a) = 1.0$. The multiplication of the three curves and the computation of the area located under the function defined by this multiplication will give the echo voltage. When the pulses center frequency is changed in the (x/a) domain, the $f^3(\omega_H)$ term sweeps the slab between $(x/a) = 0$ to $(x/a) = 1$. One can see that the echo will first be zero because the nonlinearity of the model is zero at the center of the slab, then increases following the corresponding increase in the nonlinearity as (x/a) grows, and finally drops back to zero when the faster varying $\omega_p^2(x)$ takes over.

Before leaving the weak echo case, it is interesting to derive the relation between the amplitude of the weak echo and the input power

---

* In Fig. 2.5b the $f^3(\omega_H)$ term does not look symmetrical, because it is drawn in the (x/a) domain instead of a frequency domain, see Fig. 2.5c.

used to generate it, or what might be called the "power law" of the
echo. Considering the case of the first echo with equation 2.94, the
input power is contained in the pulse spectrum, if we call $\bar{f}$ a
normalized pulse spectrum then:

$$\bar{f} = \gamma E_i f \qquad (2.96)$$

where γ = constant

E_i = peak input electric field.

Since neither γ nor E_i is a function of x, it is possible to
take them out of the integral 2.94 so that

$$V_{01}(\tau) \sim \gamma^3 E_i^3 \int_{-a}^{+a} \frac{\omega_p^2(x)}{\omega_H^4} \bar{f}^3 \tau \left[\omega_p^{2''} - \frac{2}{3} \left(\frac{\omega_p^{2'}}{\omega_H} \right)^2 \right] dx \qquad (2.97)$$

Hence the voltage generated by the first echo grows as the cube of the
incident electric field, and if one speaks of power, the power of the
first echo grows as the cube of the incident power. In general for a
weak incident power one can show that:

$$\text{Power nth echo} \sim (\text{Power incident})^{2n+1} \qquad (2.98)$$

Another peculiarity of equation 2.94 or 2.97 is that the echo power
seems to grow as τ^2 if everything else is kept constant. This will
be true only as long as $\theta\tau$, $\Delta\omega_1\tau$, $z\tau$ stay $\ll 1$. Experimentally,
even if $\theta\tau$, $\Delta\omega_1\tau$, $z\tau$ do stay very small, the echo power will not
grow as τ^2 for τ greater than 100 ns because of the effect of
electron-neutral collisions not present in the theoretical model.

Large Input Power Echo Description of Saturation Phenomena. It
was seen that considerable simplifications in the expressions giving
the echo power or voltage resulted when the approximations appropriate
to low power could be used. One of the aspects of these simplifications
(see equation 2.97) is that neither the input power nor τ has an
influence on the shape of the spectrum of the echo. The curve traced
by the peak power of the echo as the parameter (ω_c/ω) is changed, we
call an echo spectrum. For instance, Fig. 2.5a is an echo spectrum.
P and τ merely control the absolute magnitude of the echo spectrum.
This is because a low input power makes $z\tau$ small and it is possible
to expand in series and retain only the first terms of the sine, cosine
and Bessel functions present in the general expression of a_n and b_n.
However, when the input power or τ is increased to make $z\tau$ equal to
about .5, the retaining of only one term in the expansions of the above-
mentioned functions will certainly not be adequate. This value of .5
for $z\tau$ will set, as a matter of definition, a threshold for what we
call saturation phenomena of the echo. When this threshold for satura-
tion phenomena is reached, the general form of a_n and b_n will be
needed. P and τ will be present in the arguments of the trigonomet-
ric functions and Bessel functions and it will not be possible any more
to factorize them out of the integral as in equation 2.97. It is then
conceivable that the shape of the echo spectrum, among other charac-
teristics of the echo, could be a function of the input power, τ , or
for that matter any other variable which enters into the expression of
$z\tau$. The complexity of the general expressions for a_n and b_n makes
the task of finding the echo functional dependence on input power, τ ,

and electron density, seem arduous to say the least. But it is also through these functional dependences of the echo that one can best test the theory with the experiment. Blum (20) computed numerically all the interesting echo characteristics as functions of the parameters acces- sible to the experiment. His results will be presented in a following chapter. However, because of the great interest in these saturation phenomena in relation to the experiment, it is of importance to try to have some intermediary steps between the general expression of the echo voltage and the numerical calculation of these expressions.

The only way to accomplish this and then to achieve some mathe- matical if not physical insight, is to try to simplify the echo's general expression without losing too many of the interesting features of the saturation phenomena that we want to study.

We recall that the first echo power in the general case is given by (assuming equal pulses)

$$V_{01}^2(\tau) = A_1^2 + B_1^2 \tag{2.99}$$

$$A_1 = -\frac{2m}{e} \int_0^a \omega_p^2(x) \, a_1 \, dx$$

$$B_1 = -\frac{2m}{e} \int_0^a \omega_p^2(x) \, b_1 \, dx \tag{2.100}$$

with

$$a_1 = -\frac{f}{\omega_H} \left[J_2(z\tau) \cos(\frac{3}{2} z\tau) + J_1(z) \sin z\tau \right]$$

$$b_1 = \frac{f}{\omega_H} \left[-J_2(z\tau) \sin(\frac{3}{2} z\tau) + J_1(z\tau) \cos z\tau \right] \tag{2.101}$$

and with $\quad z\tau = \dfrac{1}{8\omega_H^3}\,[\,\omega_p^{2''} - \dfrac{5}{3}\,(\dfrac{\omega_p^{2'}}{\omega_H})^2\,]\;f^2\tau$ $\qquad\qquad$ (2.102)

The following pseudo-echo experiment will then be devised to simplify the mathematics. One will use very wide pulses in the time domain such that in the frequency domain the pulses spectral width is much smaller than the frequency change necessary to produce a significant variation of all other functions of ω present in the expression of the echo. Equations 2.99 to 2.102 giving the echo voltage are expressed with x as the variable and not ω . However, as pointed out earlier, see Fig. 2.5c, there exists a direct relationship between the parameter (ω_c/ω) and (x/a):

$$\frac{\omega_c}{\omega} = \left(1 - \frac{\omega_{p0}^2}{\omega^2}\,(1 - (\frac{x}{a})^4)\right)^{1/2}$$

if

$$\omega_p^2(x) = \omega_{po}^2(1 - (\frac{x}{a})^4)$$

If we use then pulses with narrow spectral width whose center frequency is such that $(\omega_c/\omega) = K$, they will involve only a very localized area of the slab given, say, by $(x/a) = L$. Then all contribution to integral 2.100 between $x = 0$ and $x = a$ will be zero except for values of (x/a) very close to L .

Then

$$A_1\bigg|_{(x/a)=L} \;\cong\; - \frac{2m}{e}[\omega_p^2(x)\;a_1(x)]\;\bigg|_{(x/a)=L} \qquad\qquad (2.103)$$

$$B_1\Big|_{(x/a)=L} \cong - \frac{2m}{e} [\omega_p^2(x)\, b_1(x)]\Big|_{(x/a)=L} \qquad (2.104)$$

If we use another center frequency K' we will involve another local-
ized area of the slab characterized by x/a = L' so that we can
follow the variation of A_1 and B_1 and of the pseudo-echo:

$$(A_1^2 + B_1^2)^{1/2} = (\omega_p^2(x)(a_1^2 + b_1^2))^{1/2}$$

as a function of (x/a).

Figures 2.6a and 2.6b represent the computation of a_1, b_1 and
of the pseudo-echo as a function of (x/a) with different input power
levels. The behavior of the pseudo-echo with power is similar to that
observed when one directly computes the general echo formula with
pulse characteristics corresponding to those of the experiment. Fig.
2.6a displays the variation of the absolute magnitude of a_1 and b_1
versus (x/a), with input power as a parameter. The obvious result is
that decreasing the input power makes $z\tau$ smaller which results in a
shift for the location of the threshold of saturation phenomena
($z\tau$ = .5). Since the nonlinearity is a growing function of (x/a), when
the power is diminished the saturation threshold will be reached for a
larger (x/a), until eventually the saturation threshold cannot be
reached anywhere in the slab as is the case for the lowest power curve
in Fig. 2.6a. After considering the three diagrams of a_1 and b_1
and the pseudo-echo, it is possible to make some predictions as to
what kind of meaningful experiments can be tried. First, choosing a
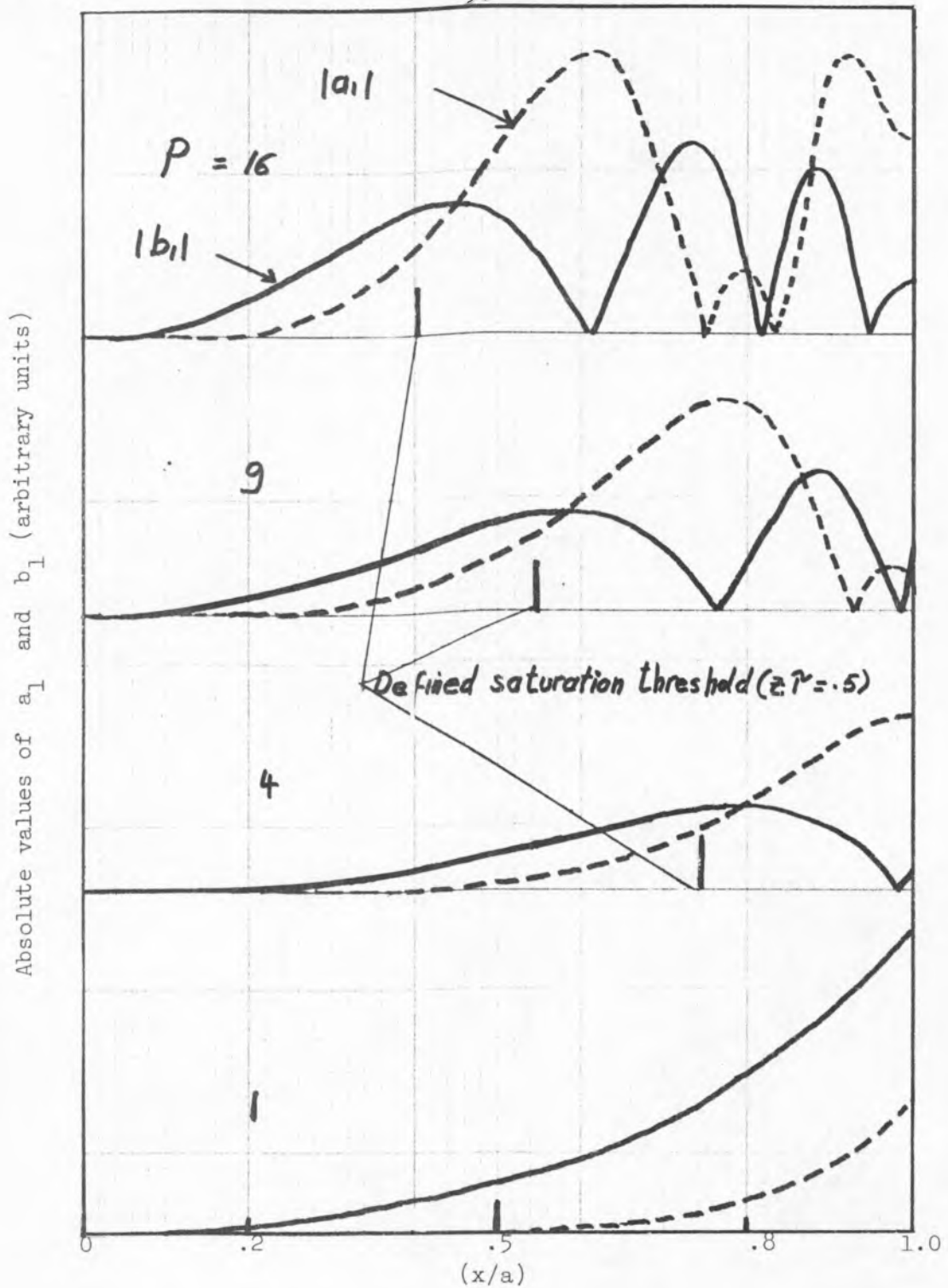certain center frequency for the exciting pulses corresponding to a

Fig. 2.6a Saturation phenomena. Computation of a_1 and b_1 vs. (x/a) in the approximation of very narrow spectrum pulses with input power (expressed in arbitrary units) as a parameter. The vertical scale has been changed for the different input power cases.
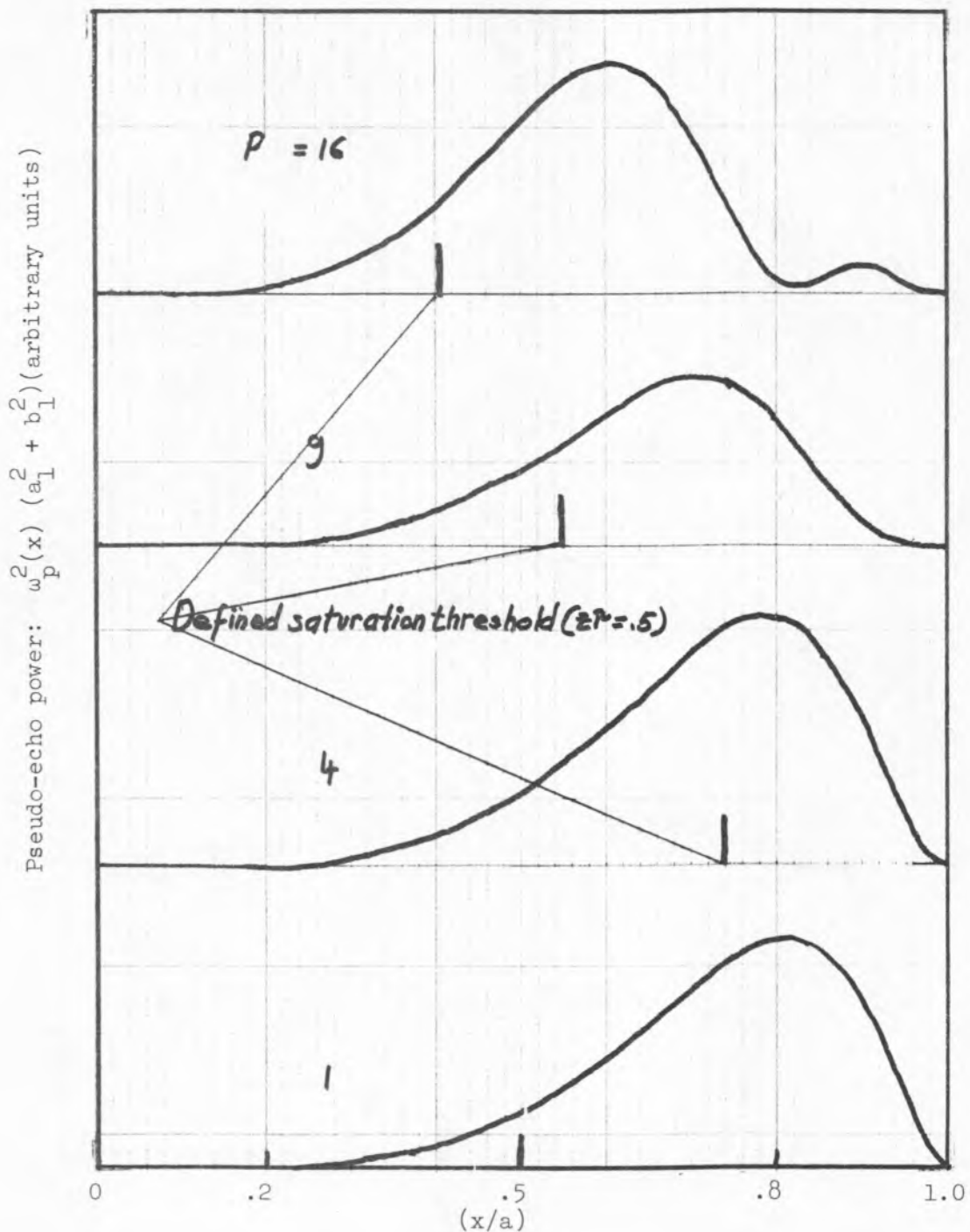
Fig. 2.6b Saturation phenomena. Computation of the pseudo-echo power
          vs. (x/a) with input power (expressed in arbitrary units)
          as a parameter. The vertical scale has been changed for the
          different input power cases.

certain (ω_c/ω) or (x/a) value, the amplitude of the echo can be moni-
tored as the input power is varied and the experiment repeated for

different (ω_c/ω). If the center-frequency of the pulses is equal to

an upper hybrid frequency close to the maximum upper hybrid frequency

(corresponding to $(x/a) \sim 0$), it will require a large input power to

reach the saturation threshold. As this point is reached, the echo

power will stop growing with input power, then decrease, and eventually

increase again depending on the complex variation of a_1 and b_1 with

input power. If, on the contrary, the center frequency of the exciting

pulses is equal to an upper hybrid frequency not very different from

the cyclotron frequency (corresponding to $(x/a) \sim 1$), the saturation

effect should be felt even for low input power levels.

Another type of experiment would be to monitor the echo power

as (ω_c/ω) or (x/a) is varied for a fixed input power level and compare

the results obtained with different input power levels. From Figs.

2.6a and 2.6b one sees that if the input power is decreased, the echo

spectrum should not peak at the same place. Its peak should shift

toward larger (ω_c/ω) or larger (x/a) until the low power case is

reached; in other words, until the saturation threshold cannot be

reached anywhere in the slab. (In that case equation 2.97 is a valid

representation of the echo.) So far the saturation phenomena have been

described only as a function of P and (ω_c/ω) or (x/a), but the other

parameters contained in $z\tau$ can produce saturation as soon as they

make $z\tau$ large enough. To discuss the influence of the other param-

eters, it is desirable to come back to the general case of finite

spectral width pulses. Calculating $z\tau$ with a density profile of the type:

$$\omega_p^2(x) = \omega_{po}^2 (1 - (\frac{x}{a})^4)$$

one has:

$$z = - \frac{\omega_{po}^2}{2a^2 \omega_H^3} [3(\frac{x}{a})^2 + \frac{20}{3} \frac{\omega_{po}^2}{\omega_H^2} (\frac{x}{a})^6] f^2(\omega_H) \tag{2.105}$$

Using a normalized pulse spectrum $\overline{f}$ to make the input power appear separately, equation 2.105 can be written (γ is a constant)

$$z\tau = \frac{\omega_{po}^2 P_i \tau \gamma}{2a^2 \omega_H^3} [3(\frac{x}{a})^2 + \frac{20}{3} \frac{\omega_{po}^2}{\omega_H^2} (\frac{x}{a})^6] \overline{f}^2(\omega_H) \tag{2.106}$$

Among the variables which could be responsible for saturation, a prime candidate seems to be $1/\omega_H^3$. However, in this paragraph we try to make suggestions for experiments and in the experiment the microwave signal generator will be fixed so that $\omega = \omega_H = $ constant. The resonance of each layer of the slab is reached by changing the magnetic field so that in the parameter (ω_c/ω) it is ω which is constant. This might seem contradictory since in previous paragraphs the words: upper hybrid frequency domain were used, it meant that ω_c was then considered to be fixed and ω variable, and then ω_H was a variable too. The first point of view is more directly related to the experiment and the second makes the theoretical expressions much easier, but the two points of view are strictly equivalent if one writes the results which might be derived from them in terms of (ω_c/ω) or (x/a). The changes from one to the other might be confusing to the reader,

but it is felt that the confusion would be even greater if it were not
done, due to the greater complication of the algebra. ω_H , here, is
then a constant and will not be one of the variables useful for the
study of saturation phenomena. As was pointed out before, (ω_c/ω) is
one variable parameter. It is contained in the term:

$$[3(\frac{x}{a})^2 + \frac{20}{3} \frac{\omega_{po}^2}{\omega_H^2} (\frac{x}{a})^6] \ \overline{f}^2 \ (\omega_H)$$

P_i,τ will play identical roles. ω_{po}^2 finally, will be involved in
two terms with the second term in the brackets very weak. So that if
(ω_c/ω) is kept constant an experiment should show the similar role of
ω_{po}^2, P,τ in saturation phenomena. This also means that if one wants
to measure the effects of a parameter, it is necessary that the other
parameters do not change during the measurement. To conclude, since
an experiment can demonstrate the presence or absence of all the
parameters thought to be contained in $z\tau$ and demonstrate whether they
have the proper predicted functional relationship, it can be said that
the saturation phenomena play an important role as a test of the theory.

2.3.3 Echo Width

In the independent particle expression of the echo current, one
recalls that it is possible to write it as the product of an echo amp-
litude factor and an echo shape factor. The echo shape factor $g(t-\tau)$,
(see equation 2.17) is just the Fourier transform of the oscillators'
spectral density, so that there is a direct relationship between the
echo width and the spectral width of the oscillators. To compare with
the cold plasma model of Blum and Gould, one has to express the nth

echo voltage as an integral over ω_H and not x ; this is done in
equation 2.78:

$$V_{on}(t) = \frac{ma}{e\,\omega_{po}^2} \int_{\omega_{Ho}}^{\omega_c} N(\omega_H)\,[a_n \sin\omega_H(t-n\tau) + b_n \cos\omega_H(t-n\tau)]\,d\omega_H$$

$$(2.78)$$

with

$$N(\omega_H) = (\omega_H^2 - \omega_c^2)\,\omega_H \bigg/ \left(\frac{\omega_{Ho}^2 - \omega_H^2}{\omega_{po}^2}\right)^{3/4} \qquad . \qquad (2.79)$$

With $\left\{ \begin{matrix} a_n(\omega_H) \\ b_n(\omega_H) \end{matrix} \right\} N(\omega_H)$

one has defined two "equivalent oscillator spectral densities" whose
sine and cosine transforms will give the echo voltage. The knowledge
of $\left\{ \begin{matrix} a_n \\ b_n \end{matrix} \right\} N(\omega_H)$ without going through the integral defined in equation
2.78 is then sufficient to describe the echo width. To test the prac-
ticality of this idea, one can investigate the low power limit of
equation 2.78. Using equations 2.97, 2.78 and 2.105, the first echo
voltage is:

$$V_{01}(t) \sim t\,E_i^3$$

$$\times \int_{\omega_{Ho}}^{\omega_c} \left\{ \frac{(\omega_H^2 - \omega_c^2)\left\{ 3\left(\frac{\omega_{Ho}^2 - \omega_H^2}{\omega_{po}^2}\right)^{\frac{1}{2}} + \frac{20}{3}\frac{\omega_{po}^2}{\omega_h^2}\left(\frac{\omega_{Ho}^2 - \omega_H^2}{\omega_{po}^2}\right)^{\frac{3}{2}}\right\}\bar{f}^3(\omega_H)}{\omega_H^3\left(\frac{\omega_{Ho}^2 - \omega_H^2}{\omega_{po}^2}\right)^{3/4}} \right\} \cos\omega_H(t-\tau)\,d\omega_H$$

$$(2.107)$$

This can be written:

$$V_{01}(t) \sim t \; E_i^3 \int_{\omega_{Ho}}^{\omega_c} \frac{(\omega_H^2 - \omega_c^2)[3 + \frac{20}{3}(\frac{\omega_{Ho}^2 - \omega_H^2}{\omega_H^2})] \; \bar{f}^3(\omega_H)}{(\frac{\omega_{Ho}^2 - \omega_H^2}{\omega_{po}^2})^{1/4}} \cos \omega_H(t-\tau) d\omega_H$$

(2.108)

From equation 2.108 one sees that the "equivalent oscillators' density" has a singularity at $\omega_H = \omega_{Ho}$. It seems meaningless, then, to relate the "half-power" width of the oscillators' spectral density and that of the echo as it is done in the independent particle theories. However, one can show (18) that there is still a relation between the total spectral width of the oscillators and that of the echo. In fact in the simple case where the pulse spectrum is much larger than that of the oscillators, the echo width will be inversely proportional to that of the oscillators. Since the latter scales with the electron density, one can expect a dependence of the echo width on the electron density. To obtain the exact echo width in that low power limit and in the general case, one must then perform the integration as defined by 2.78 and 2.108. Some other observations can also be made from equation 2.108 on the echo width behavior. Since it was possible to factorize out of the integral t and E_i^3, the echo width in the low power limit will not depend on the input power or τ. As the power or any other variables contained in $z\tau$ is raised, saturation phenomena will take place and affect the echo width. An experimental study of the echo width will then offer one more way of testing the adequacy of the theory.

III.   INSTRUMENTATION AND EXPERIMENTAL TECHNIQUES

3.1   Instrumentation

In the introduction we indicated the sequence of the most important events present in the experiment. First the plasma is fired with a 21 MHz pulse. Then at a time T_a after the end of the discharge, two high power microwave pulses about 20 ns wide, separated typically by 100 ns are sent through waveguides to interact with the plasma. If the pulse center frequency is chosen correctly, bursts of radiation at times $t = n\tau$ $(n=1,2,\cdots)$ after the second microwave pulse are observed. They are the echoes. In this section the instrumentation which was used to create the microwave pulses, the plasma, the magnetic field, and to observe the echoes will be described. In a following section we will give more details on the properties of the plasma and how the basic characteristics of the echoes are measured.

As was pointed out before, the experiment is performed in an afterglow plasma. Among other quantities, the plasma electron density will decrease in an approximately exponential fashion, through recombinations. The corresponding e-folding time of that decrease will determine the frequency at which the experiment can be repeated in order to have a sufficiently wide variation of density for each experiment. This repetition rate was chosen to be 60 c/s. In Fig. 3.1 it is the "master timing unit" triggered by the line which gives this repetition rate. The master timing unit is composed of several Tektronix waveform and pulse generators of the 160 series. Their triggering pulses permit firing the plasma first and then choosing the
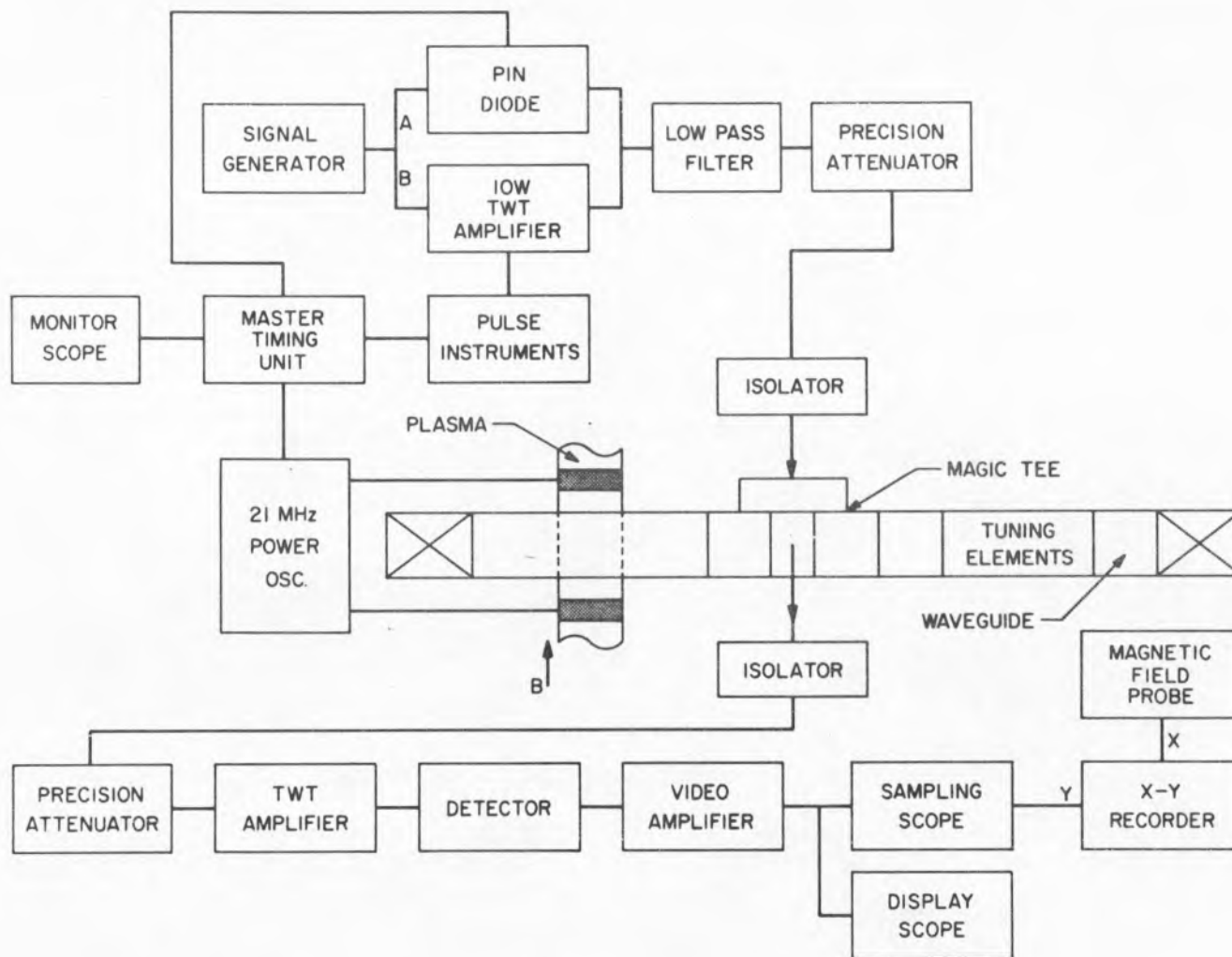
Fig. 3.1 Block diagram of the experiment electronics

time after the end of the discharge at which the microwave pulses will
be sent to interact with the plasma. The delay between the two events
is observed on the monitor scope. The microwave pulses are generated,
looking at Fig. 3.1, by the three blocks "signal generator", "10W TWT
Amplifier" and "pulse instruments". The signal generator, an UHF
oscillator (Hewlett-Packard Type 616A) is set to produce a continuous
wave signal of frequency 3 GHz and power of about 1 mW. The signal
then goes through path B (path A is used in continuous wave scattering
measurements described later) to a Litton traveling wave tube amplifier
Type L5010. The grid on the tube is held at about -50V with respect to
the cathode. The traveling wave tube is then not operating; no output
can be detected. If one applies to the grid a positive pulse such that
it drives the grid potential with respect to the cathode to its
nominal value (+60V with respect to the cathode) during, say 20 ns,
the tube operates for the corresponding length of time. It will thus
generate a microwave pulse with a peak power of 10 watts, 20 ns wide.
The difference in peak power output of the tube between off and on
conditions was difficult to ascertain, but it is believed to be more
than 60 db, 20 ns after the beginning of the pulse's trailing edge. To
bring the grid from its preset -50V with respect to the cathode to the
operating voltage of 60V during 20 ns, 110V pulses, $\sim$ 30 ns wide are
needed. They were obtained using two Hewlett-Packard Type 214A pulse
generators; since the maximum pulse voltage given by the instruments
is only 50V, they were stepped up with two blocking oscillators in
parallel (one is described in Fig. 3.2) or with a simple 3 to 1 pulse
transformer (Pulse Engineering Type PE-5775). The blocking oscillators

are used when very narrow pulses are needed, and the transformer is
practical for pulses whose widths are not required to be narrower than
the minimum available from the HP 214A (minimum half-power width ∿ 30 ns).
It further provides for variable width pulses through the corresponding

Figure 3.2.   Pulse Producing Blocking Oscillator

feature of the HP 214A's until a critical value of about 200 ns is
reached, at which point the saturation of the ferromagnetic material
of the transformer sets in and causes a significant alteration of its
operation.   Two HP 214A's and two blocking oscillators were used
because of the slow recovery of these instruments after one pulse is
produced.   A second pulse could not be obtained directly after the

first from just one of the instruments. In fact, even with the doubl-
ing of the pulse electronics, a certain amount of interaction and
interference was observed when the pulse separation was smaller than
60 ns, so that no echo measurement was taken for lower values of τ
than the above given limit. The 10W traveling wave tube was always
operated close to its maximum peak output; under these conditions a
certain amount of harmonics of the input signal frequency was produced.
To avoid a possible complication in the data interpretation, a low pass
filter was then placed after the traveling wave tube to reject the
harmonics. A precision attenuator followed, permitting us to adjust
the pulses' peak power. Before reaching the waveguide section, the
pulses went through an isolator which eliminated troublesome multiple
reflections due to unavoidable mismatches.

Several remarks can be made about the waveguide arrangement.
First, the glass tube in which the plasma is created, is inserted into
the S band waveguide through two holes in its narrower side. The mag-
netic field lines are parallel with the tube axis. The geometrical
relation between the wave vector $\underline{k}$ of the pulses propagating in the
waveguide, their electric field $\underline{E}$, and the magnetic field lines is
then such that $\underline{k} \perp \underline{E} \perp \underline{B}$.

Second, a certain symmetry in the waveguide configuration with
respect to the magic tee can be observed from Fig. 3.1. It is a
consequence of a property of the magic tee (23) that if its H-arm
(input) and E-arm (output) are terminated in matched loads and if a
signal E_{in} enters the H-arm, the signal at the E-arm will be

$$E_{out} = (\Gamma_1 - \Gamma_2) \frac{E_{in}}{2} \tag{3.1}$$

where Γ_1 and Γ_2 are the reflection coefficients looking from the magic tee into arms one and two respectively. Supposing that the plasma is located in arm 1 and that the coefficient of reflection due to the plasma Γ_p , and that due to the glass and the waveguide holes Γ_g , superpose, one has

$$\Gamma_1 = \Gamma_p + \Gamma_g \tag{3.2}$$

so that

$$E_{out} = (\Gamma_p + \Gamma_g - \Gamma_2) \frac{E_{in}}{2} \tag{3.3}$$

Equation 3.3 gives the output signal when some plasma exists. If there is no plasma, equation 3.3 becomes:

$$E_{out} = (\Gamma_g - \Gamma_2) \frac{E_{in}}{2} \tag{3.4}$$

This means that with no plasma, one can, by acting on Γ_2 through tuning elements in arm 2, have no output signal. And when the plasma is turned on the output signal for $\Gamma_2 = \Gamma_g$ is just:

$$E_{out} = \frac{\Gamma_p E_{in}}{2} \tag{3.5}$$

The experimental output signal is just a measurement of the coefficient of reflection of the plasma alone which can be easily compared with its theoretical equivalent. Ideally, when no plasma is present, we showed that it is possible to have no output signal by properly adjusting Γ_2 .

However, experimentally the maximum isolation between input power and output power was about 30 db for the 20 ns microwave pulses used in an echo experiment. For a pulse 200 ns wide, the isolation can be as good as 60 db. The difficulty with short pulses can be traced to the relatively strong frequency dependence of conventional tuning elements such as slide-screw tuners and the wide frequency spectrum of the short pulses.

This microwave bridge arrangement is not especially useful as far as echo investigations are concerned, but it permits a much better observation of the plasma stimulated radiation directly following the exciting pulses. By monitoring the amount of power reflected from a continuous wave by the plasma as a function of (ω_c/ω), it will also give some valuable information on the plasma which will be described later. On the output path there is an isolator to remove multiple reflections, and a precision attenuator for the calibration of the signals' magnitude. Finally, the signal is amplified by two 1-watt traveling wave tube amplifiers (Hewlett-Packard Type 491A), giving a total signal power amplification of about 55 db with a noise figure around 30 db. The signal is then detected, sometimes video amplified, and displayed on a Tektronix 585A oscilloscope or on a Hewlett Packard Type HP 185B sampling oscilloscope. The sampling oscilloscope, with its 100 ps rise time, permits a detailed study of the echo. Also, through its "manual scanning" feature, one is able to sample a single point of the repetitive waveform of interest. The y axis output of the sampling oscilloscope is fed into the y axis input of an X-Y recorder. On the x axis input of the recorder is a signal whose voltage is proportional to the

magnetic field intensity and thus (ω_c/ω). The recorder will then
directly trace the variation of the deflection of the sampling oscillo-
scope beam as 'a function of (ω_c/ω). As was pointed out in Chapter II,
the value of (ω_c/ω) is changed, not through ω which is kept constant,
but through ω_c or the magnetic field. The reason for that particular
choice lies in the frequency dependence of too many elements in the
system. For instance, the 10 watt TWT and the signal generator which
feeds it do not have a flat frequency response as far as power output
or amplification are concerned. It could be expected, however, that
changing the magnetic field would affect the plasma parameters. But it
was not believed to be very important in the case of echo experiments,
since the magnetic field is not changed by more than 25%.

The plasma is generated in the following manner. The plasma
vessel is a tube of glass about 1 m long and of 1.8 cm I.D. It is
connected through a stainless steel flexible tubing to a conventional
vacuum system (see Fig. 3.3). After their assembly, the glass and
flexible tubing were baked at $400^{\circ}C$ for twelve hours so that a vacuum
of 1×10^{-7} mm of mercury could be reached. Then neon or argon gas
of research grade purity was leaked in the system through a variable
leak valve (Granville-Phillips). A weak continuous flow through dif-
ferential pumping of the diffusion pump (the valve between the diffu-
sion pump and the system being almost closed) was arranged to insure
the highest possible purity of the gas involved in the plasma formation.
The gas was then ionized by 100 watt peak power pulses of 21 MHz, 50µs
long, fed into large copper sleeves (10 cm long) tightly fitted around
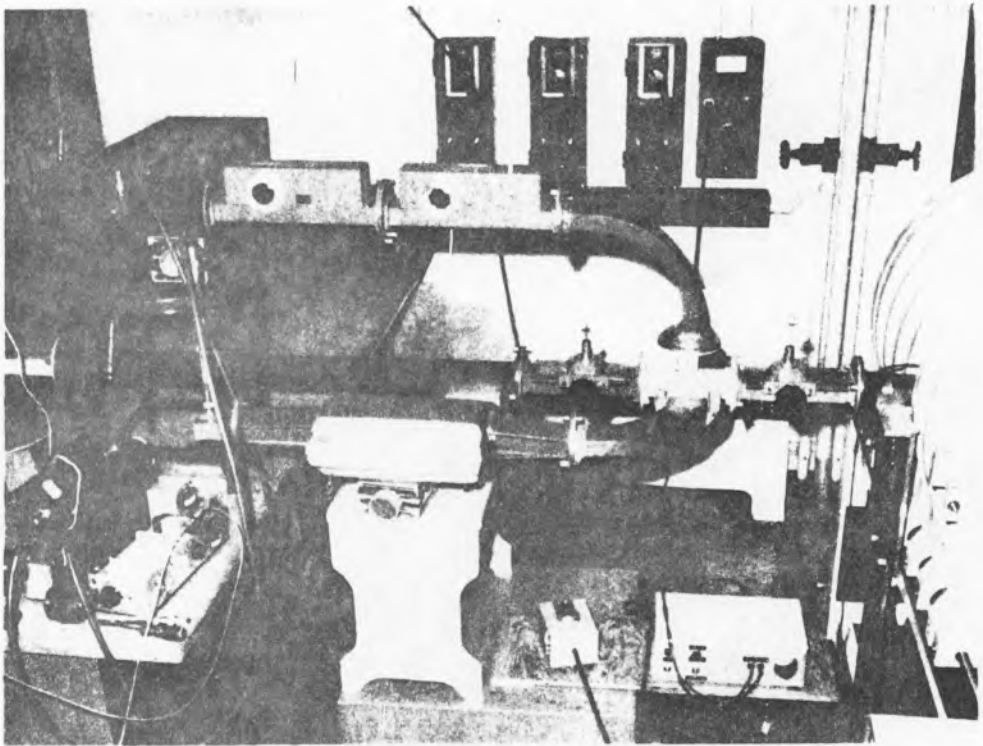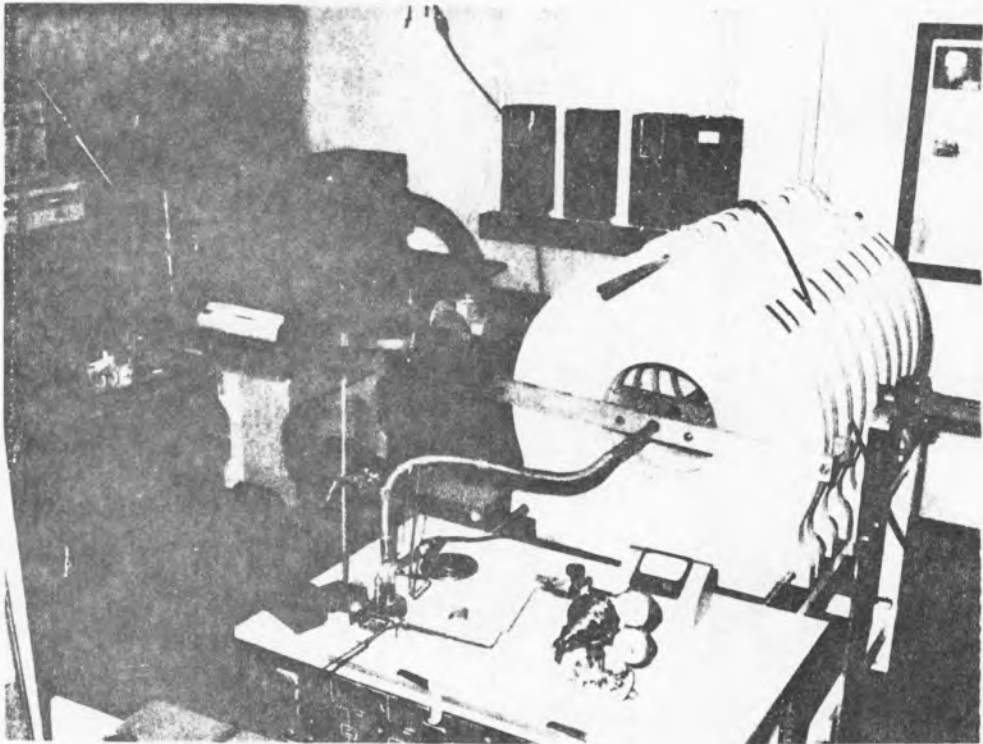the glass vessel and symmetrically situated with respect to the

Fig. 3.3 Photographs of the solenoidal magnet and waveguide apparatus

waveguide. To produce a 21 MHz high power pulse, a VHF signal generator (Hewlett-Packard type HP608D) with an output of 4 mW was used. The output was modulated and fed to a simple tuned three-stage power amplifier whose power tubes were two 6146 in parallel, in class C . The peak power of the 21 MHz pulses seems to be an important factor in obtaining an easy and reproducible breakdown of the plasma. Some fluctuations in the first few microseconds of the discharge were observed. They were undesirable because they provoked density fluctuations making studies of the echo properties difficult, since the latter were strongly dependent on the electron density. These fluctuations of the breakdown from shot to shot diminished appreciably if the 50 watt peak power was increased to a 100 watt peak power. The situation was even better when 500 watt peak power was used (24). The explanation is thought to lie simply in the higher initial electron density created, leaving a higher final electron density when the next pulse comes along. The latter breaks down the gas easily because of the relatively high number of electrons left. Another way to correct this difficulty would be to increase the repetition rate of the experiment. However, synchronizing with the line frequency is experimentally preferable. It is more convenient to increase the power of the breakdown pulse.

There was difficulty in avoiding some density variations which occurred over time periods of the order of one hour or so. One of the reasons for their existence could be the progressive elimination of impurity molecules trapped on the inner surface of the glass due to the intense ion bombardment occurring during the discharge. In fact, a somewhat more stable plasma over long periods of time can be obtained if

during the first half-hour of operation the breakdown of the gas is made
by very long pulses ($\sim$ 500 μs) instead of the usual 50 μs . The 50 μs
width of the breakdown pulses was chosen because it gave the highest
density for a fixed peak power. The measurement of the plasma parameters
is discussed in Section 3.2.

The magnetic field was obtained with an air core solenoid con-
sisting of 10 pancake type coils; see Fig. 3.3. The positions of the
coils could be adjusted so as to minimize inhomogeneities due to the
end effects. A computer calculation showed that if a space of 3.2
inches was left between the two center coils to accommodate S-band
waveguide, a homogeneity of .01% could be achieved over the plasma
volume if the other coils had the same distance between them, except
for the last pair which should be separated by a space of only .8". The
coil dimensions were the following: inner diameter 12", outer diameter
27", coil width 1-5/8". They were wound with hollow copper conductor
through which water could be pumped for cooling. About 110A and 40V
were necessary for the field intensity to reach 1 kg in the region of
interest (the volume of plasma contained in the waveguide) with the above
described positions of the coils.

The computer calculations of the magnetic field intensity were
experimentally checked. Using a nuclear magnetic resonance probe and a
digital frequency counter, the expected high longitudinal and radial
homogeneity over the volume of interest was observed. The voltage across
a constantan shunt by the solenoid current was measured with a
digital voltmeter and calibrated against the NMR probe readings. This
voltage was then fed into the x-axis of the recorder. The accuracy in

the magnetic field readings was of the order of .1%, but (ω_c/ω) was known only within $\pm$ .2% due to cumulative errors introduced by other elements of the instrumentation.

3.2 Experimental Techniques

3.2.1 Measurement of the plasma characteristics.   It soon became apparent that the echo was a strong function of the plasma electron density. Some measurement of that quantity was needed. Due to the critical dependence of the r.f. loading on the exact location of the sleeves on the glass tube with respect to the waveguide and on the orientation of the tube with respect to the magnetic field, such a measurement had to be made in rapid succession with those of the echo, without modifying the magnetic-field-waveguide-glass-tube geometry. We were then led to study the reflection of a low power continuous wave by the plasma as a function of (ω_c/ω). Fig. 3.4ab shows the results of such a measurement in neon with the time in the afterglow at which the experiment was done, as a parameter. Most of the features seen are known to other workers (25,26) who made reflection, absorption and emission studies of active discharges as a function of (ω_c/ω). However, the appearance of a sharp scattering peak at $(\omega_c/\omega) = 1.0$ at large times in the afterglow is new, and not explained by previous theories. Blum (20) has studied the new aspects of these CW reflections as well as those seen in emission in different gases. Here the features of the CW scattering which are understood will be used to obtain an estimation of the plasma parameters. The peak in the scattering that significantly shifts and broadens at high electron densities is one of these features.
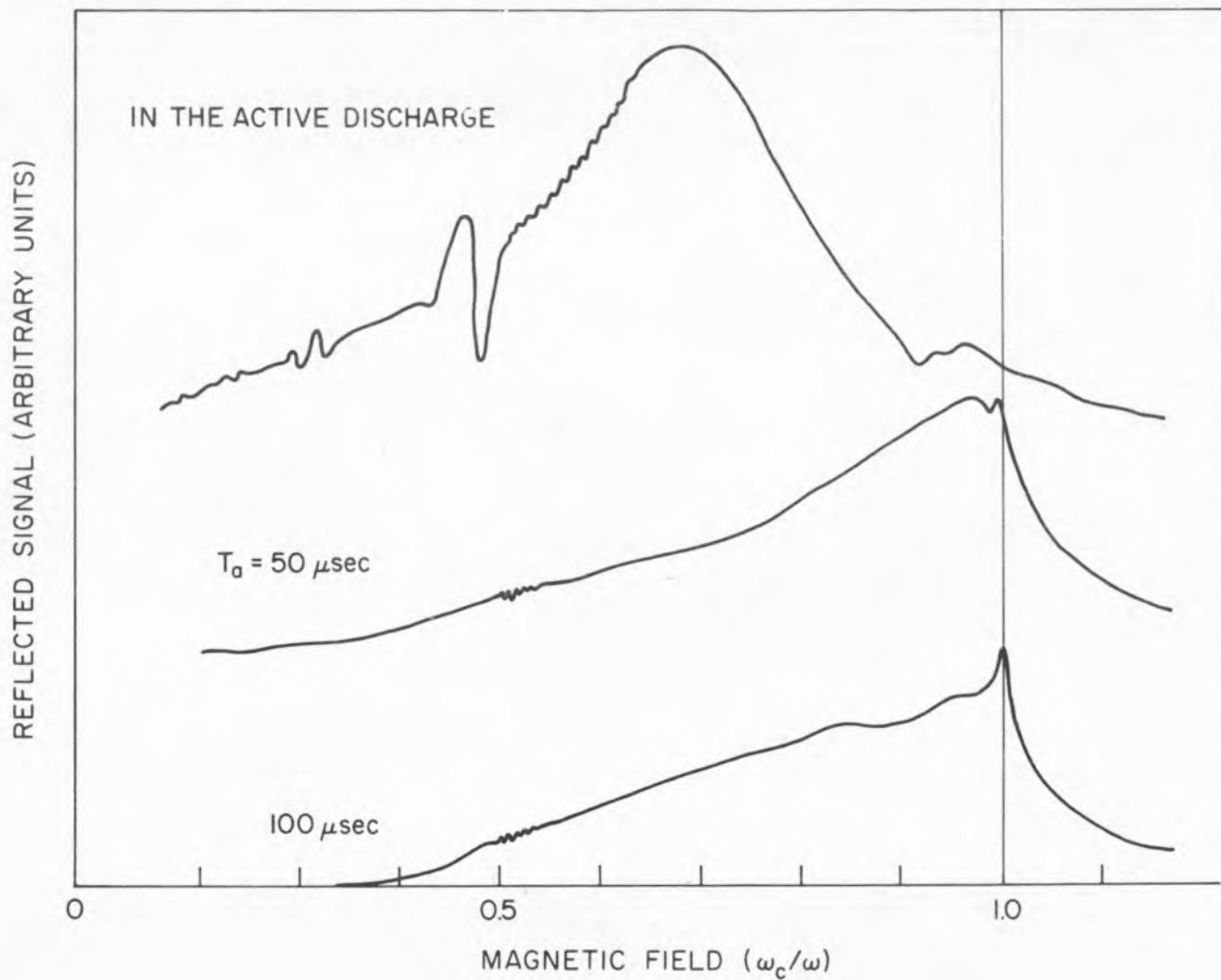
Fig. 3.4a "Continuous wave" (8 μsec pulse) scattering at early times in a neon afterglow at a pressure of 25 microns. Peak input power = -10 dbm, signal frequency = 2.76 GHz.
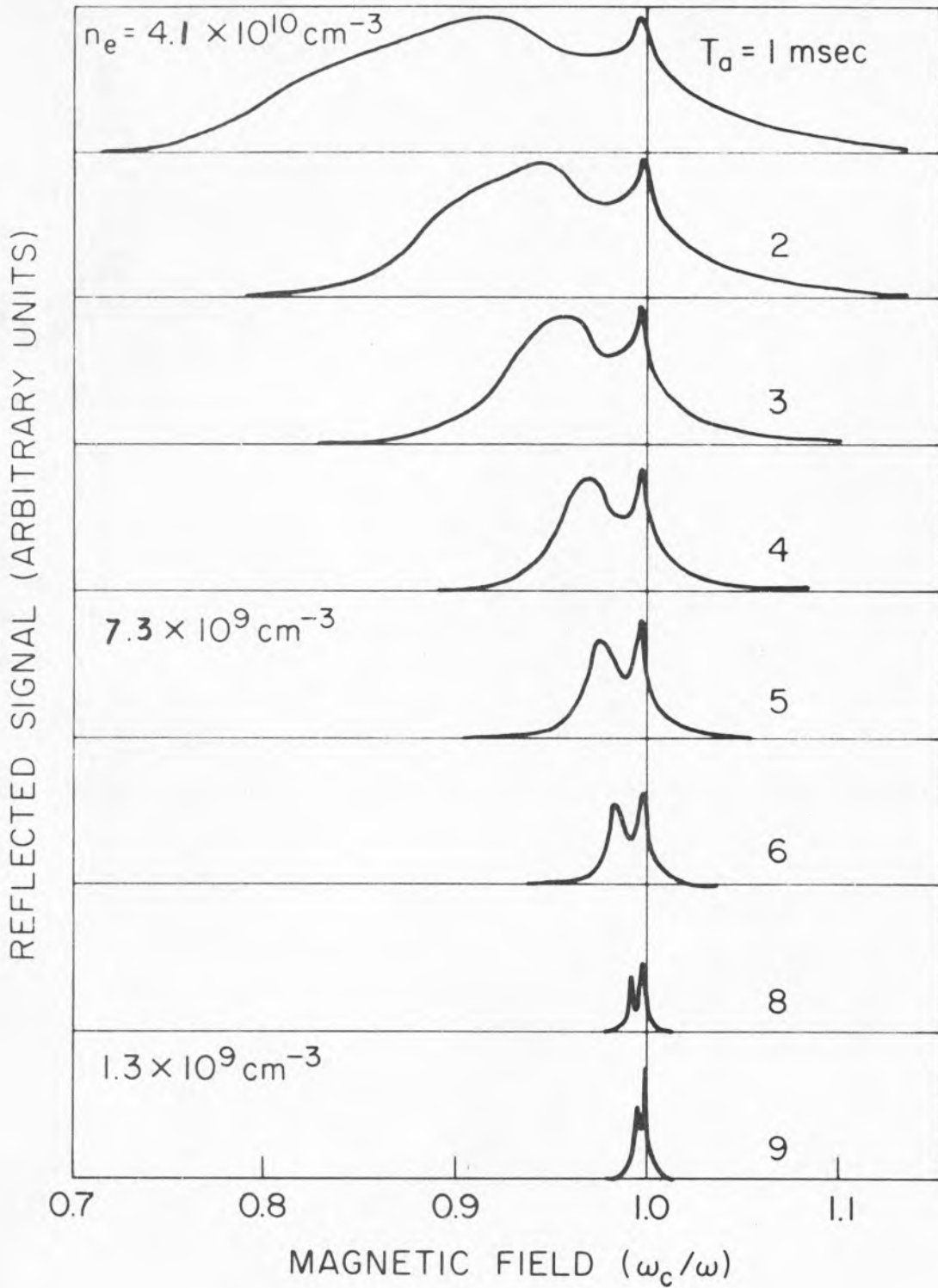
Fig. 3.4b. Late afterglow "continuous wave" (200 nsec pulse) scattering of an S-band signal (3.0 GHz, -30 dbm) from a 35 micron neon plasma.

It is attributed to the upper hybrid resonance of a cold, inhomogeneous plasma (27), excited by the so-called extraordinary wave. The onset of significant scattering at low values of (ω_c/ω) has proved to be a good measurement of the maximum electron density of nonuniform plasma columns (26). At the onset point on the (ω_c/ω) axis, the incident signal frequency is equal to the maximum upper hybrid frequency of the plasma, i.e.

$$\omega^2 = \omega_{Ho}^2 = \omega_c^2 + \omega_{po}^2 \qquad (3.6)$$

where $\omega_c/2\pi$ is the cyclotron frequency and $\omega_{po}/2\pi$ is the maximum local plasma frequency. This interpretation is the source of our density determination. For consistency and minimum graphical error, the maximum upper hybrid frequency was postulated to correspond to a scattering amplitude of 20% compared to the maximum observed. The results of such a density determination using the CW scattering of Fig. 3.4 are shown in Fig. 3.5. The data points show an expected exponential decay of the density. The points taken at the lowest densities show some dispersion because a precise determination of the value of (ω_c/ω) for the 20% scattering amplitude is more difficult under these conditions. The accuracy of such a density measurement is difficult to ascertain because of the lack of a quantitative theory. For instance, Blum observed changes in the shape of the upper hybrid resonance when different gases were studied. It is not known if they were due to corresponding changes in the density profile or to some other effects such as the influence of collision frequency. However, Lustig (26) using both the
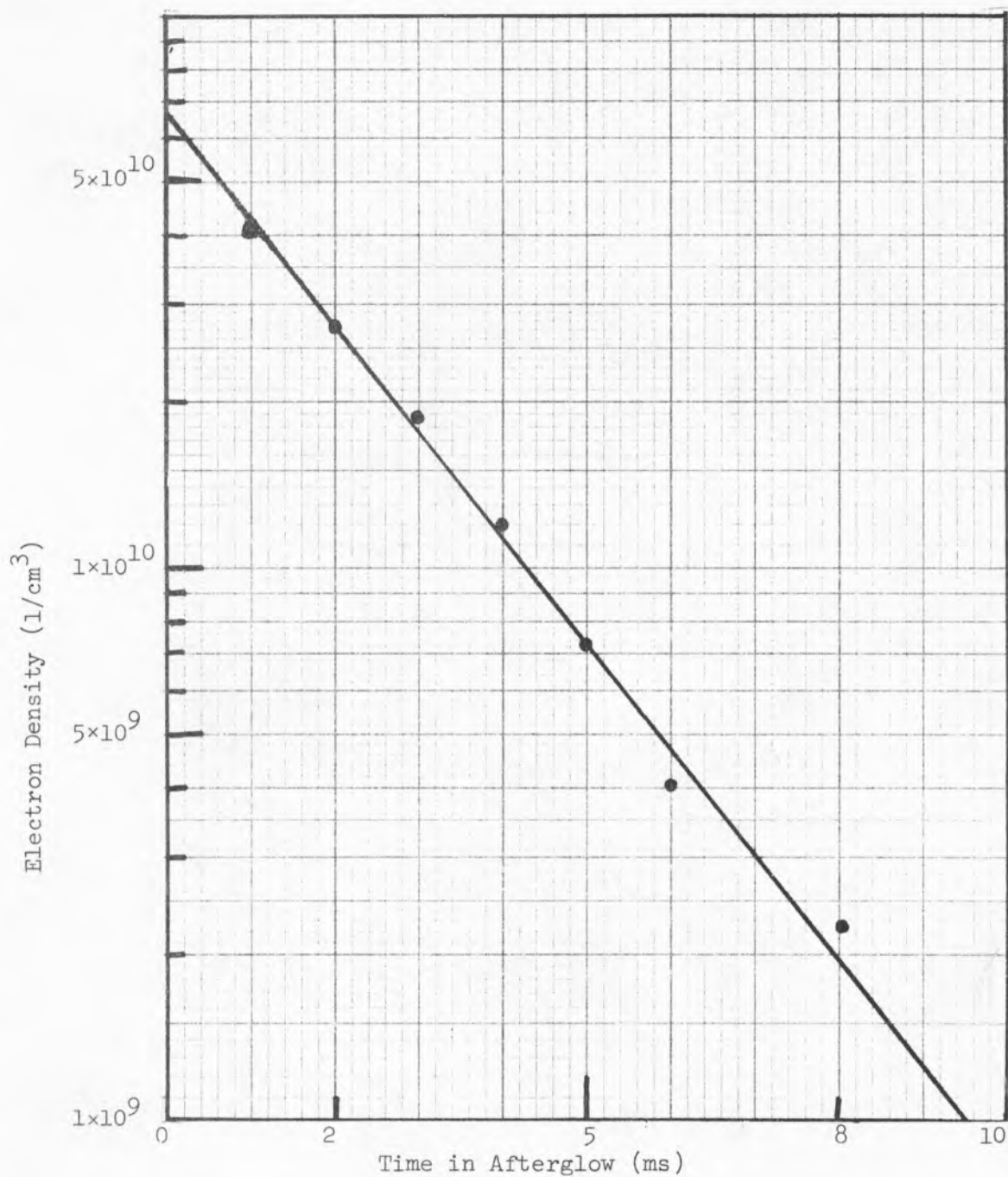
Fig. 3.5 Decay of the electron density in a 35 micron afterglow
neon plasma as measured by the scattering of an S-band
signal (3 GH_z, -30 dbm).

onset of absorption and a cavity measurement of the average electron
density of a d.c. discharge, showed that the two methods offer consis-
tent results. It can then be reasonably stated that our peak density
measurements are accurate to within 30% when the density is not too low.

Some other interesting features are seen during the discharge
and in the early afterglow. Superimposed on the wide "cold plasma upper
hybrid resonance" one can see broad resonances occurring close to the
harmonics of the cyclotron frequency during the active discharge. Their
existence is not well understood. Just above the second harmonic, one
can distinguish the familiar Buchsbaum-Hasegawa resonances due to
standing longitudinal waves in the column. They can be seen in the
afterglow until the maximum upper hybrid location is at $(\omega_c/\omega) = .5$.
These two types of feature are indications of the electron temperature.
It is apparent that their temperature is rapidly decaying. This was
confirmed by a measurement of the plasma radiation of argon and neon in
a similar neutral pressure range (1-30 microns of mercury) by Stenzel
(24) who showed that the electron temperature dropped to $\sim 2000^{\circ}K$ in
the first few hundred μs after the end of the active discharge. When
an echo experiment is done, usually at a time in the afterglow between
2 and 10 milliseconds, the electrons are probably very close to room
temperature. A word of caution must now be added as to the experimental
conditions under which the CW scattering curves should be obtained. It
was observed that a CW signal of only 100 mW could break down the plasma
when the signal frequency corresponds to the cyclotron frequency. It is
therefore important to keep the CW signal power much lower than -30 dbm

so as to not disturb the plasma by a too strong heating of the electrons. Rather than going to these extremely low powers, the scattering measurements were made using wide ($\sim$ 500 ns) relatively low power (-30 dbm) pulses. These wide pulse experiments yield results essentially identical with those of extremely low power CW experiments provided the spectral width of the pulses is narrow compared with the normal mode spectrum width of the plasma. Considering Fig. 3.1 the signal generator CW output was fed through path A to a PIN diode modulator (Hewlett-Packard type 8732B); 500 ns microwave pulses were then obtained. They were attenuated to a -30 dbm peak power before arriving in the waveguide. The plasma reflected pulses were monitored with the sampling oscilloscope. Only a few ns of the center section of the pulses were sampled using the manual scanning feature. This provided a signal for the Y axis of the recorder, while the magnetic field was automatically slowly varied, tracing curves such as those of Fig. 3.4ab.

3.2.2 Measurement of echo characteristics. The echo width and echo peak amplitude or power are the two most often measured quantities. The echo width can be roughly estimated on an oscilloscope such as the Tektronix 585A, but the rise time of that fast conventional oscilloscope is too slow to hope for a quantitative measurement. This can be done using a sampling oscilloscope such as the HP 185B. Fig. 3.6 is a polaroid picture of the echo displayed on that scope.

As far as echo peak power is concerned, it is often wanted as a function of (ω_c/ω). To measure it, the echo is displayed on the sampling scope and using the manual scanning one samples just the top of the
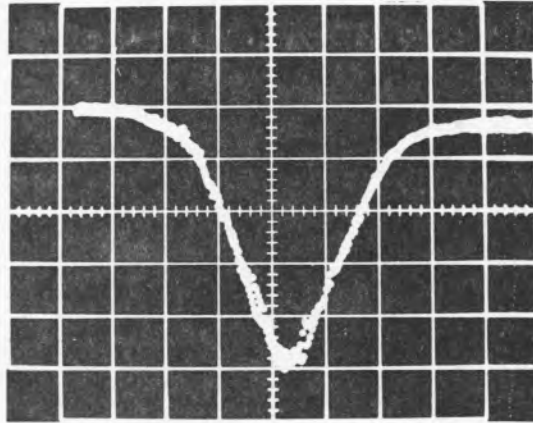
Fig. 3.6 Typical upper hybrid echo shape as displayed
by a sampling oscilloscope (Horizontal scale:
10 ns per division)

echo while sweeping (ω_c/ω). The scope's vertical output is plotted

against (ω_c/ω) on the X-Y recorder. Because the echo power after being

amplified is relatively weak and does not change by more than a factor

of ten over the range of (ω_c/ω) usually studied, the problems caused by

departures of the crystal detector from a square law response are not

believed to be serious. However, when the echo power is measured as a

function of input power and then varied over three or four orders of

magnitude, these difficulties could become critical. To avoid them one

displays the echo on the Tektronix 585A oscilloscope and chooses a con-

venient echo amplitude. Then the input power is, say, decreased,

through the input power precision attenuator, this causes a corresponding decrease in echo power. One compensates for it with the receiver precision attenuator until the same echo amplitude is displayed on the scope. The changes in the two attenuator readings give an exact relation between input and echo power, even if the chosen amplitude of the echo on the scope did not correspond to a true square law detection.

IV. EXPERIMENTAL RESULTS

4.1 Introduction

The echo was first observed in the narrow gap of the Varian elec-tromagnet V-4007-1, with a short plasma vessel (1.8 cm I.D., 7 cm long) and using X-band frequency, more or less reproducing the conditions of the experiment of Hill and Kaplan. Then the dependence of the echo's width on electron density as shown in Fig. 2.2 was found. Furthermore, the echo was seen to be peaking not quite at the cyclotron frequency but at $(\omega_c/\omega) \sim .98$. These rather fine measurements were possible because of the high homogeneity of the magnetic field. However, it was felt that these "plasma effects" could be better measured if the fre-quency of operation were lowered to make the ratio (ω_p/ω_c) greater. An experiment at a frequency of 3 GHz was planned. A change seemed also necessary in the magnetic field geometry for different reasons.   For instance, the CW scattering from the short tube showed some complicated structure near the cyclotron frequency. Tentatively explained as scat-tering from longitudinal standing waves superimposed on the broad "cold plasma" type of scattering, this structure made the measurement of den-sities more difficult. It was felt that these end effects could also make the understanding of the echo harder. So, a solenoidal magnet was built (whose characteristics were described in the previous chapter). A long tube was used (1 m long, 1.8 cm I.D.) for the discharge.   The first experiment in the new setup brought the discovery of an echo associated with the maximum upper hybrid frequency that we will call the "upper hybrid echo" (21). Section 4.2 will describe the different

characteristics of that upper hybrid echo and their changes when the
saturation phenomena (described theoretically in Section 2.3.2) set in,
and compares them with the calculations of Blum (20). For a while it
was thought that the peak in the echo spectrum at the maximum upper
hybrid frequency was the only one, as the cold plasma model predicts,
but more careful measurements showed that there is always an often
smaller secondary peak at a frequency less than 1% distant from the
cyclotron frequency. Some of the properties of that new "cyclotron
echo" will be discussed in Section 4.3.

4.2 The Upper Hybrid Echo

Before discussing detailed properties of the echo, it is useful to
recall the general experimental conditions. The measurements were per-
formed in neon and argon with a neutral gas pressure between 10 and 30
microns. The microwave pulses were typically 20 ns wide, separated by
a time interval τ between 80 ns and 400 ns. If the pulses were too
narrow, their spectral width was too large, not permitting a detailed
investigation of the echo spectrum; if they were too wide, the echo
power decreased rapidly because, probably, the narrow spectral width of
the pulses did not permit excitation of enough oscillators. The maximum
signal amplification available was about 55 db with a noise figure of
about 30 db. This permitted us to see the echo over a 20 db pulses'
peak power range down from the maximum of 5 watts. Over that range the
echo **always** displayed some saturation effects. Remembering what was
said about saturation phenomena in Section 2.3.2, all characteristics
of the echo were studied, keeping three of the four parameters entering

in $z\tau$ $((\omega_{po}/\omega)^2, (\omega_c/\omega), \tau, P)$ fixed, and changing the fourth.
Finally, the density over which the upper hybrid echo was seen, ranged
from 4×10^{10} to 5×10^8 electrons/cm^3. At the higher limit, the echo
became very weak; at the lower, the peak of the echo spectrum at the
maximum upper hybrid frequency became experimentally indistinguishable
from that at the cyclotron frequency.

4.2.1 Echo spectra. By definition an echo spectrum is the
curve which represents the variation of the echo's peak power when the
parameter (ω_c/ω) is varied. One is left then with three other variables:
P, τ, $(\omega_{po}/\omega)^2$. Two will be fixed and one will be used as a parameter
to see the variation of the echo spectra with it.

Echo spectra as a function of $(\omega_{po}/\omega)^2$. The most obvious choice
of parameters for a study of echo spectra is the density or $(\omega_{po}/\omega)^2$.
Figs. 4.1a and 4.1b show echo spectra in argon and neon, respectively.
Fig. 4.2 is a calculation of Blum with parameters chosen to match those
of the experiment in neon. As predicted by the theory, the location of
the echo spectra peak is very close to the maximum upper hybrid ω_{Ho},
shifted by as much as 25% in (ω_c/ω) units from the cyclotron frequency.
A slight difference (2% in the (ω_c/ω) domain) in the location of the
echo's spectra peak, if referred to the maximum upper hybrid frequency,
can be detected between neon and argon. It is not possible to interpret
this as a change of the echo properties, because a difference of 2% in
the location of the maximum upper hybrid frequency in the (ω_c/ω) domain
corresponds to a $\sim$ 10% difference in the electron density when the maxi-
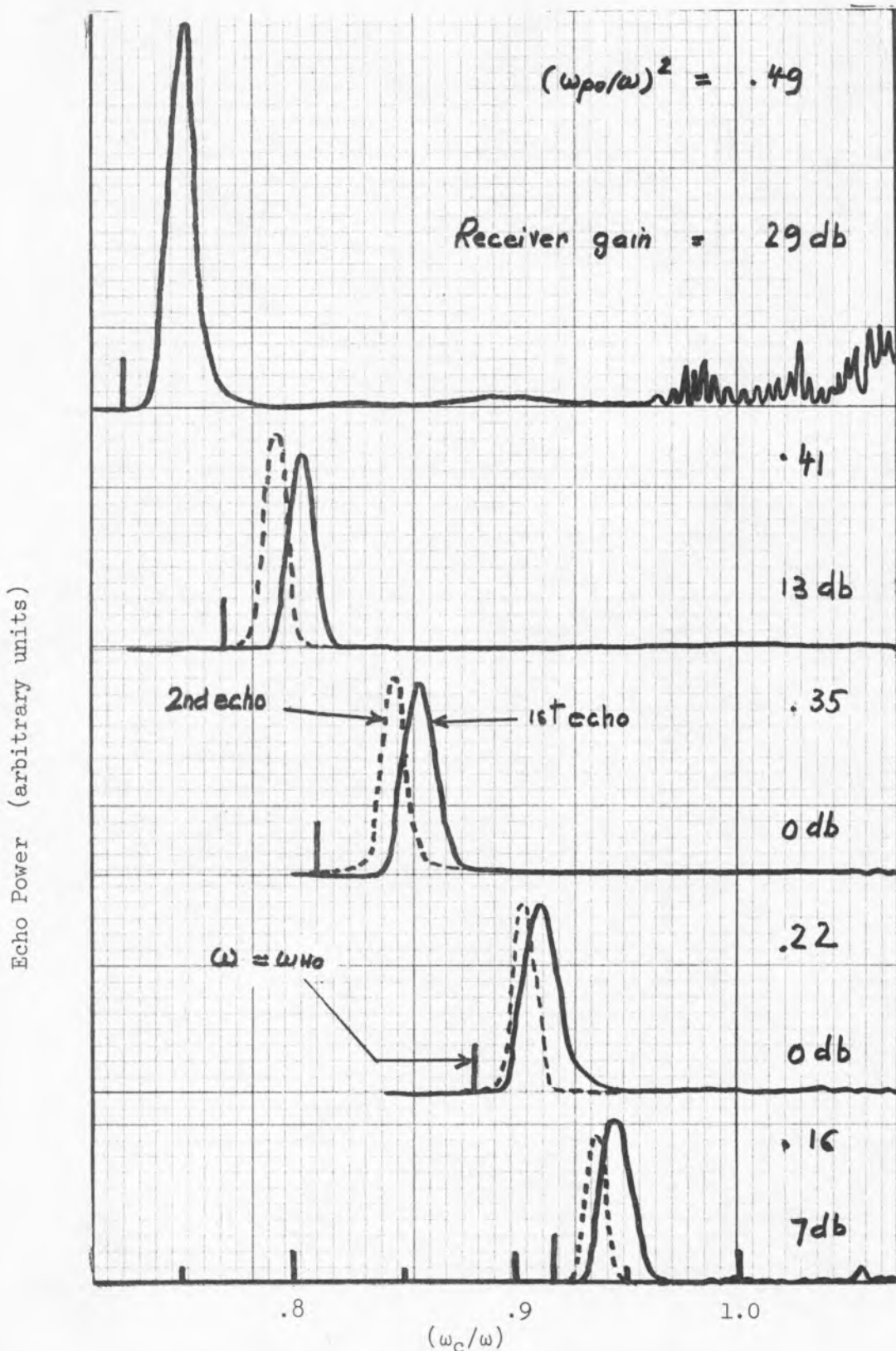mum upper hybrid is located at a typical $(\omega_c/\omega) = .8$. This 10%

Fig. 4.1a Echo spectra vs.$(\omega_{po}/\omega)^2$ with pressure = 20 microns argon, τ = 80 ns, input power = 5W, pulses' center freq = 3 GHz.
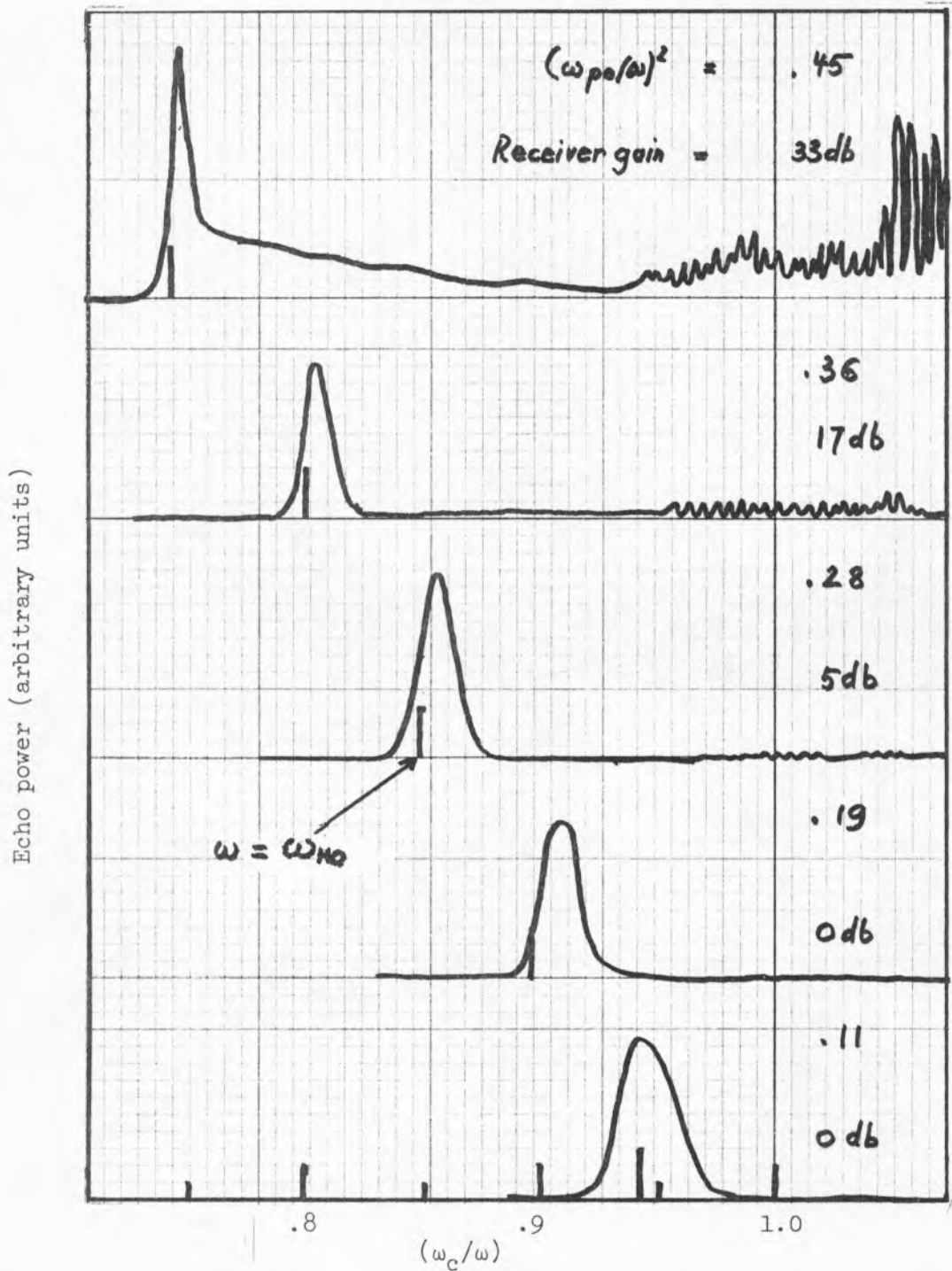
Fig. 4.1b Echo spectra vs. $(\omega_{po}/\omega)^2$ with pressure = 20 microns neon,
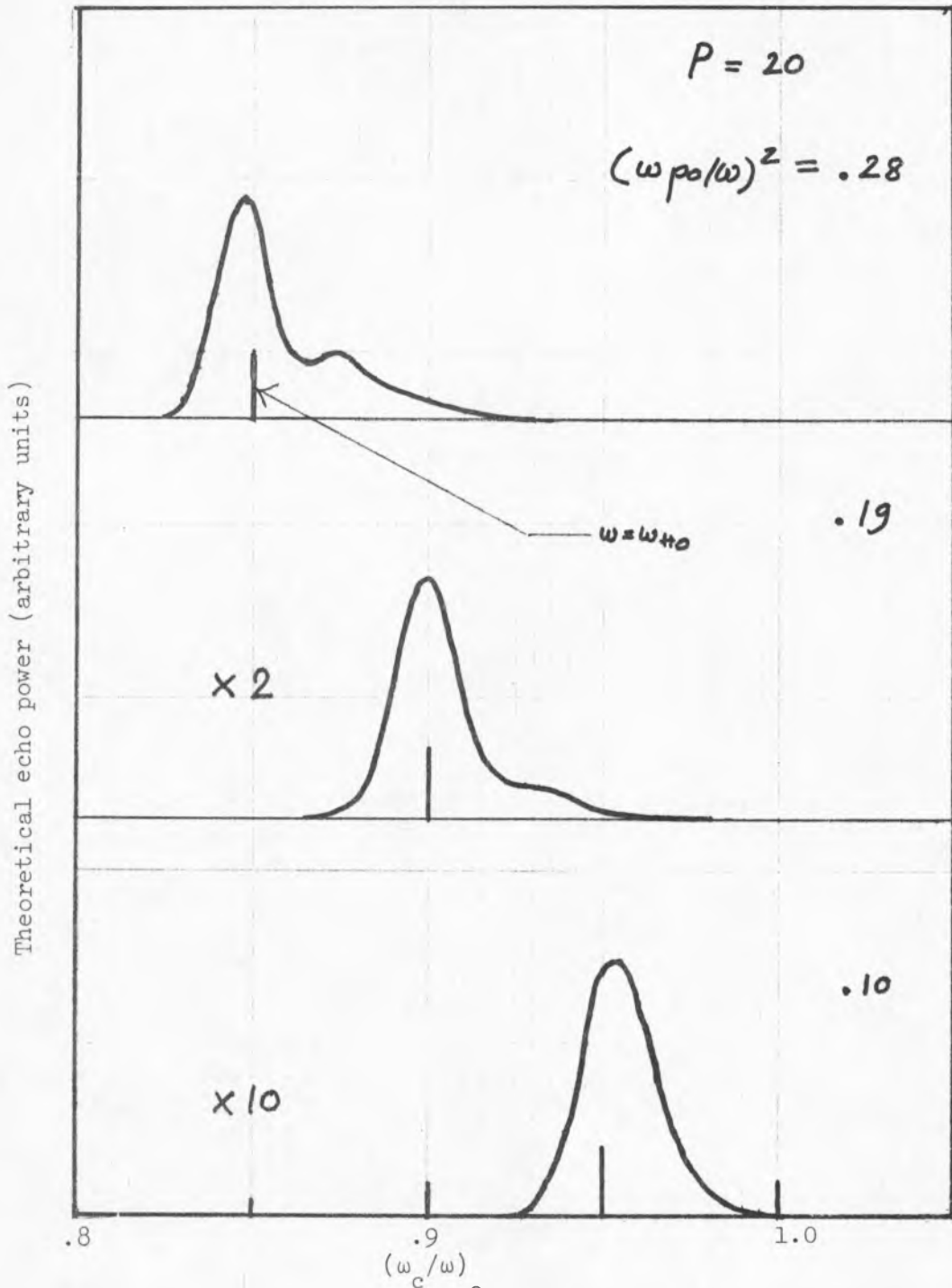τ = 80 ns, input power = 5W, pulses' center freq. = 3 GHz.

Fig. 4.2 Echo spectra vs. $(\omega_{po}/\omega)^2$, computed by Blum. (Level of
theoretical power given in arbitrary units.)

difference, in turn, is well within the minimum 30% expected inaccuracy of the experimental determination of the electron density (see Chapter III).

Another characteristic of the echo spectra is their width. The theory and experiment again agree qualitatively on magnitude and density dependence. As the density increases, the spectra get narrower. This is the first example of saturation effects; it shows that the density or $(\omega_{po}/\omega)^2$ does enter into the expression of $z\tau$. The presence of saturation is also clearly indicated by the spectra of the second echo in Fig. 4.1a. The second echo peaks at a slightly lower value of (ω_c/ω) than the first. The model's nonlinearity, it is recalled, is a growing function of (x/a) or here (ω_c/ω). Then, if the peak of the first echo spectrum is obtained when the threshold for saturation is reached for a certain value of (ω_c/ω), the same threshold for the second echo will be reached for a lower value of (ω_c/ω). This is so because τ has doubled from the first to the second echo. The second echo should then, as observed, peak at a lower value of (ω_c/ω) than the first. A slight complication arises from the fact that the saturation threshold condition for $J_2(z\tau)$ and $J_1(z\tau)$ involved in the definition of the first echo is not quite the same as that of $J_2(z\tau)$ and $J_3(z\tau)$ characterizing the second echo. However, one can show that the doubling of τ is the more important factor, leaving the simple picture previously exposed, qualitatively true. Finally, one can remark on the variation of the echo's peak power as a function of the density for both neon and argon. Starting with low density and going toward higher

density, the echo power first increases as predicted by the theory and then drops sharply in complete contradiction with it. More will be said later about that peculiar behavior with density of the echo power and probable reasons will be given for the disagreement with the theory. The signals near the cyclotron resonance will be discussed later in Section 4.3.

Echo spectra as a function of the pulses' peak power: P. Another way of studying the echo spectra is to keep $(\omega_{po}/\omega)^2$ and τ fixed and to vary the power. Figs. 4.3a and 4.3b show the results of such an experiment in argon and neon respectively. Fig. 4.4 is a calculation of Blum with parameter values close to those of the experiment. The evolution of the shape of the spectra in Figs. 4.3a, 4.3b and 4.4 is remarkably similar; it shows the characteristic narrowing when saturation becomes important. At the highest power level in argon and neon, the experimental curves display a small secondary peak in the spectrum which is also seen in Fig. 4.4. In fact, this establishes an absolute reference level of power for the theoretical computations. Furthermore, the echo spectra in the three figures are moving toward higher (ω_c/ω) as the power is decreased. This results also from saturation. Let us suppose that the echo peaks for a value of $z\tau$ close to the saturation threshold which is reached at a certain value of (ω_c/ω) for the chosen values of P, τ, $(\omega_{po}/\omega)^2$. If the power is decreased, the threshold can be reached only for a higher value of (ω_c/ω), thus causing the observed variation of the echo's spectra peak with power. There is a quantitative disagreement between Figs.4.3a, 4.3b and 4.4 as to the amount of
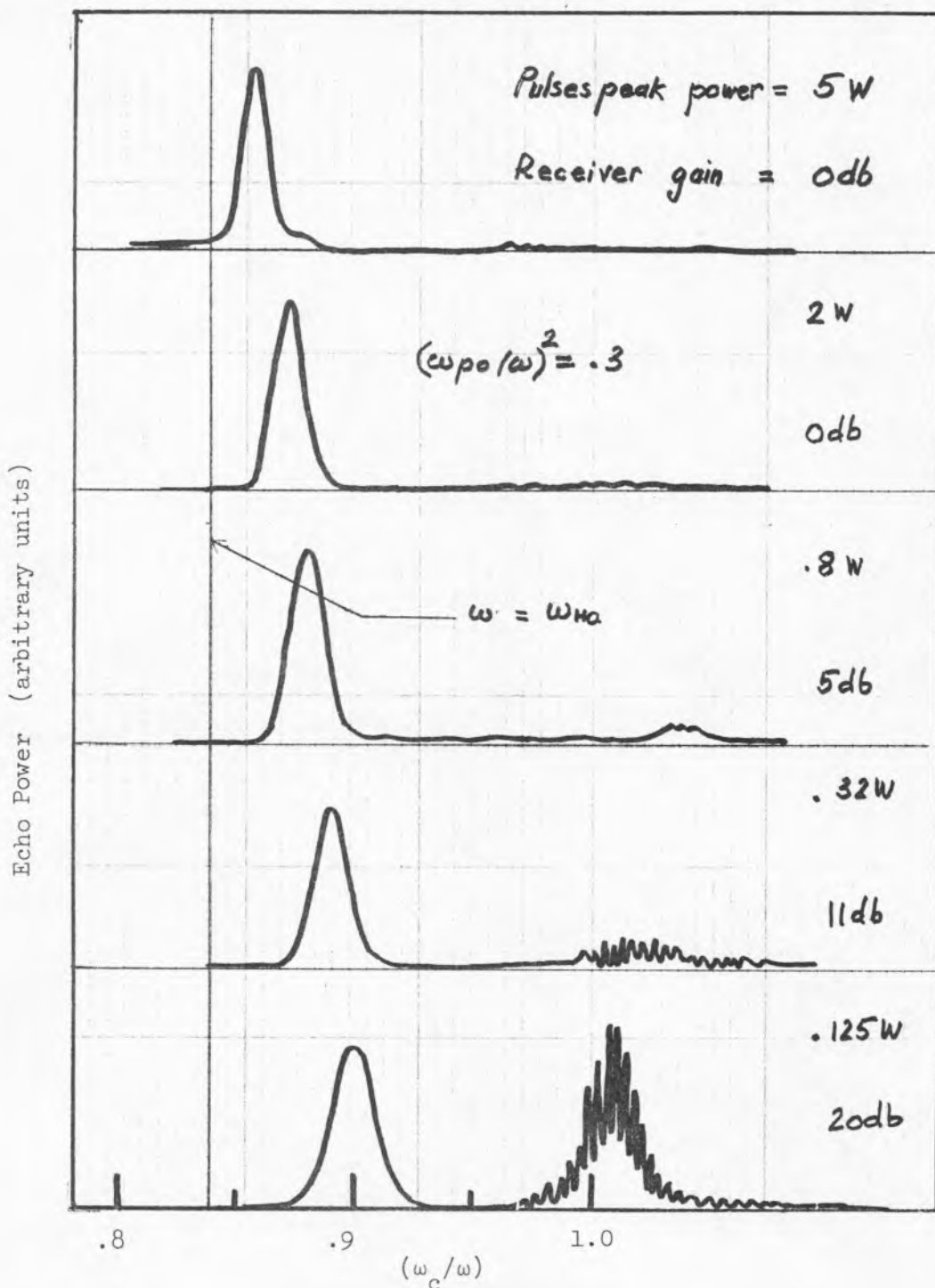
Echo Power (arbitrary units)

Pulses peak power = 5 W

Receiver gain = 0db

2 W

0db

$(\omega po /\omega)^2 = .3$

.8 W

$\omega = \omega_{H\alpha}$

5db

.32 W

11db

.125 W

20db

.8   .9   1.0
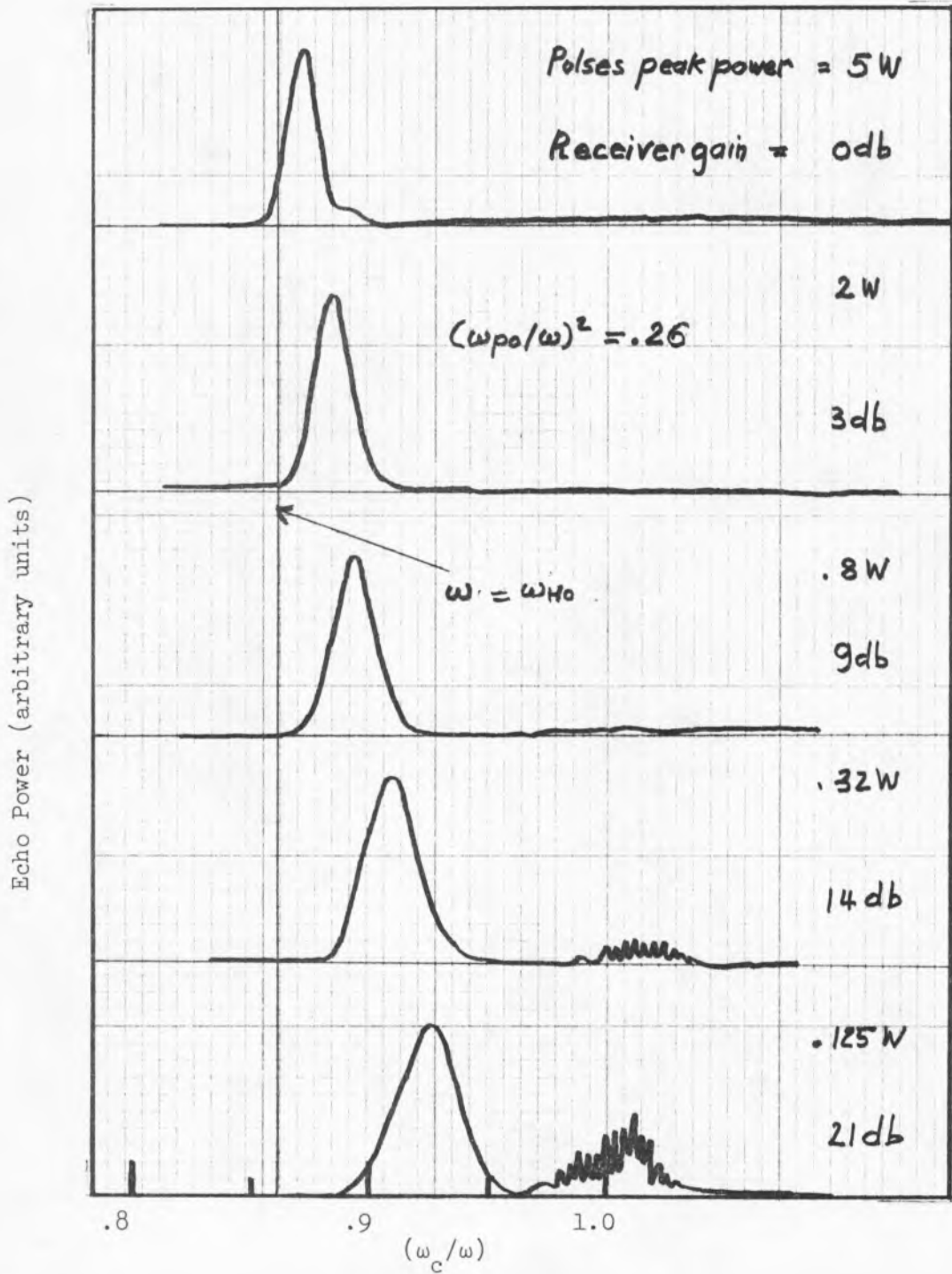
(ω_c/ω)

Fig. 4.3a   Echo spectra vs. input power with pressure = 20 microns
argon, τ = 80 ns, pulses' center frequency = 3 GHz.

Fig. 4.3b Echo spectra vs. input power with pressure = 20 microns
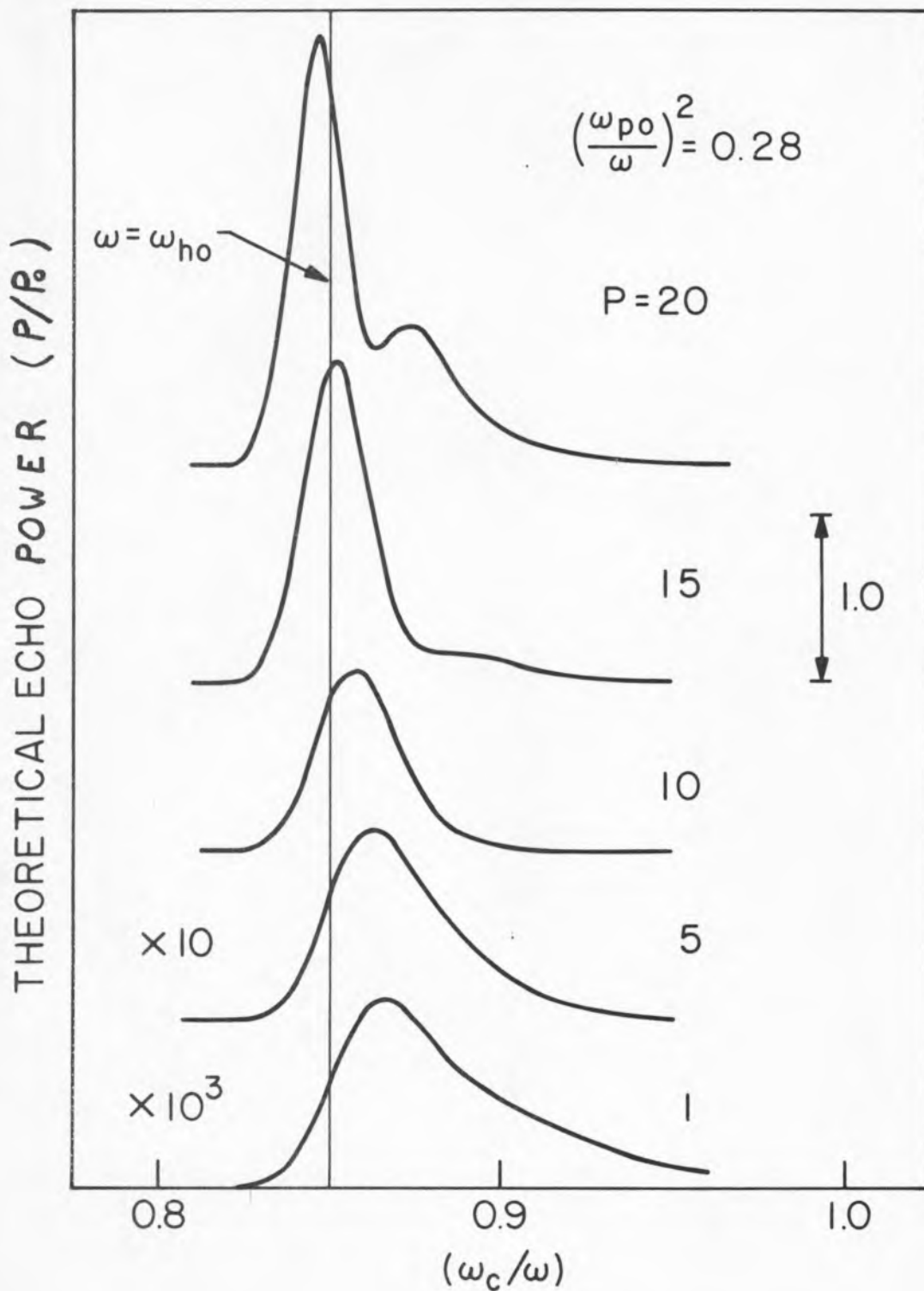neon, τ = 80 ns, pulses' center frequency = 3 GHz

Fig. 4.4 Echo spectra vs. input power, computed by Blum

the shift of the echo spectra for a certain power change. Also, experimentally, the spectra peak never stops to shift even with a 20 db decrease in power, indicating that saturation still exists at this low power level. In Fig. 4.4 decreasing the power level below its lowest value shown will not, on the other hand, produce any further shift of the echo spectra. There is then, theoretically, only a 12 db difference in power between the appearance of a secondary peak in the echo spectra and the disappearance of all saturation effects.

Echo spectra as a function of τ . Finally one can keep $(\omega_{po}/\omega)^2$ and P fixed and vary τ . Fig. 4.5 shows the spectra in argon obtained from such an experiment. Since the same relative change in P or τ will produce the same change of $z\tau$, Fig. 4.4 which described the theoretical dependence of echo spectra on power due to saturation effects will also be adequate to illustrate the saturation effects caused by τ . In Fig. 4.5 the typical narrowing and shift of the echo spectra are again observed. The measurement was performed in argon, but a similar behavior is seen in neon. This type of experiment is more difficult than the previous one, when the power was the variable parameter. The dynamic range of τ over which one can observe the echo is always less than 10 db. For very short τ (< 80 ns) one has diffi-culties with the pulse electronics. When τ is increased, the echo power decreases rapidly because of saturation, but also because of the phase randomization effect of electron collisions. This lack of dynamic range with τ will produce small echo spectra shifts and one has to be absolutely sure that none of the other "fixed" parameters changes. In
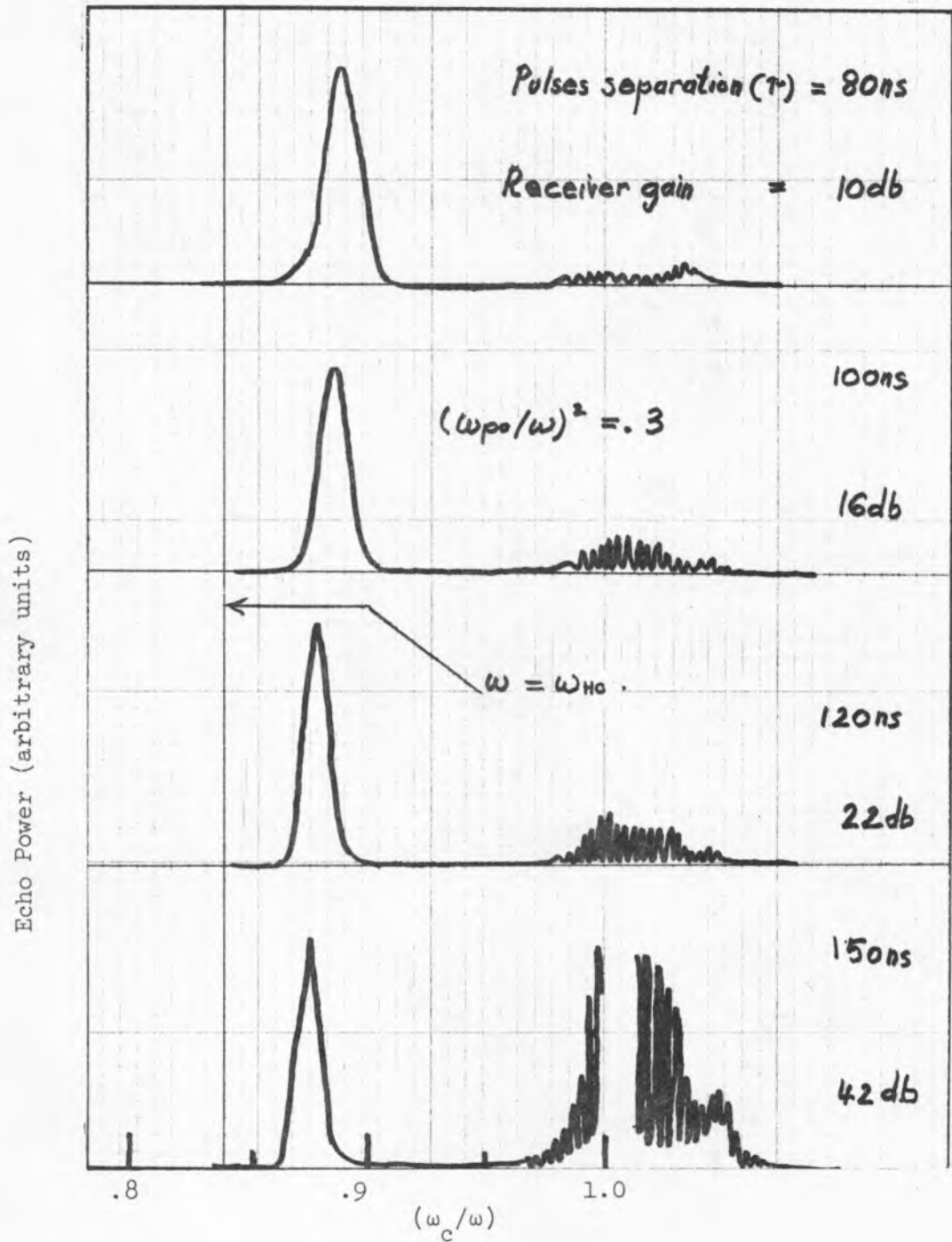
Fig. 4.5 Echo spectra vs. τ , with p = 20 microns argon,
input power = .5W, pulses' center freq. = 3 GHz

fact the only one causing problems is $(\omega_{po}/\omega)^2$ or the density.

Echo spectra peak shift as a function of P with $(\omega_{po}/\omega)^2$ as a parameter. The echo spectra give useful information. Unfortunately their measurement requires some care and therefore some time. As a consequence errors due to unavoidable density variations are introduced. In fact, if the influences of the three free parameters $(\omega_{po}/\omega)^2$, P, τ are to be compared in one experiment with a reasonable degree of accuracy, one has to find an easier and faster way to retrieve the needed information than through the echo spectra.

There is a solution to this dilemma. If only the shifts of the echo spectra are measured, they can be obtained in a very simple manner. The variation of the echo power as a function of the magnetic field is observed on a wide band oscilloscope. An optimum value of the magnetic field will be found corresponding to the echo's spectrum peak. The magnetic field value is noted and one can change the value of the parameter of interest. The whole process is simple and fast. Fig. 4.6 presents the results of such an experiment in argon. It was done in two phases; the echo spectra shifts were taken vs. power for a few different values of $(\omega_{po}/\omega)^2$ with τ fixed, and then, starting again with the power fixed, the shifts were measured as a function of τ for the values of $(\omega_{po}/\omega)^2$ taken in the first phase. The data were plotted as a function of $P\tau$ with $(\omega_{po}/\omega)^2$ as a parameter. The theoretical equivalence of P and τ in saturation phenomena is once more confirmed. Furthermore, considering Fig. 4.6 , the shifts seem to be logarithmic
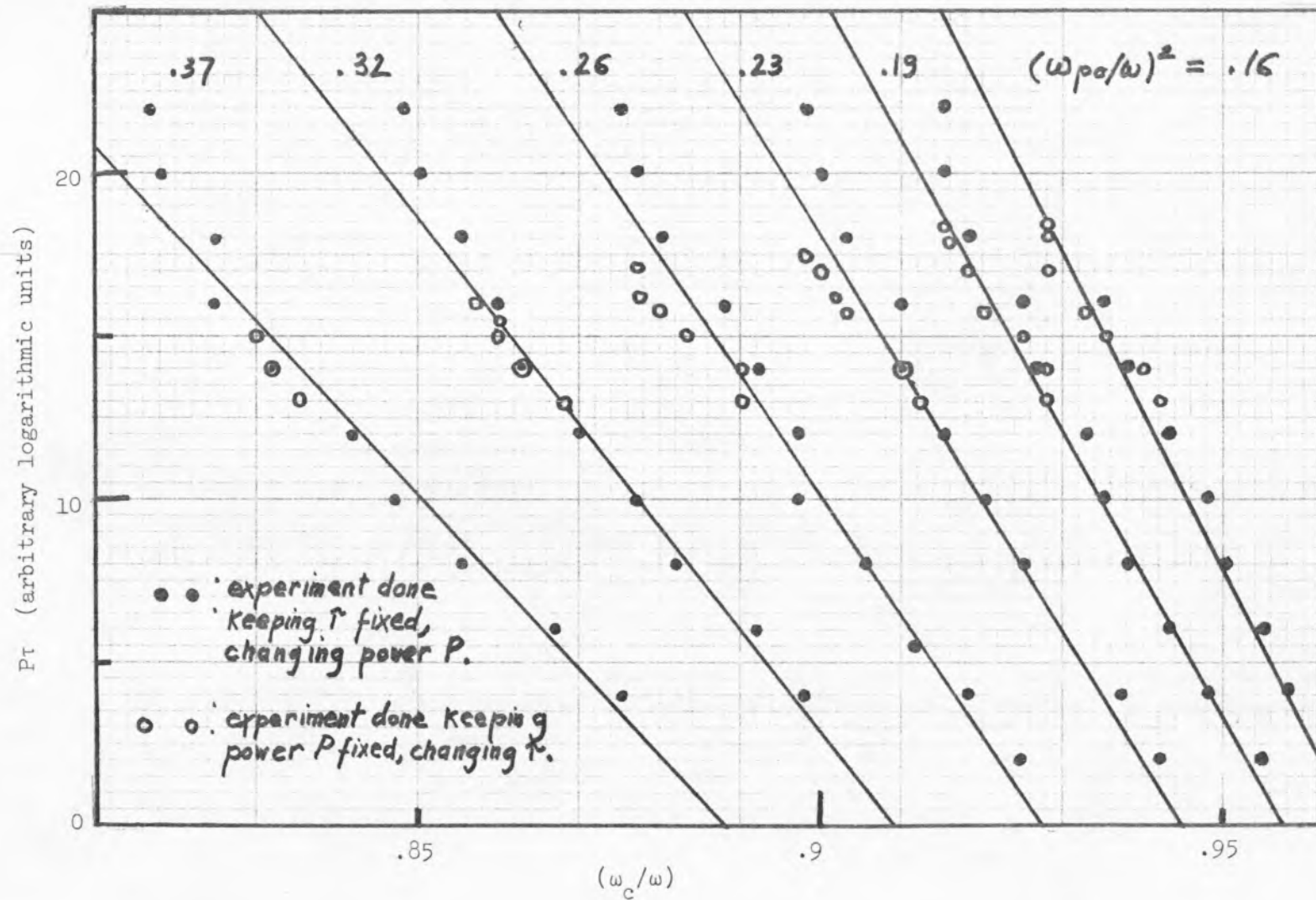
Fig. 4.6 Echo spectra peak shift vs. Pτ with $(\omega_{po}/\omega)^2$ as a parameter. Pressure = 20 microns argon, and pulses' center frequency = 3 GHz.
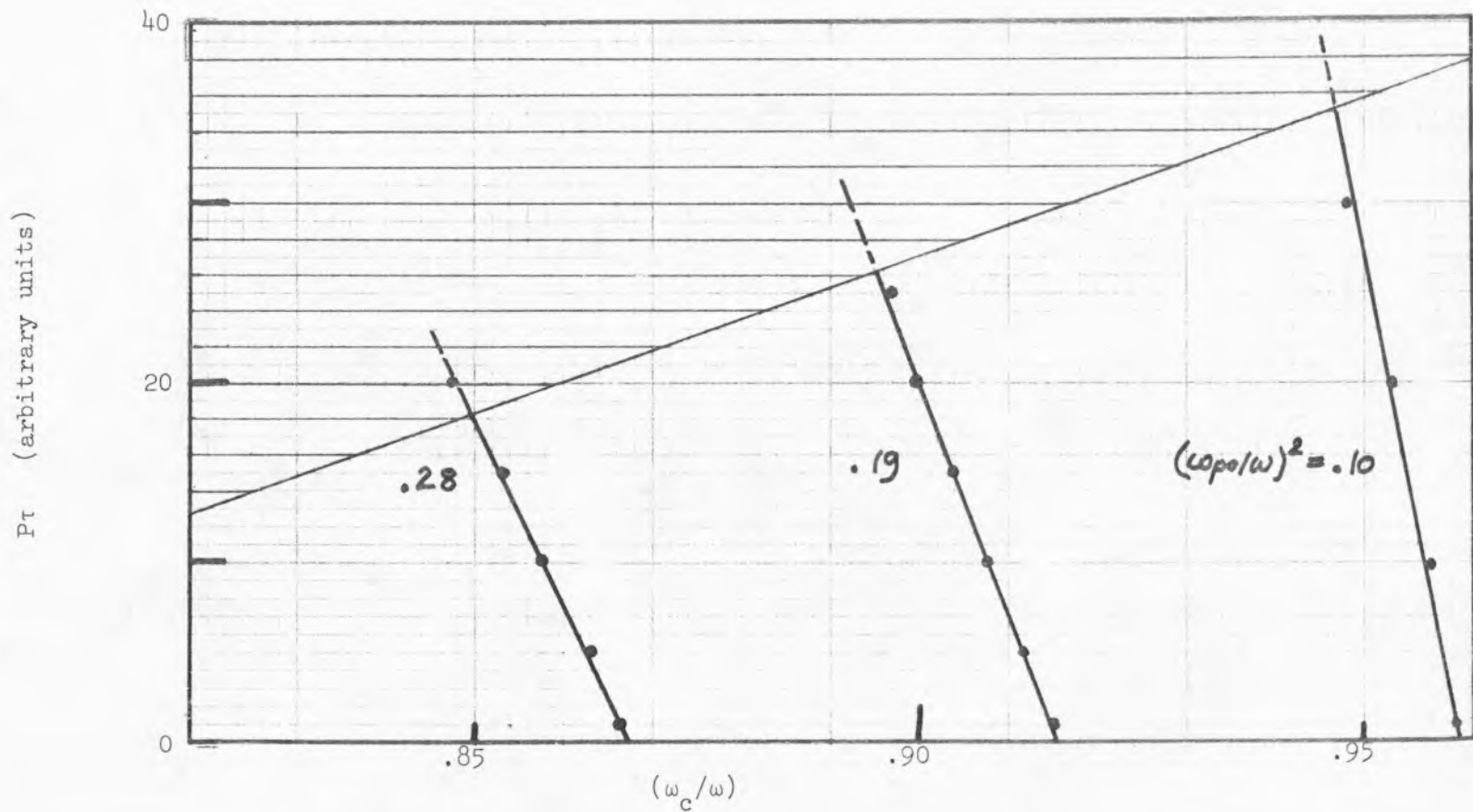
Fig. 4.7 Theoretical echo spectra peak shift vs. P$_T$ with $(\omega_{po}/\omega)^2$ as a parameter, after Blum. In the shaded area, the echo spectra are double peaked.

functions of $P\tau$ and the parameter $(\omega_{po}/\omega)^2$ adjusts the slope of the shift's dependence on $P\tau$ in the expected way. For a certain change of $P\tau$, the corresponding change in $z\tau$ will depend on the parameter $(\omega_{po}/\omega)^2$. If $(\omega_{po}/\omega)^2$ is large, a large change in $z\tau$ will occur, causing a large shift of the echo spectra peak. If $(\omega_{po}/\omega)^2$ is small a smaller increase in $z\tau$ will be observed causing a corresponding smaller shift in the echo spectra peak. Fig. 4.6 then represents a partial success of the cold plasma model, since we can explain qualitatively the intricate variations of the echo spectra peak shifts. When one looks for a quantitative comparison to Fig. 4.7 representing the corresponding theoretical shifts, the difficulties begin.

First, the theoretical echo spectra shifts are seen to be <u>linear</u> functions of $P\tau$ and not <u>logarithmic</u> functions as in the experiment. Second, over the range of power used, the experimental spectra peak shifts are too large. Third, above the thin line (shaded area) crossing the theoretical shifts of Fig. 4.7 is a region of strong saturation where the echo spectrum becomes double peaked, see for instance Fig. 4.4. The power necessary to reach that saturation level is theoretically decreasing as the peak density is increasing. Experimentally, such a behavior is only partially seen. Starting from a low density and using the maximum available power, the double peaking of the echo spectra at first cannot be seen as expected, and the density increasing barely appears (see Figs. 4.3a and 4.3b), only to disappear again. This is consistent with the reported variation of the echo spectra power as the parameter $(\omega_{po}/\omega)^2$ is changed. All indications are, then, that for a peak density high enough the microwave pulses do
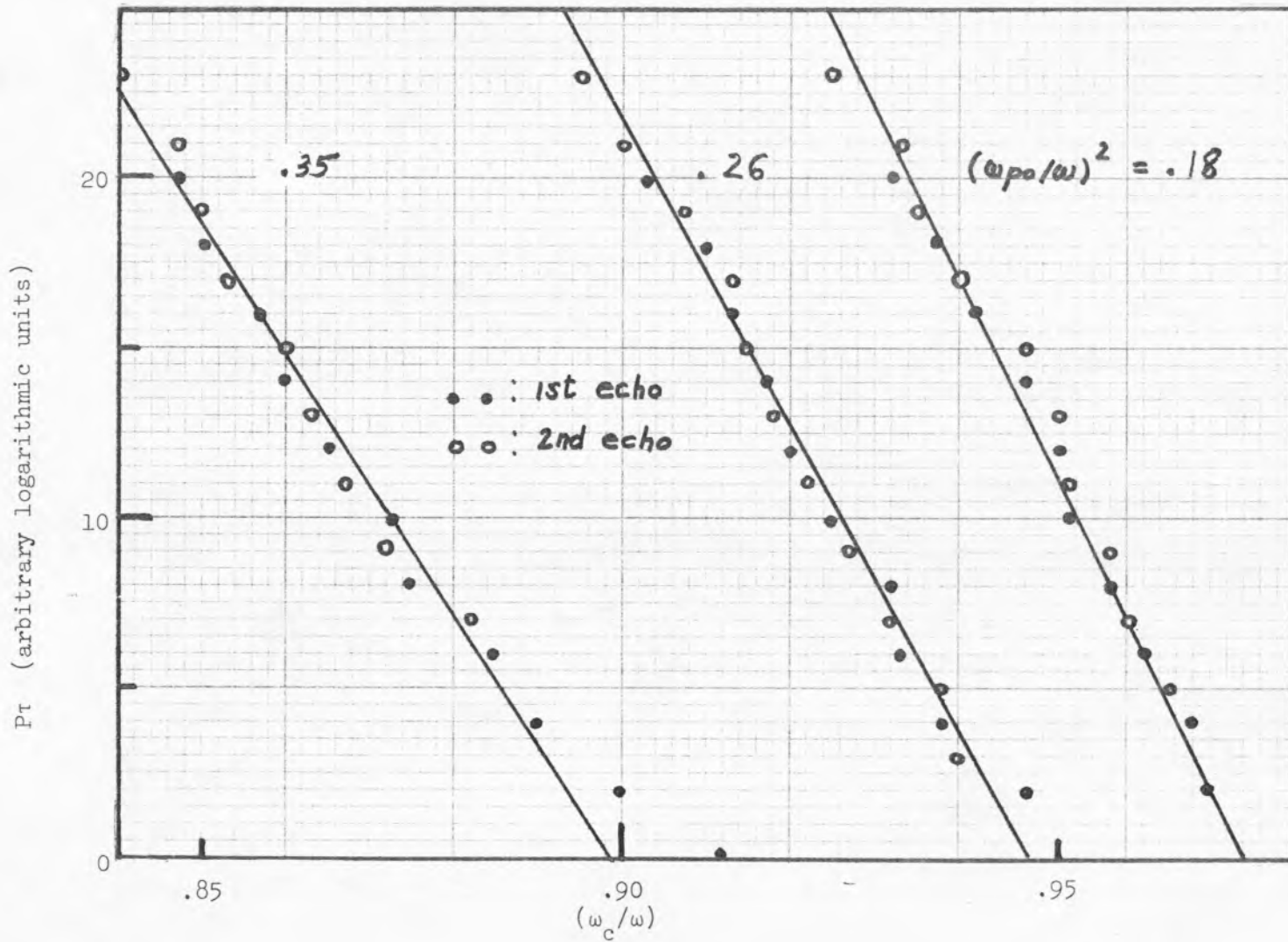
Fig. 4.8 Echo spectra peak shift vs. P_τ of first and second echo, with $\tau = 80$ ns, pressure = 20 microns argon, pulses' center frequency = 3 GHz.

not seem to couple effectively to the "oscillators". This puzzling
phenomenon, probably similar to the problem of coupling to upper hybrid
resonances in a Q machine (28), is studied in another experiment
described in Section 4.2.2.

Figure 4.8 represents the shifts of the first and second echo
spectra peaks as a function of $P\tau$. If one plots the first and second
echo shifts vs. P only, the second echo shifts lie on lines parallel
to those representing the first echo shifts such that a vertical trans-
lation of 3 db would make them coincide. When plotted vs. $P\tau$ this
translation is done since $\tau_{2nd\ echo} = 2\tau_{first\ echo}$. This measurement
is relatively easier and faster than that presented in Fig. 4.6, which
is probably why less dispersion in the data is seen in Fig. 4.8.

Echo spectra peak shift as a function of electron collisions.
The theory is collisionless, but in the experiment the collision fre-
quency of electrons with neutral or ions is an important parameter that
can be adjusted by changing the neutral gas pressure, the electron tem-
perature and the density. The electron neutral collision frequency
depends on the neutral gas pressure and on the electron temperature.
The Coulomb collision frequency depends on electron and ion densities
and temperatures. For some numbers on these quantities in the usual
experimental conditions, see Appendix B. Figure 4.9 represents echo
spectra peak shifts in neon as a function of $P\tau$ for a fixed density
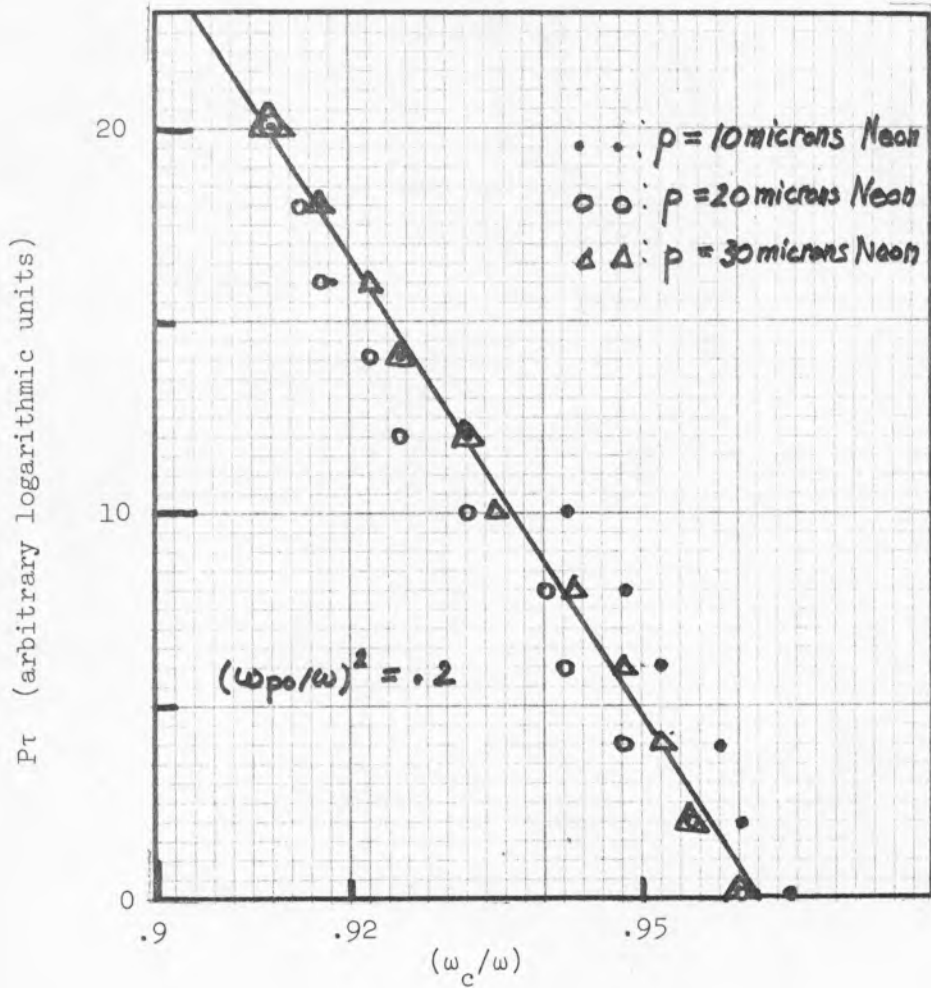and for three different neutral gas pressures.

Fig. 4.9 Echo spectra peak shift vs. Pτ for different neutral
pressures, τ = 80 ns, and pulses' center freq. = 3 GHz

In this figure the purpose of the measurement was, hopefully, to resolve an old controversy about which nonlinearities are more important in the echo formation. The previous experiment with echo spectra have confirmed the qualitative correctness of the cold plasma nonlinearity arising from the nonuniform density profile. The parameters (ω_c/ω), $(\omega_{po}/\omega)^2$, P, τ were seen to play qualitatively, the roles determined by their being part of $z\tau$. The question which arises is the eventual presence of factors in $z\tau$, not theoretically predicted, such as the energy-dependent electron neutral collision. From Section 2.2 one recalls that this nonlinearity enters as a factor $\partial\nu/\partial V^2$ in the argument of the Bessel functions of the echo amplitude factor in the independent particle theories (see Eq. 2.6). In neon the electron collision frequency can be closely approximated by

$$\nu = a(P) \, V^2 \tag{4.1}$$

where $a(P)$ is a factor depending linearly on the neutral gas pressure, so that

$$\frac{\partial\nu}{\partial V^2} = a(P) \tag{4.2}$$

Now this factor $a(P)$, if present in the experimental $z\tau$, should produce an effect on the spectra shifts when the neutral pressure is changed. One can show that it would merely translate them up or down along a line parallel to the vertical axis. The straightforward way to check this effect experimentally is the following. A neutral gas pressure and a certain density are chosen, an echo spectra shift vs.

Pτ is taken. Then the pressure is changed, a CW scattering is made
to determine to what time in the afterglow the previously chosen
density in the new situation corresponds. Once this is found, an echo
spectra shift measurement is taken at that time in the afterglow (Ta).
One might then check the existence of the predicted effect on the
spectra shifts, however, this process would take too long to hope for
any meaningful results for reasons previously explained (density fluc-
tuations). Instead, the following is done. A pressure and a density
are chosen. Then the value of (ω_c/ω) which corresponds to the largest
echo for the maximum available power is noted, and an echo spectra
shift measurement is made. The pressure is changed. Using again
maximum power and the same value of (ω_c/ω), one looks for the value of
Ta which gives the strongest echo. An echo spectra shift measurement
is obtained at that value of Ta. Now suppose that a term of the form
$\partial v/\partial V^2$ does enter in zτ . When the pressure increases zτ must
increase too. So if in the two phases of the experiment the echo peaks
at the same value of (ω_c/ω), it is because the density was changed to
compensate for the increase in zτ due to the pressure dependent
nonlinear term $\partial v/\partial V^2$. But as was seen in Figs. 4.6 and 4.8, the
"slope" of the echo spectra shifts vs. Pτ is a function of density.
So in Fig. 4.9 if a term $\partial v/\partial V^2$ has a strength comparable to the
parameters involved in the model's nonlinearity, a change in the
"slope" of the echo spectra shifts would be seen. It is not, so the
old dilemma seems to be solved in favor of the "energy-dependent gyro-
frequency" type of nonlinearity. Unfortunately, a qualification must

be added to the last statements. In the independent particles view, the electron-neutral or Coulomb collisions can be straightforwardly considered as a relaxation of the oscillators involved in the echo experiment. But what is the relaxation of the oscillators in the collective effects model? It is certainly related to the electron-neutral or Coulomb collsions too, but it is not clear how. This raises some doubts as to the conclusions reached from the results presented in Fig. 4.9.

4.2.2 Echo Power Law

The echo spectra gave some insight into the upper hybrid echo properties and in particular how saturation phenomena can affect it. Another type of measurement which could confirm those results was indicated in Section 2.3.2. The idea was to measure the echo power as a function of the exciting pulses peak power or input power P for different areas of the slab. It was predicted that near the center of the slab, corresponding to the maximum upper hybrid frequency in the frequency domain, saturation phenomena would appear for a higher input power than near the edge of the slab, corresponding to the cyclotron frequency. Fig. 4.10 explains how these measurements are taken. One recognizes echo spectra obtained at a fixed density with the input power as a parameter. The thin lines show for what value of (ω_c/ω) the relation between the echo power and input power is studied. Figs. 4.11a, 4.11b show typical results of such experiments in argon and neon respectively. Fig. 4.12 shows the corresponding calculations of Blum. The maximum upper hybrid for Fig. 4.11a is located at (ω_c/ω) = .89; for
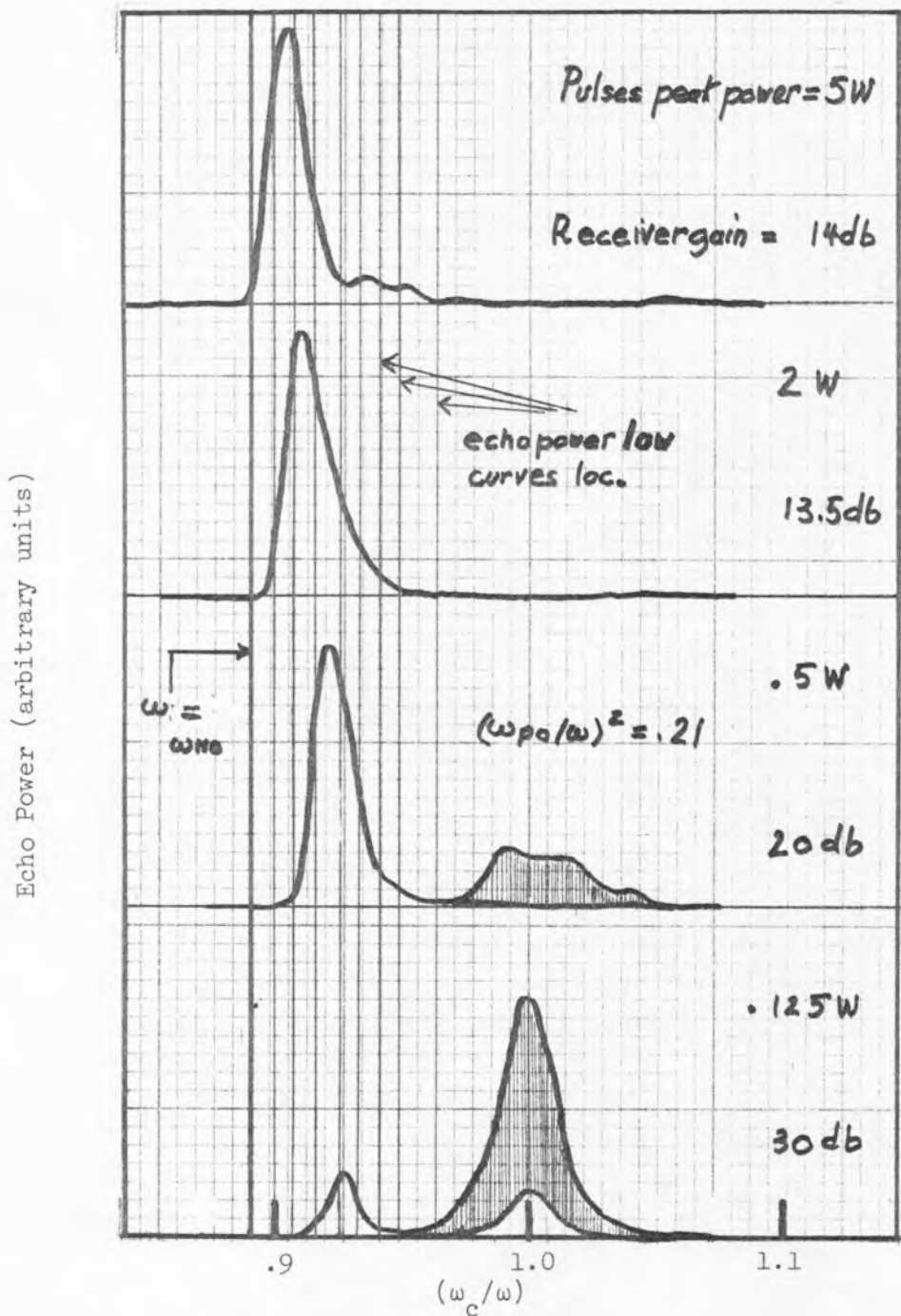
Fig. 4.10 Echo spectra vs. input power, to show how echo power
law curves are measured. τ = 140 ns,
pressure = 18 microns argon, and
pulses' center frequency = 3 GHz.

Fig. 4.11b ω_{Ho} is located at $(\omega_c/\omega) = .855$; and for Fig. 4.12 at

$(\omega_c/\omega) = .90$. In the beginning of Section 2.3.2 the behavior of the

echo power as a function of input power in the low input power limit

was described. One recalls that the echo power in that limit is pro-

portional to the cube of the input power. Since the data in Figs.

4.11a,b and 4.12 are plotted on log-log scales, the low power regime

should correspond to straight lines with a slope of 3. As can be

guessed from Fig. 2.6a,b when the saturation begins, the echo power

should depart from a cubic law, stop growing, and even decrease with

input power. These behaviors are very well seen in Figs. 4.11a,b. When

an "echo power law" curve is taken at a value of (ω_c/ω) close to the

location of ω_{Ho} , it looks almost like a straight line, barely bending

for the maximum available power and displaying very little saturation.

However, when a higher value of (ω_c/ω) is chosen, the echo reaches a

maximum for a certain input power, then decreases; the echo is saturated.

If the qualitative behavior of the echo power law curves is

understood, a quantitative study gives rise to some problems. One is

associated with the previously noted quantitative disagreement in the

echo spectra shift's magnitude. Here, comparing Figs. 4.12 and 4.11a,b,

the decrease of input power necessary to just reach saturation when a

certain increase of (ω_c/ω) is made, is larger than expected. With the

echo spectra, the shift for a given change of power was too large. The

information given by the two different experiments permit a guess as to

what could be a reason for the noted quantitative disagreement. The

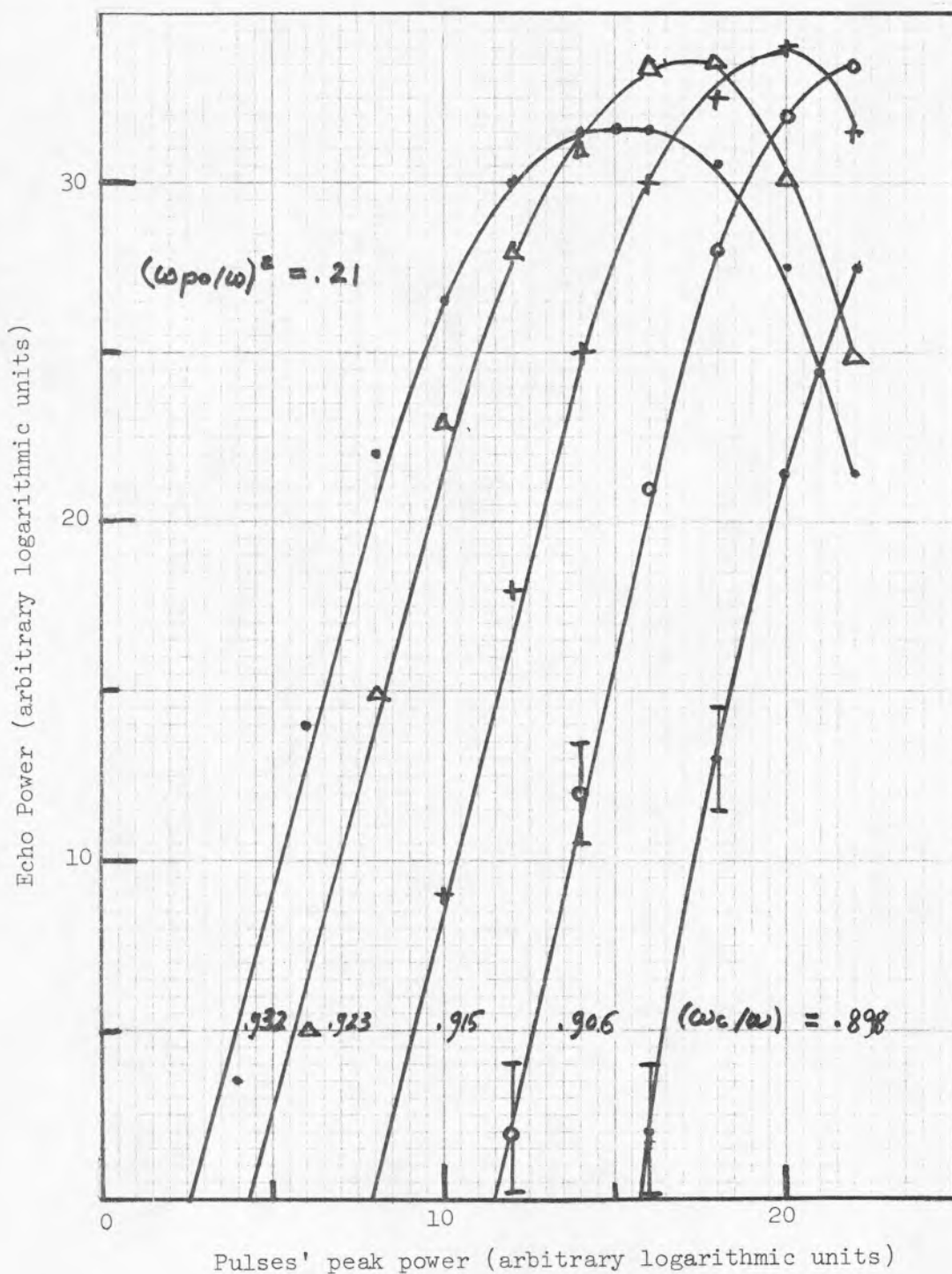nonlinearity as displayed by the experiments is a stronger function of

Fig. 4.11a "Echo power law curves" with (ω_c/ω) as a parameter.
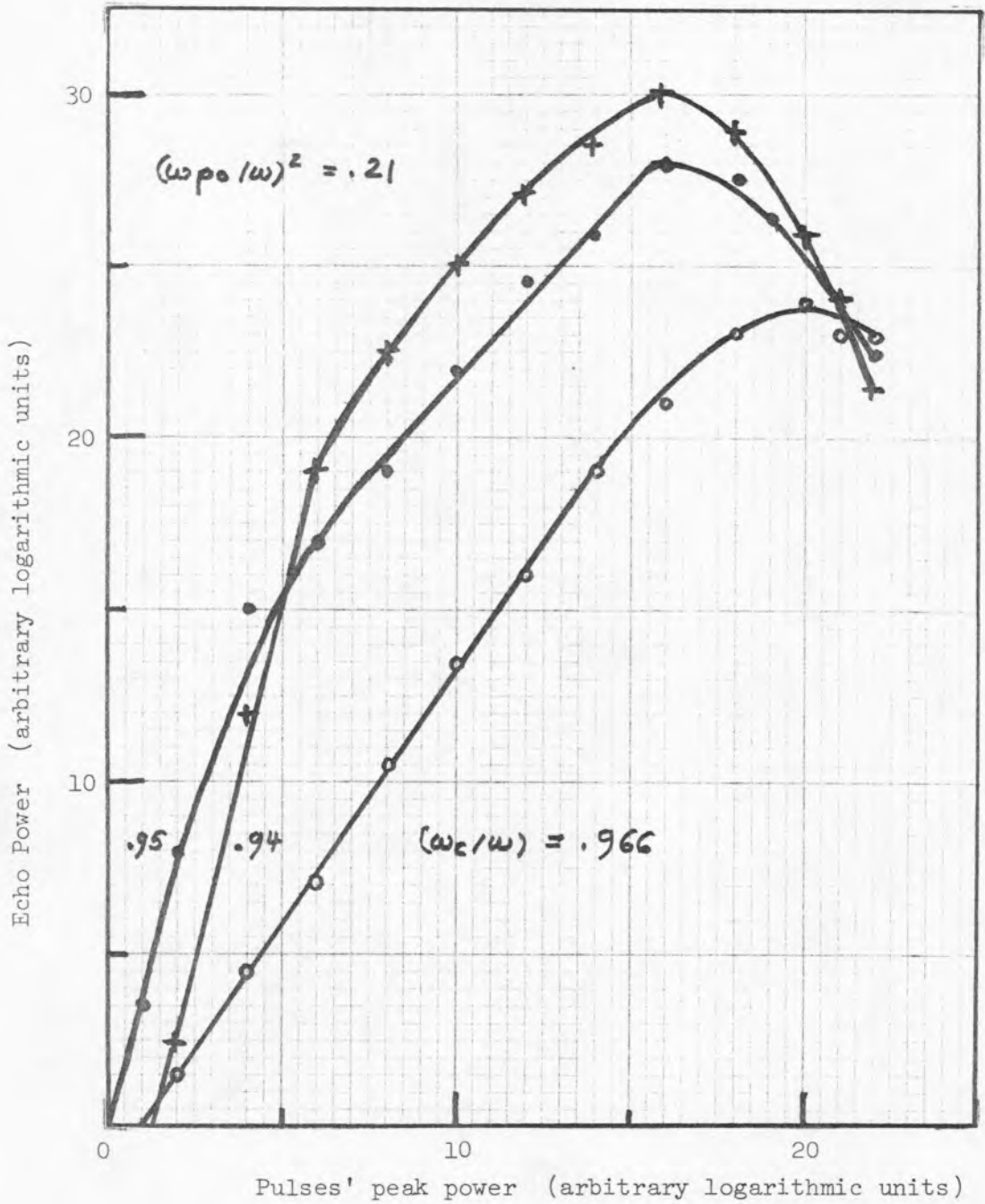τ = 140 ns, pressure = 18 microns argon,
pulses' center frequency = 3 GHz.

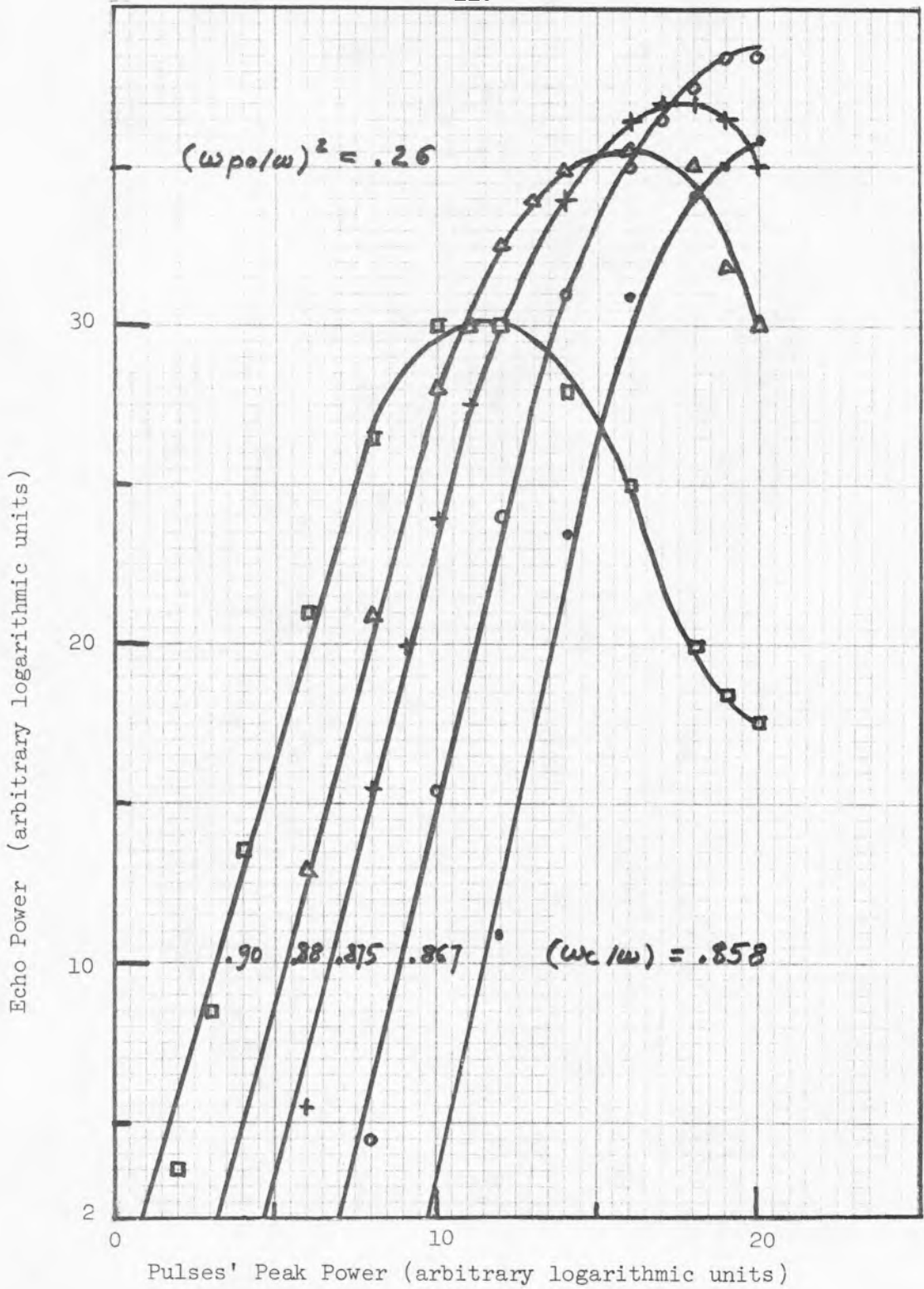Fig. 4.11a (continued) "Echo power law curves" with (ω_c/ω) as a parameter.

Fig. 4.11b "Echo power law curves" with (ω_c/ω) as a parameter,
τ = 80 ns, pressure = 20 microns neon, and
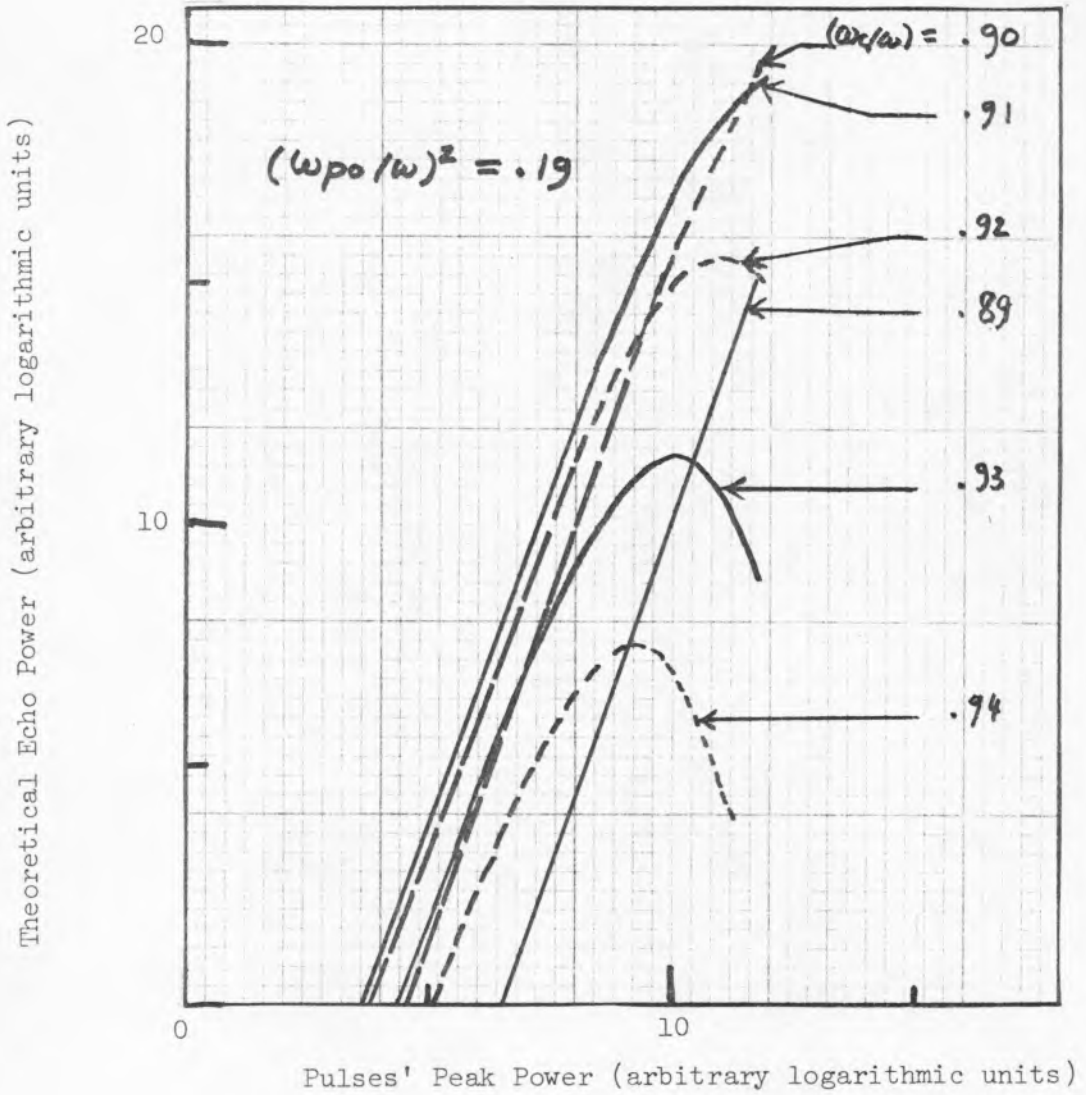pulses' center frequency = 3 GHz.

Fig. 4.12 Theoretical "echo power law curves" with (ω_c/ω) as a parameter, after Blum.

(ω_c/ω) than predicted. Translated in the point of view of the slab, that means that a density profile with a stronger dependence over (x/a) than the chosen $(x/a)^4$ is needed. There is, then, a certain temptation to obtain the best possible agreement with the experiment by modifying the density profile of the slab. However, in our opinion, to expect a quantitative agreement from such a simple model is asking too much. And some of the experimental results, for example the peak of the echo spectra at the cyclotron frequency, will not be explained whatever the model's density profile is. A new theory will have to be found to explain quantitatively all the experimental results. But at least the Blum and Gould model has qualitatively explained many aspects of the experiment not at all understood with the independent particle theories. Another quantitative discrepancy is observed in the low power region. A cubic echo power law is expected (Fig. 4.12). But Fig. 4.11a shows for large values of (ω_c/ω) a very different and complicated behavior. When (ω_c/ω) is $\leq$ .932 the experimental data form parallel lines, quali- tatively reproducing the general aspect of Fig. 4.12. However, they represent a quadratic echo power law rather than a cubic one. An average over 12 curves in neon and argon (with no noticeable difference between the two gases) concludes that if

$$P_{echo} = (P_{input})^{\alpha} \qquad (4.3)$$

then

$$\alpha = 3.92 \pm .6 \qquad (4.4)$$

A possible reason for the disagreement is the effect of Coulomb colli- sions. In Fig. 4.11b, for instance, at the lowest input powers, the

data points indicate that the echo decreases even faster than the lines
representing an approximately fourth power dependence. Supposing
that the electrons acquire an energy of 3eV with the maximum power
available, and using the electron density of 2.2×10^{10} corresponding
to Fig. 4.11b, at full power, the Coulomb collision frequency is of the
order of 3×10^5c/s. When the power is reduced by 10 db it becomes
$\sim 4 \times 10^6$c/s, and for a 20 db power attenuation it is $\sim 6 \times 10^7$c/s.
The last number means that on the average an electron experiences a
collision each 17 ns, or since $\tau = 80$ ns, about 9 collisions between
the first pulse and the time of the echo. The functional relation
between the echo power and the input power could then be drastically
affected by the Coulomb collisions at these lower powers.* The numbers
given seem impressive, but as was pointed out before, should only give
an order of magnitude feeling for the importance of Coulomb collisions,
since it is probably improper to assume that the relaxation of collec-
tive oscillations is given just by the electron-neutral or electron-ion
collision, whichever dominates. Furthermore, the energy acquired by
the electrons from the pulse is difficult to estimate (29). An
experiment similar to that reported by Fig. 4.11b was tried at a lower

---

*The corresponding electron-neutral collisions for 20 microns of neon
are at full power $\nu_{en} = 2 \times 10^7$c/s, with an attenuation of 10 db in
power: $\nu_{en} = 1.6 \times 10^6$c/s, for an attenuation of 20 db, no data are
available at that low electron temperature. We will suppose it is at
least as small as the value given for an attenuation of 10 db so the
electron-neutral collision will not affect the low power regime of the
echo.

density: $(\omega_{po}/\omega)^2$ was $\sim.18$. The coefficient α defined in equation 4.3 was:

$$\alpha = 3.55 \pm .2 \qquad \text{for } (\omega_{po}/\omega)^2 = .18$$

compared to:

$$\alpha = 4.02 \pm .5 \qquad \text{for } (\omega_{po}/\omega)^2 = .26$$

as obtained from Fig. 4.11b.

The possibility of Coulomb collisions playing a role is therefore reinforced by this steepening of the echo power law with electron density since their frequency is a growing function of that quantity.

Echo power laws for the first and second echo. The same type of experiment was made to compare the behavior of the first and second echo (see Fig. 4.13). As one expects, the saturation is reached for a lower power for the second echo than for the first, since $\tau_{\text{second echo}} = 2\tau_{\text{first echo}}$. Another interest in the simultaneous study of the two echoes is to see if they have the proper power law. The results of the 12 measurements of the first echo already discussed and 10 for the second echo for neon and argon are shown in the following table.

Coefficient α of:	Theory	Experiment
First Echo	3.0	$3.92 \pm .6$
Second Echo	5.0	$4.12 \pm .8$

The discrepancy between the theoretical and experimental value of the coefficient α of the second echo is not understood.
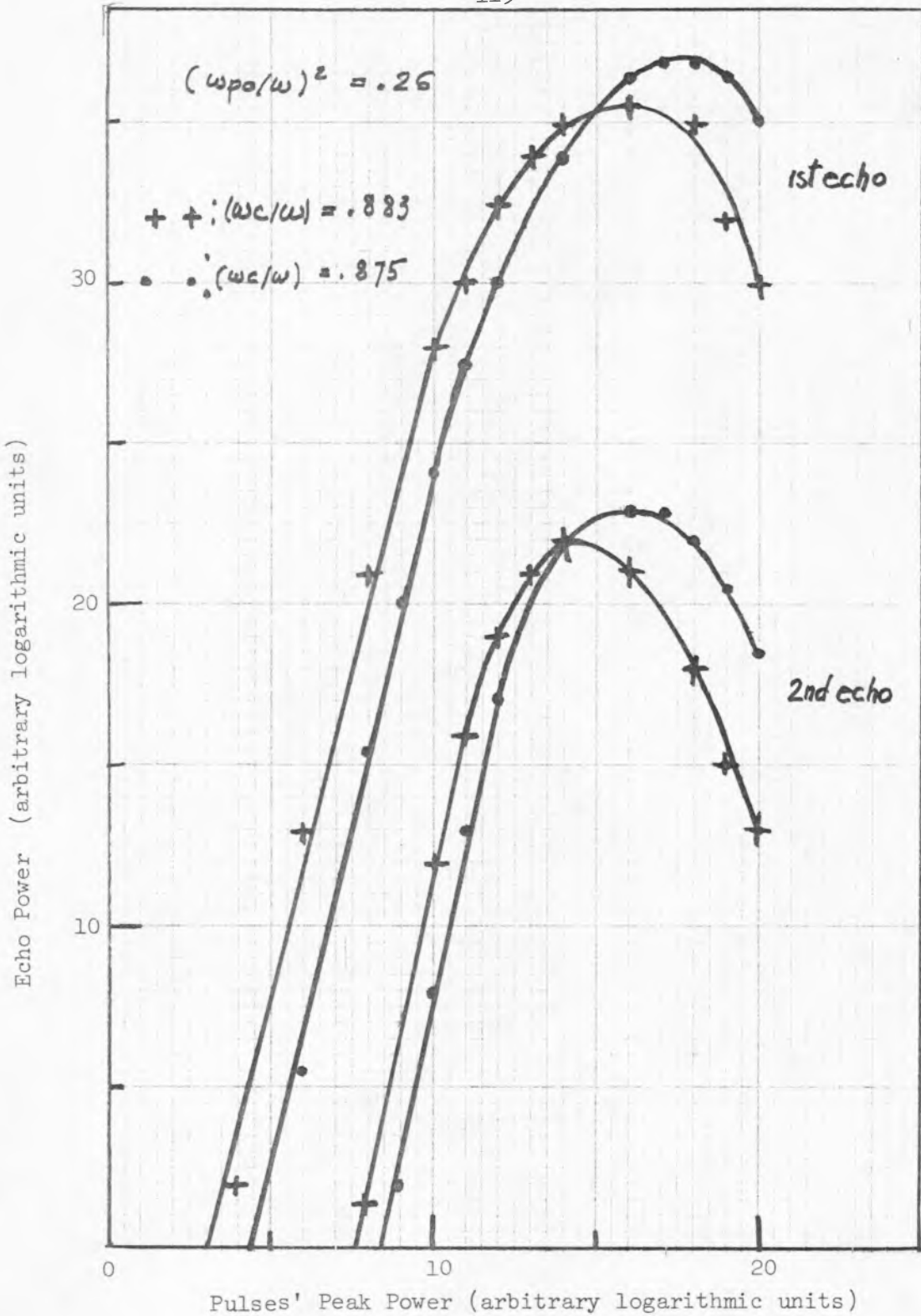
Fig. 4.13 "First and second echo power law curves" with (ω_c/ω) as a parameter, p = 20 microns neon, τ = 80 ns, and pulses' center frequency = 3 GHz.
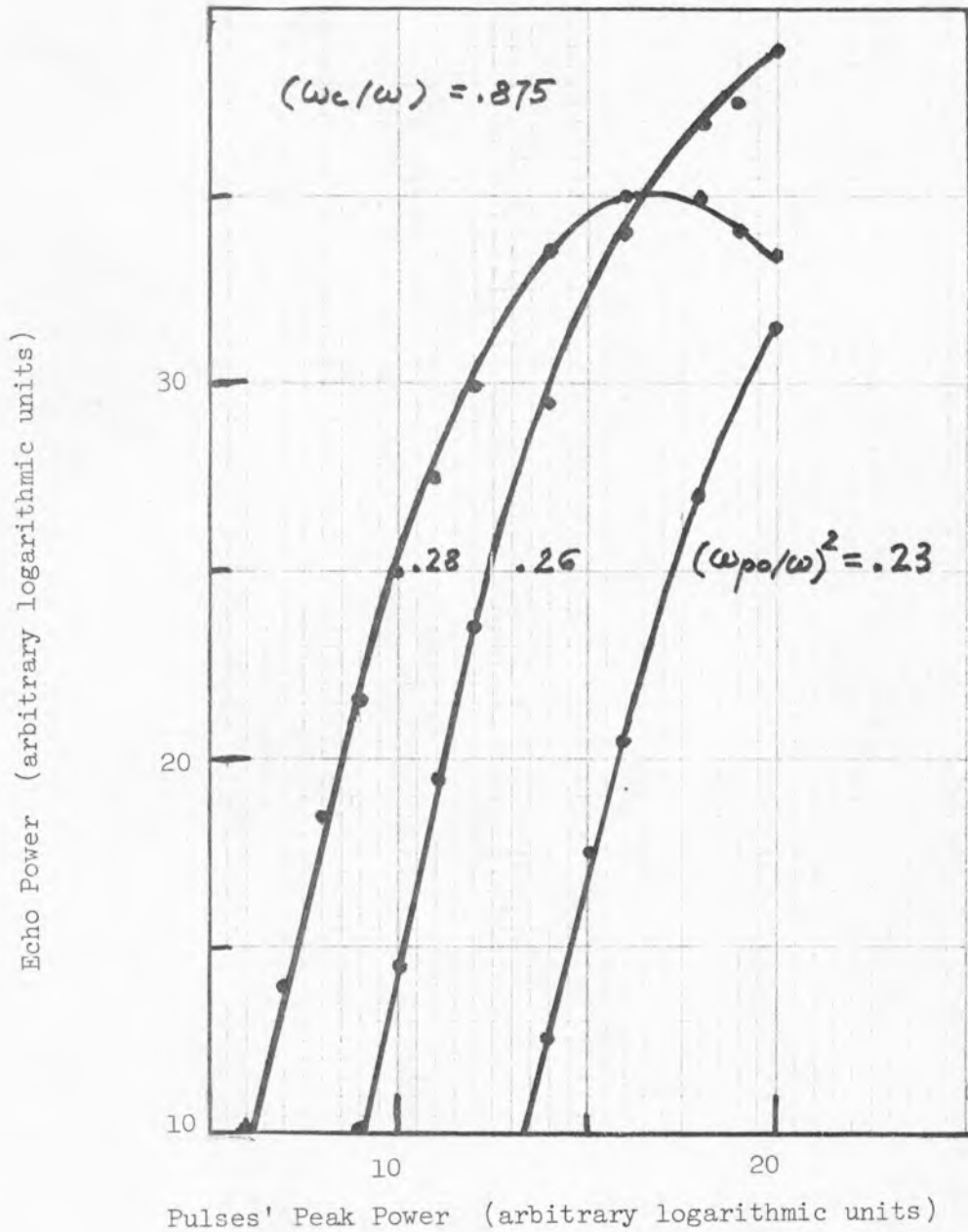
Fig. 4.14 "Echo power law curves" with $(\omega_{po}/\omega)^2$ as a parameter
$\tau = 80$ ns, pressure = 20 microns neon, and
pulses' center frequency = 3 GHz.

Echo power law with the peak density as a parameter.   In Figs.
4.11 to 4.13, the peak density or $(\omega_{po}/\omega)^2$ was kept constant and the
role of saturation on echo power law curves was studied through (ω_c/ω),
one variable entering into $z\tau$.   Fig. 4.14 shows that if the parameter
(ω_c/ω) is fixed, one can observe saturation effects on the echo power
laws by changing the parameter $(\omega_{po}/\omega)^2$ also contained in $z\tau$.   A
comparison between Fig. 4.14 and Fig. 4.11b permits us to estimate the
relative strength of the parameter (ω_c/ω) and $(\omega_{po}/\omega)^2$ in the nonline-
arity.   The three curves of Fig. 4.14 can be likened to the curves of
Fig. 4.11b defined by (ω_c/ω) = .858, (ω_c/ω) = .867 and (ω_c/ω) = .88 .
So that a change of $\sim 2.5\%$ in the parameter (ω_c/ω) will produce the
same saturation increase as a 20% change in the density.

Echo power law as a function of the neutral pressure.   Fig.
4.15a,b,c represents an effort which had similar objectives as that of
Fig. 4.9.   The question was to check whether the electron-neutral col-
lision frequency could be a possible competitor through its energy
dependence to the cold plasma model's nonlinearity.   The experiment was
done in the following way: A pressure was chosen and a certain density
was fixed and measured.   The value of the magnetic field giving the
largest echo for the maximum available power and chosen τ was noted.
(In Fig. 4.15a, for instance, it would correspond to (ω_c/ω) = .9 .   An
"echo power law curve" was taken for that value of (ω_c/ω) and for two
other values not very different from the first.   The pressure was
changed.   With the help of CW scattering measurements, the time in the
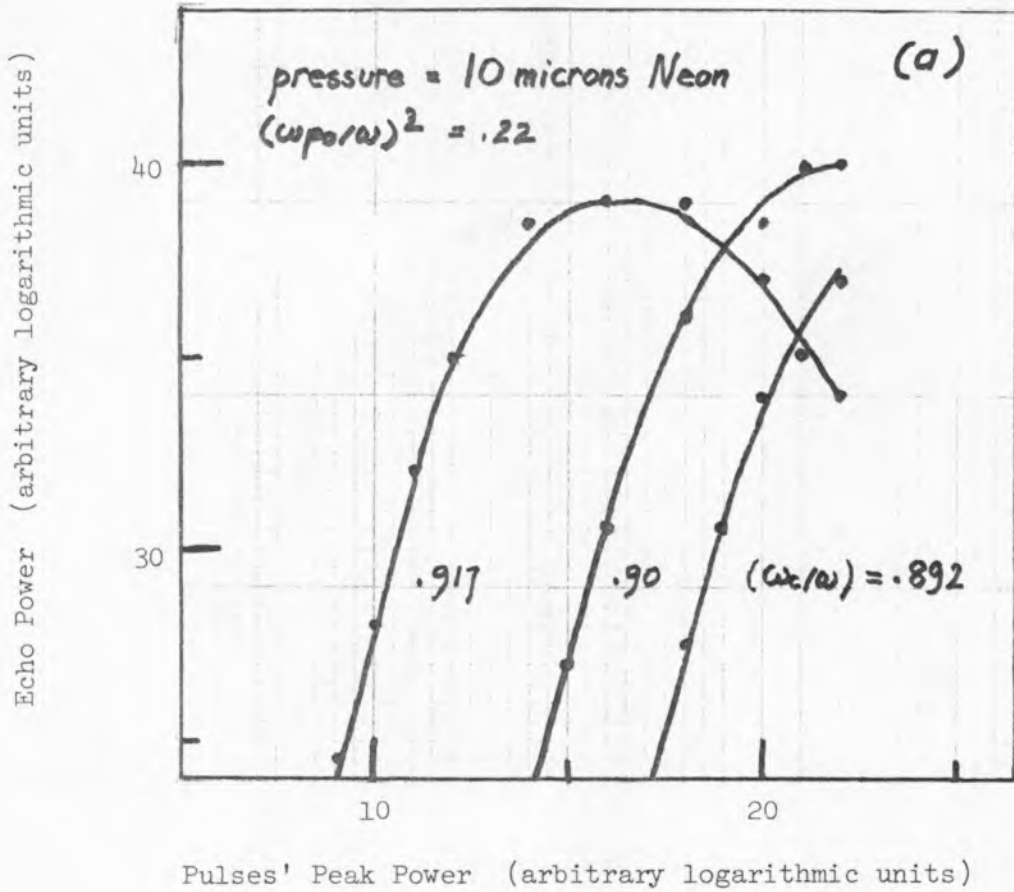afterglow giving the same density as before could be found and fixed.

Fig. 4.15 "Echo power law curves" with (ω_c/ω) as a parameter.
$\tau = 80$ ns, pulses' center frequency = 3 GHz, and
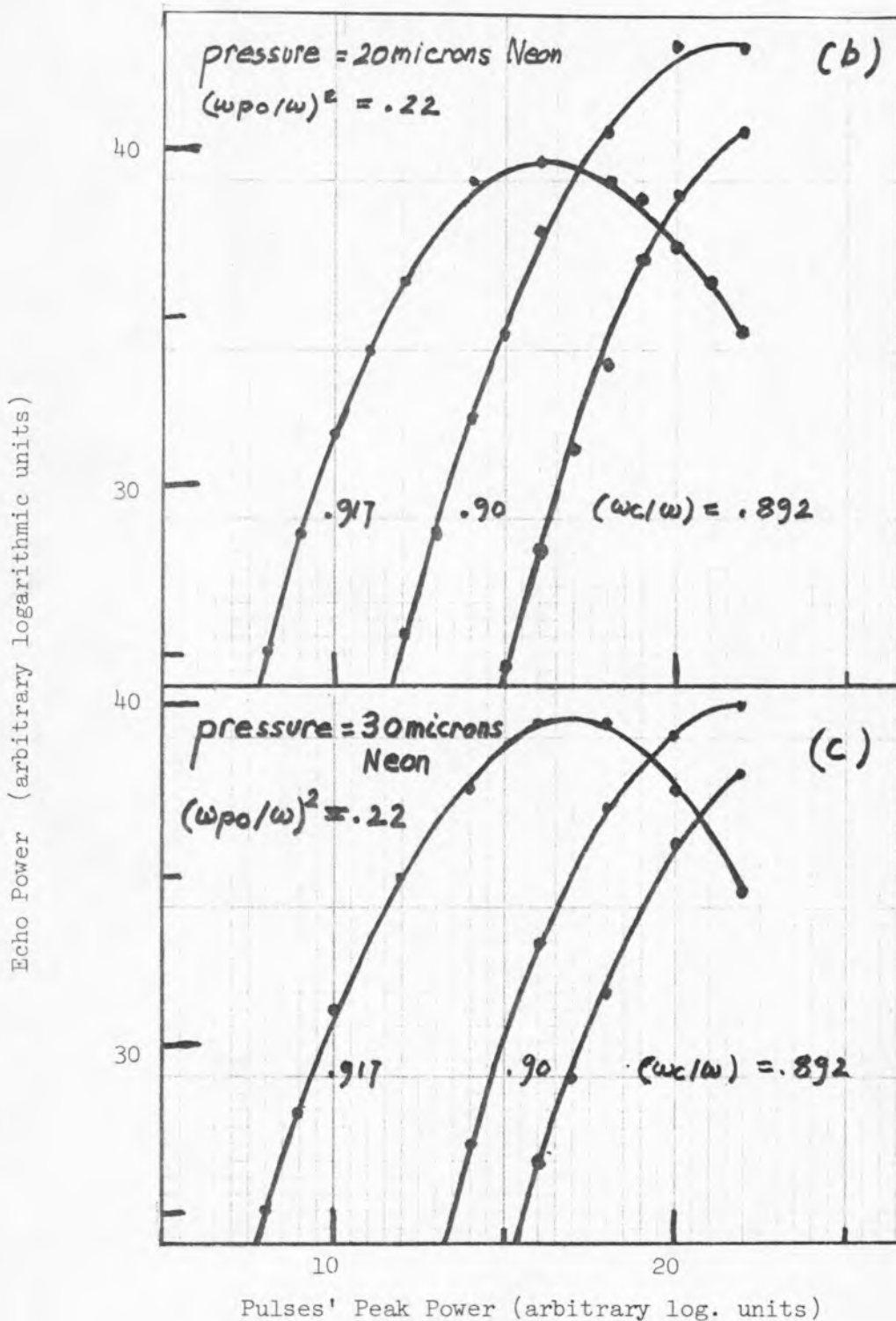(a) pressure = 10 microns neon.

Fig. 4.15 Echo power law curves with (ω_c/ω) as a parameter.
$\tau = 80$ ns and pulses' center frequency = 3GHz.
(b) pressure = 20 microns neon,
(c) pressure = 30 microns neon.

"Echo power law curves" were then taken for the three previously chosen values of (ω_c/ω). If the collisions, through a term $\partial \nu/\partial V^2$ participated in the nonlinearity, an increase of pressure provided an increase of the nonlinearity. The input power values for which the echo saturated should then have been diminishing as pressure increased. As can be seen, no significant changes in the saturation of the echo can be found for the three values of (ω_c/ω) and for the three different pressures. So with the reserve expressed previously, the energy dependent collision frequency does not enter the nonlinearity. (In this experiment one was obliged to measure the density for each pressure. It was impossible to use the same trick as in the measurement of the echo spectra shifts vs. pressure because, here, it would have been impossible to distinguish the contributions of the peak density and energy dependent collision frequency. The measurement shown in Figs. 4.15a,b,c took longer to perform and in principle was more subject to errors).

Another interesting result of Fig. 4.15a,b,c is the fact that the power law coefficient α , stays constant for the three different pressures, thus confirming our previous assumption that the electron neutral collisions should not affect the echo power law in the low input power regime.

Echo power as a function of $(\omega_{po}/\omega)^2$. The behavior of the echo power with P, τ fixed, when $(\omega_{po}/\omega)^2$ is varied was already described in connection with the echo spectra. Fig. 4.16 shows the variation of the echo power as a function of $(\omega_{po}/\omega)^2$ with the input power as a parameter. The theory (20) predicts a monotonic increase of
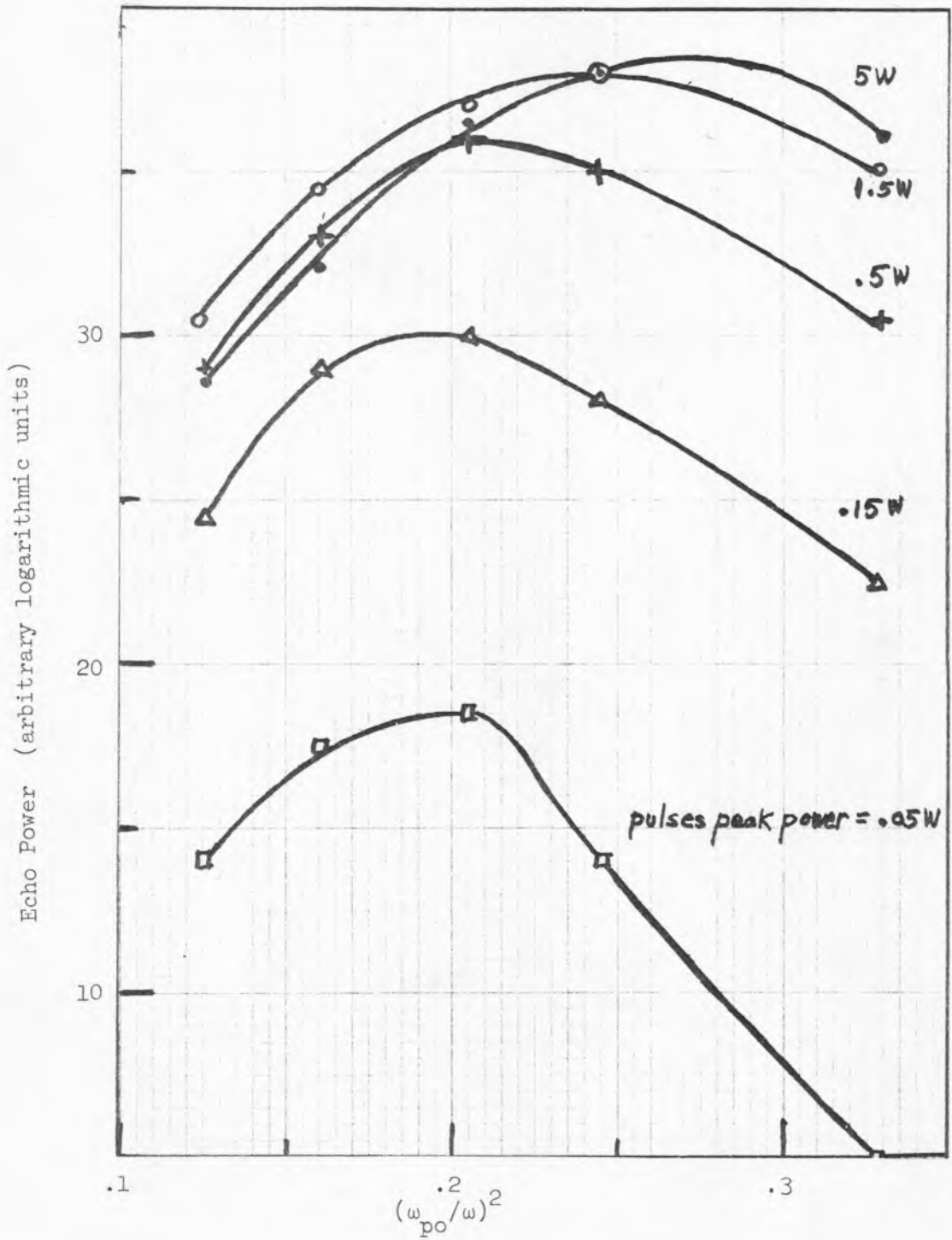
Fig. 4.16   Echo power vs. $(\omega_{po}/\omega)^2$. $\tau = 100$ ns, pressure = 18 microns argon, and pulses' center frequency = 3 GHz.

echo power with the density, but the theory is collisionless and uses the electrostatic or infinite wave length approximation. So neither Coulomb collision effects nor the problem of the efficiency of coupling to the upper hybrid oscillations in a nonuniform plasma have been taken into account in the model. These two effects, though, are probably responsible for the decrease of echo power once $(\omega_{po}/\omega)^2$ is larger than a certain critical value. It is difficult from the information we have to decide which one is dominant.

4.2.3 Echo Width

The echo width is defined to be the half power width of the echo in the time domain. It is an easily measured echo characteristic. In fact, it brought the first evidence for the importance of collective effects. In Section 2.3.3 it was shown that, in the low input power regime, the echo width should be independent of P and τ. It was further argued that if a saturation situation exists, the echo width should be a function of all parameters contained in $z\tau$. Fig. 4.17 represents the experimental variation of the echo width as a function of input power with (ω_c/ω) as a parameter in argon. (Similar results in neon are observed). The value of (ω_c/ω) corresponding to the maximum upper hybrid is .89. As the input power is raised, the echo width increases with the dependence on power influenced by the value of (ω_c/ω). This can be understood as follows. When (ω_c/ω) is very close to .89 (location of the maximum upper hybrid frequency), the factor of the nonlinearity which depends on (ω_c/ω) is very small so that the maximum input power will barely induce saturation. As
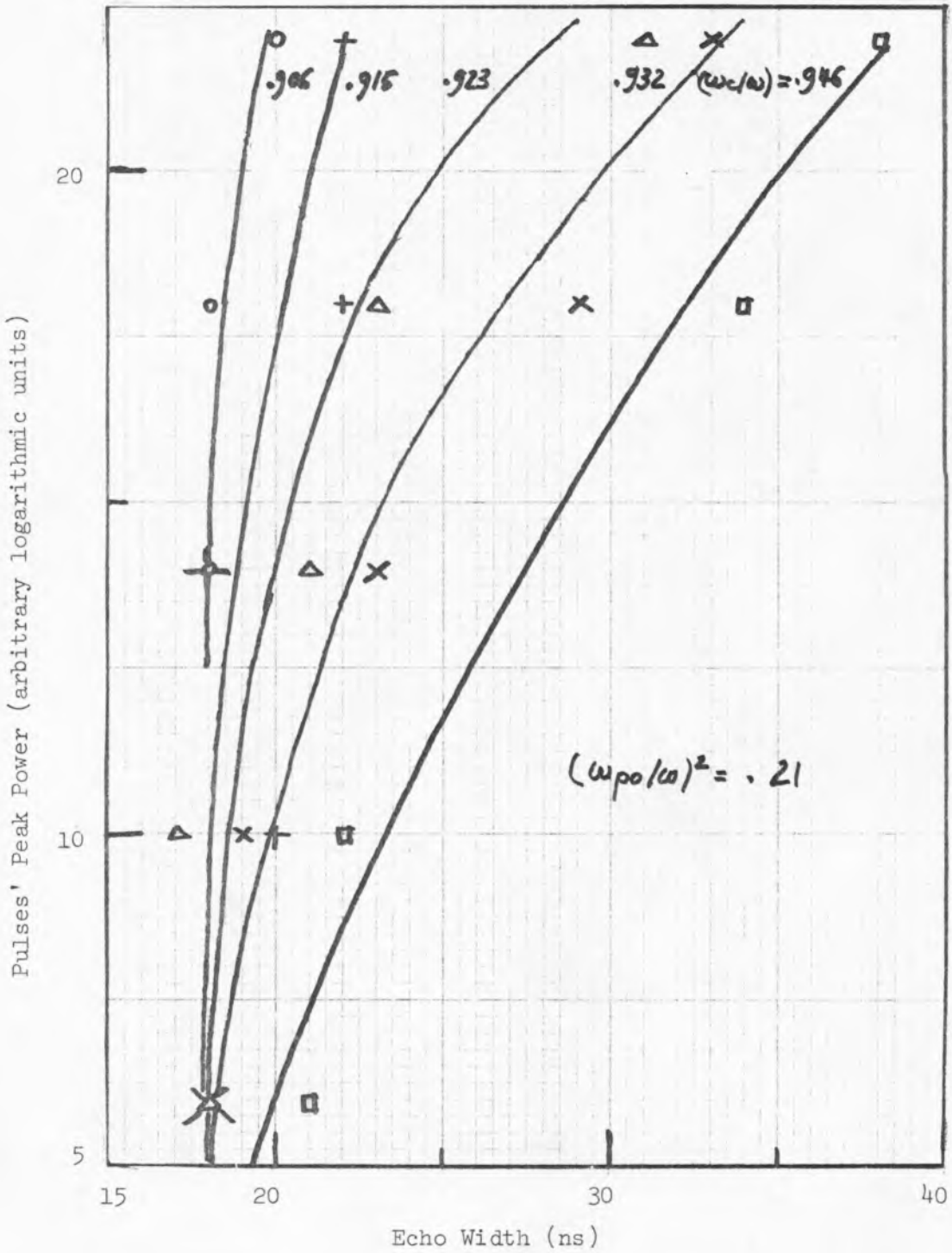
Fig. 4.17 Echo width vs. pulses' peak power with (ω_c/ω) as a
parameter. $\tau = 140$ ns, p = 18 microns argon,
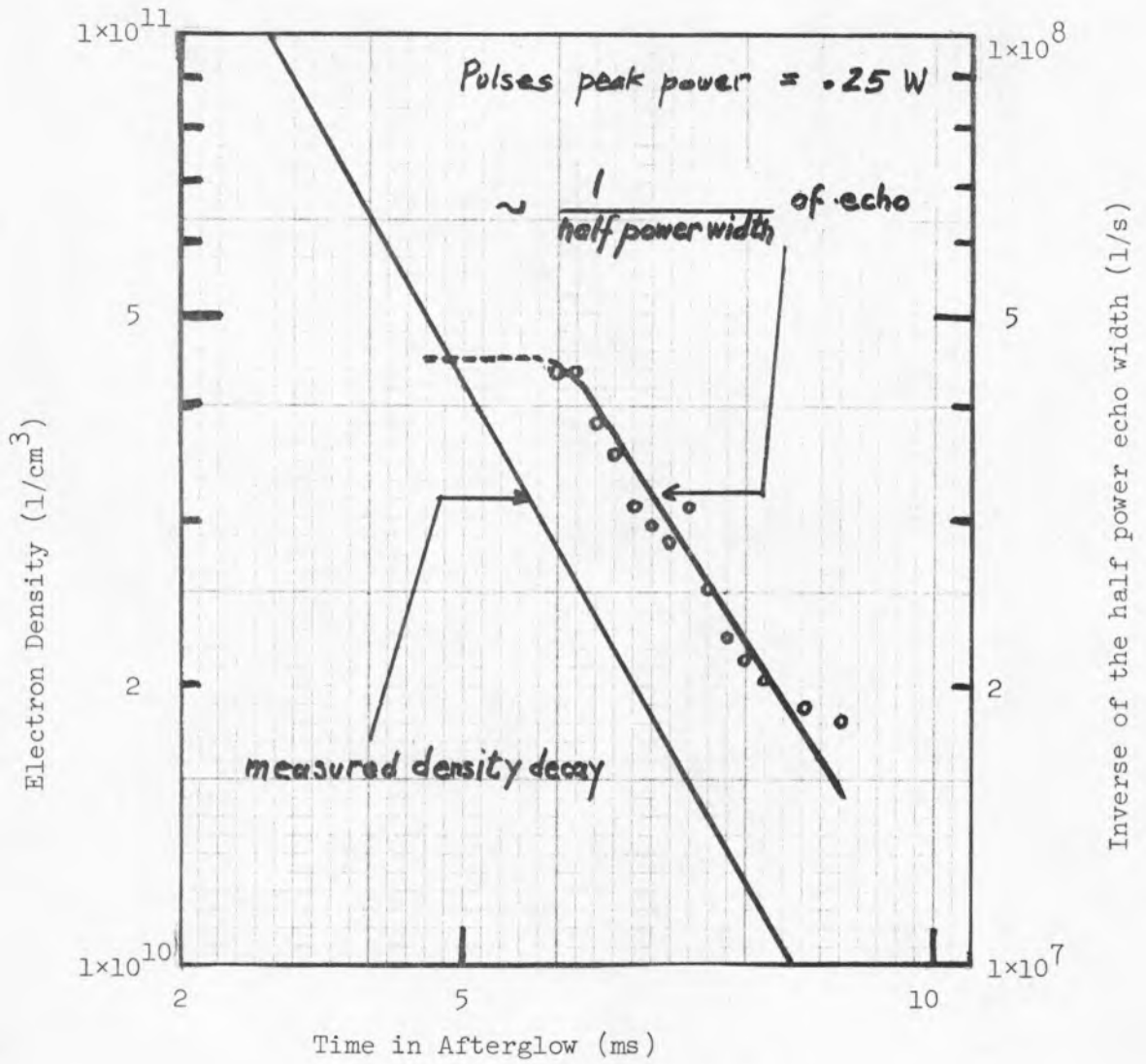pulses' width $\sim$ 15 ns, and pulses' center freq. = 3 GHz

Fig. 4.18 Echo width vs. electron density. Pressure = 18 microns
argon, input power = .25 W, τ = 260 ns, and
pulses' center frequency = 9 GHz.

(ω_c/ω) is increased, however, the input power will be more efficient
at producing saturation. When the input power is lowered, whatever the
value of (ω_c/ω) is, the echo width becomes a very weak function of power
agreeing with the low power regime theoretical predictions. A qualita-
tive agreement has been reached once more. Other experimenta have been
made to measure the echo width variation as a function of τ with
(ω_c/ω) as a parameter. As expected, quite similar results are obtained,
reinforcing the conclusions of other experiments that P and τ play
a similar role in the saturation. In Fig. 4.18 we tried to reproduce
the results of early experiments showing a variation of echo width with
peak density. In order not to be affected by the parameters (ω_c/ω), P,
τ, through saturation and to observe only the influence of $(\omega_{po}/\omega)^2$, a
low input power was chosen corresponding to about 8 in the logarithmic
units of Fig. 4.17. Ta, the time in the afterglow, was changed and the
echo width monitored. Its inverse was then plotted as a function of
Ta jointly with the measured density as a function of the same param-
eter. This particular way of plotting the echo width is a carry-over
from the independent particle theory thinking. In those theories, the
echo width is proportional to the inverse of the oscillators' spectral
width. Since, in the cold plasma model the spread of oscillators is a
function of the density, it is then logical to plot the inverse of the
echo width and the density as a function of Ta .

Looking at Fig. 4.18, the inverse of the echo width appears to
be proportional to the density over a certain range of that parameter.
On the high density side the echo ceases to narrow and stays more or

less constant. This is probably caused by relative width effects of
the pulses and oscillators' spectra. On the low density side the echo
ceases to widen and shows some complicated structures (discussed in
Section 4.3) when the pulses' spectrum is wide enough to excite at the
same time the peak of the echo spectrum at the maximum upper hybrid
and that at the cyclotron frequency.

Finally, although the main properties of the echo width have
been described and qualitatively explained here, there are a host of
fine variations of the echo shape left to be investigated and under-
stood.

4.2.4 Echo Envelope

An "echo envelope" is the curve which represents the variation
of the echo's peak power when τ is varied. Theoretically, because of
the equivalence of P and τ in the expression of the nonlinearity,
an "echo envelope" is similar to an "echo power law curve". Experimen-
tally, though, an echo envelope will show some markedly different
features due to the intervention of electron-neutral and Coulomb col-
lisions. The collisions intervene in any echo power expression as a
factor $\exp[-2f(\nu,\omega_{po}^2,\cdots)t]$, where $f(\nu,\omega_{po}^2,\cdots)^*$ is a function among
other variables of the appropriate collision ν frequency and t is
the time counted from the first pulse. When an echo power law curve is
measured, τ is fixed and the term $e^{-2f(\nu)t}$ will just be a constant
amplitude factor. When an envelope is taken, τ is varied and the term

---

* In the case of independent particle theories, $f(\nu) = \nu$.

e^{-2ft} could play a dominant role. It is this aspect of the echo envelopes which attracted a lot of interest on the echo as a possible collision diagnostic tool. This will not be the main point of emphasis in our study. We will rather try to see if some features predicted by the cold plasma model can be recognized. Fig. 4.21 shows what they should be. The maximum upper hybrid is defined by $(\omega_c/\omega) = .848$. With the density and power fixed, envelopes can be studied with (ω_c/ω) as a parameter. When (ω_c/ω) is close to the value characterizing the maximum upper hybrid, a larger τ will be necessary to produce a peak or saturation in the envelope than when (ω_c/ω) has values closer to that defining the cyclotron frequency. The shape of the envelope maximum is also seen to be dependent on the value of (ω_c/ω). These two characteristics, namely the envelope peak location and the shape of that peak, will be accessible to the experiment and worth studying. The rise of the echo envelope is not accessible because of electronic difficulties with the pulse producing apparatus (see Chapter 3). The fall of the envelopes could be dominated by a mixture of effects much as electron-neutral collisions, Coulomb collisions, diffusion of electrons out of the volume of observations whose consequences are difficult to distinguish and calculate. Fig. 4.19a is a composite diagram of experimental envelopes with the power and (ω_c/ω) as parameters. Taking the case of an input power = .5 watts, the predicted shifting and broadening of the envelope peak as (ω_c/ω) decreases is observed. The same effect, as expected, is seen when the power is decreased for a fixed value of (ω_c/ω). Although the observed behavior of the envelope holds a reasonable resemblance to those of Fig. 4.21, it could possibly be
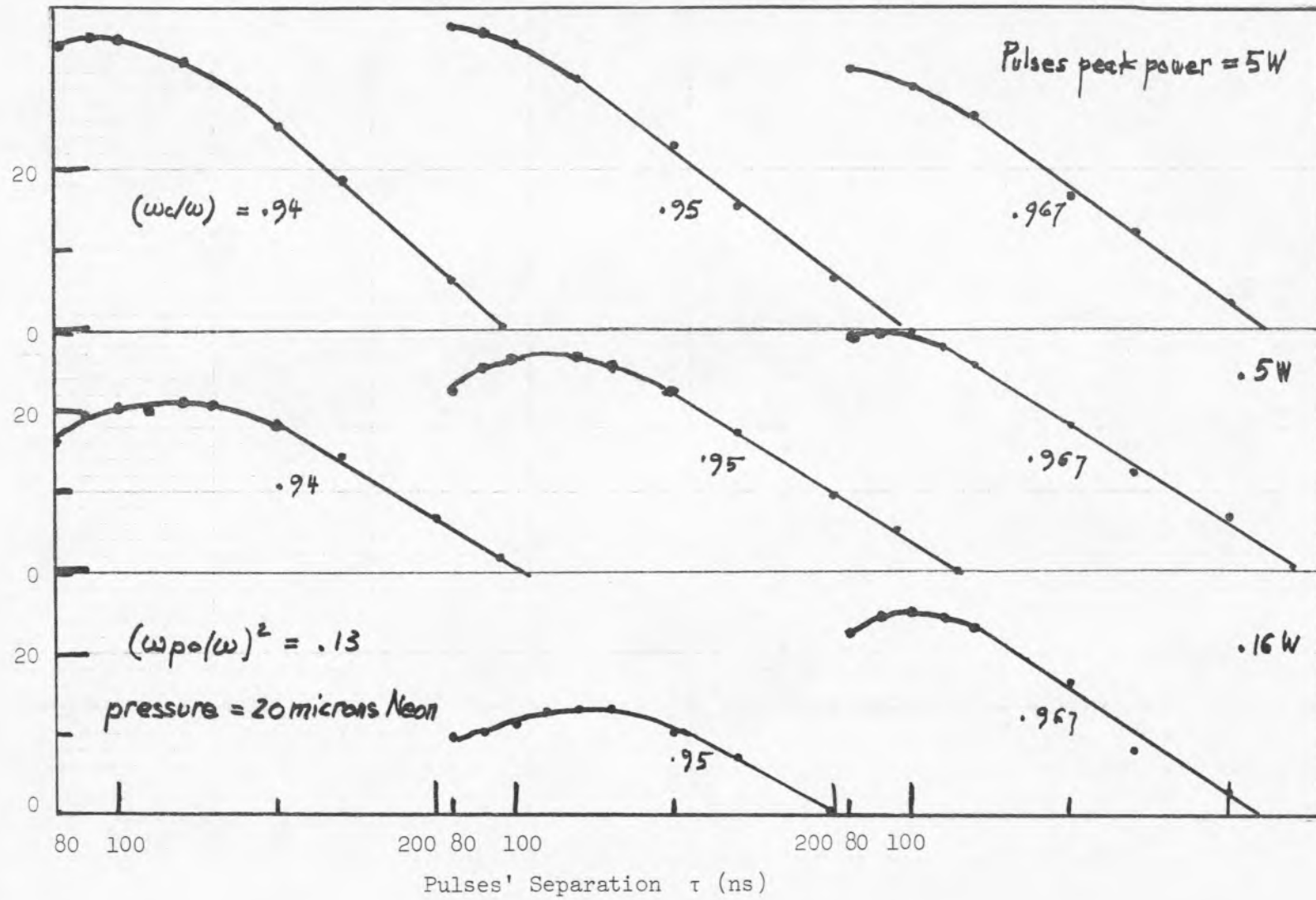
Fig. 4.19a Echo envelopes with (ω_c/ω) and input power as parameters. p = 20 microns neon, and the pulses' center frequency = 3 GHz
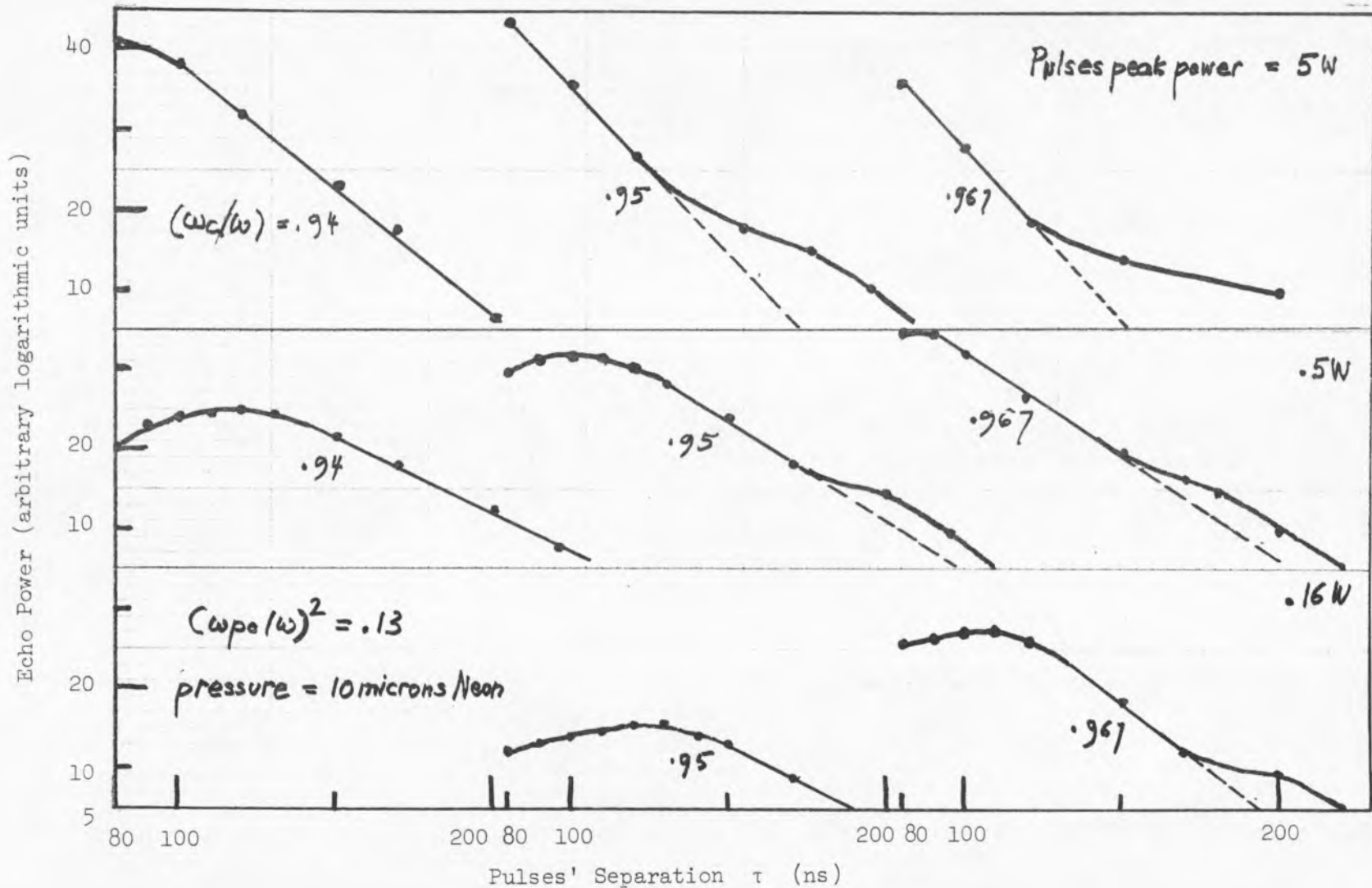
Fig. 4.19b Echo envelopes with (ω_c/ω) and input power as parameters. Pressure = 10 microns neon, and pulses' center frequency = 3 GHz.

$(\omega p \alpha / \omega)^2 = .28$

.85 .866 $(\omega_c / \omega) = .84$

Theoretical Echo Power (arbitrary units)
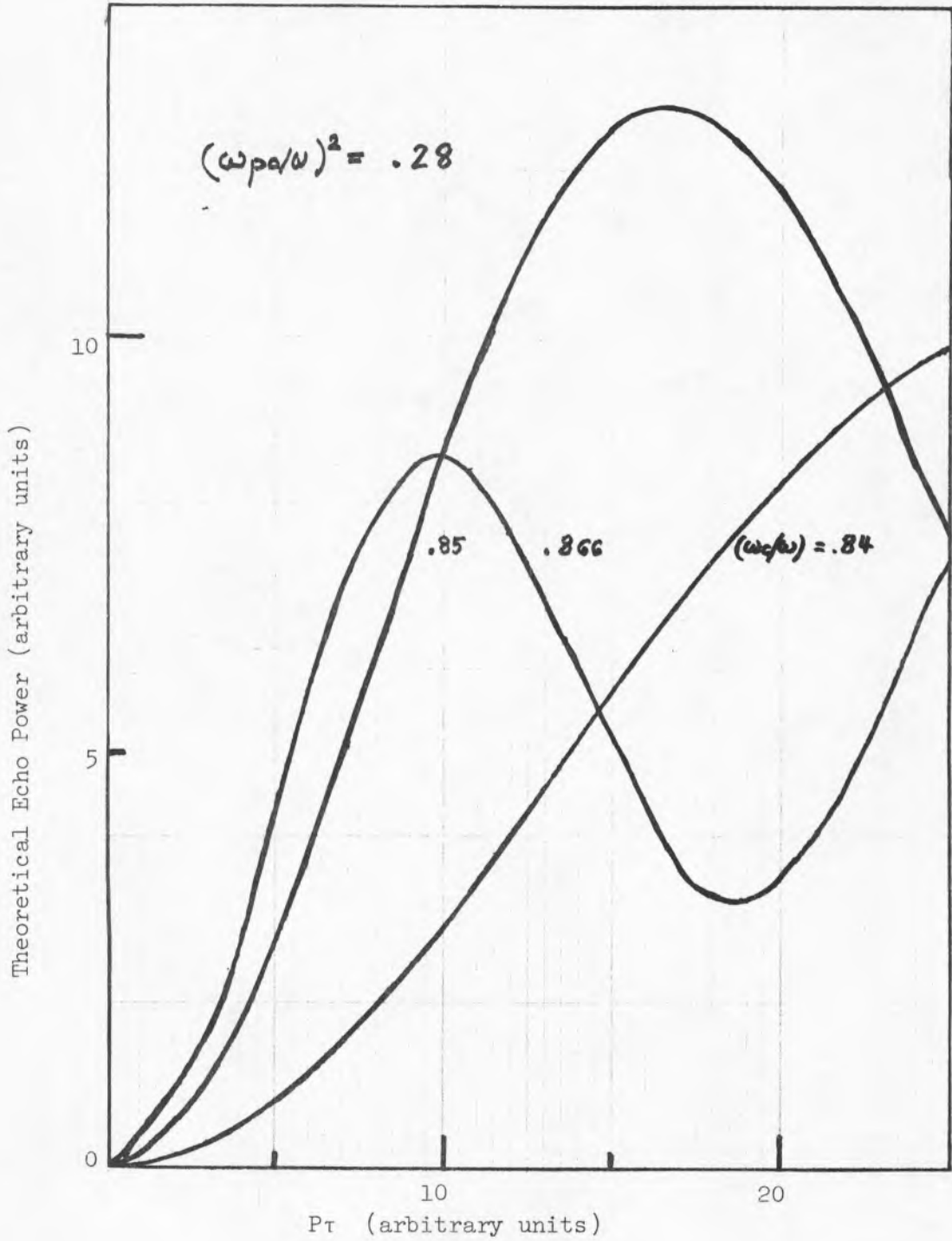
10

5

0

10 20

P_τ (arbitrary units)

Fig. 4.21 Theoretical echo power vs. P_τ with (ω_c / ω) as a parameter, after Blum.

caused by, say, the electron-neutral collisions. Their effects were investigated by lowering the pressure of neutral gas and choosing Ta so as to obtain the same density as before. The results are exposed in Fig. 4.19b. The envelopes maxima are seen to have almost the same shape and location as those of the higher neutral pressure case for all values of the parameters except for the envelopes corresponding to the highest power. Furthermore, the rate of decrease of the echo power with τ is almost equal for the two pressures and for all values of the parameters until the secondary bump of the lower pressure envelopes is reached. (The dashed lines on Fig. 4.19b help to visualize the similarity of the echo rate of decrease for the two pressures). Postponing for the moment the discussion of the bump in the low pressure envelopes, it seems that one could have ignored the role of electron neutral collisions, as can be seen by comparing the echo rate of decrease for different power levels with those given by the electron neutral collision frequency in the experimental conditions of Fig. 4.19a. (One assumes that the electrons acquire an energy of 3eV for the highest power level.) Adding Coulomb collisions for more generality, the comparison can be written as follows:

	P = 5w	P = .5w	P = .16 W
T_{exp}	13 ns $\pm$ 1 ns	16 ns $\pm$ 1 ns	16 ns $\pm$ 3
T_{en} (p = 20 microns)	35 ns	250 ns	> 250 ns
T_{ei}	5000 ns	500 ns	150 ns

The times T_{exp}, T_{en}, T_{ei} are the times sufficient to produce a factor

e decrease of the echo power as measured experimentally, due to the electron-neutral collisions and to the Coulomb collisions, respectively if their effects can be described through a simple term $e^{-2\nu t}$.

It seems then, that except in the case of the highest power level, the collision effects can be entirely neglected. When such a reasoning was used, it was usually remarked that the above collision frequency numbers should not be taken as quantitative, because it is improper to equate the relaxation of the plasma collective phenomena to independent electron collisions with neutral atoms or ions. The secondary bumps in the envelopes of Fig. 4.19b furnish an example of this problem. They are believed to be the results of the superposition of the upper hybrid echo envelopes and of those of the echo associated with the cyclotron frequency. The effect on that echo of the electron-neutral collision frequency is seen to be apparently larger than the term $e^{-2\nu t}$ would suggest. This is probably due to the special nature of the collective modes which give rise to the echo at that frequency. Some caution must therefore be used when one discusses the quantitative effects of collisions on the upper hybrid echo also. Gould, Herrmann and others (8,13) investigated the role of another factor on which the echo envelopes could depend. Taking an independent particle approach, one can show that the longitudinal drift or diffusion of electrons along the field lines of a slightly inhomogeneous magnetic field could produce a randomization of phases similar to that produced by collisions, and thus determine an echo envelope characteristic of the phenomenon. In our experiment the spread of oscillator frequencies is more important across the field lines and one can also imagine that electrons under the
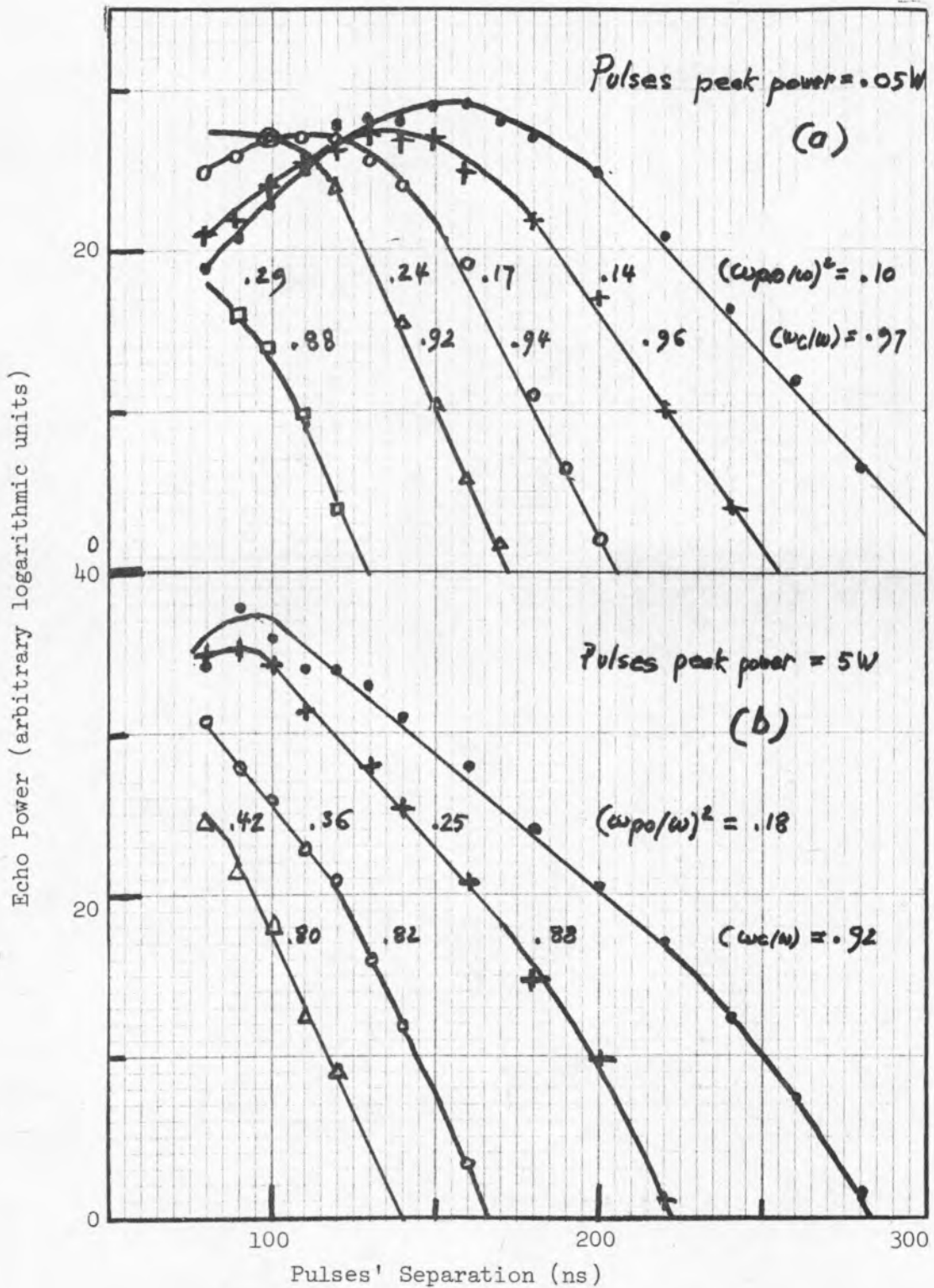
Fig. 4.20a,b Echo envelopes with $(\omega_{po}/\omega)^2$ as a parameter for two
values of input power. Pressure = 20 microns argon,
and pulses' center frequency = 3 GHz.

influence of ambipolar electric fields which exist in the plasma (due to a steady state diffusion situation) could be experiencing radial drifts, producing again randomization of the electrons' phases. The reasoning could be made quantitative using this independent particle approach, but the echo studied arose from collective oscillations, making the consequences and analyses of the previously described effects difficult to realize, to say the least.

Another experiment was tried, measuring envelopes as a function of density. Fig. 4.20a represents echo envelopes for different densities at a very low power. The maximum shape and shifts, as well as general echo envelope shapes, are believed to be controlled by Coulomb collisions. The relative change in echo envelopes as the peak density is increased; the qualitative agreement between the measured echo power rate of decrease with τ and the numbers given by the Coulomb collisions sustain that idea.[*] These conclusions are only tentative for the previously explained reasons. Fig. 4.20b shows another study of echo envelopes as a function of density for the maximum available power. In this case the maxima and beginning of the fall of the envelopes are probably determined by the saturation phenomena of the cold plasma model. To conclude this echo envelope study, one can say that there is a qualitative agreement between measurements and theory, but the evidence provided is not as solid as that given by the other measurements of the upper hybrid echo. A simple comparison between the theory and

_____

[*] It could also be expected that in argon the sharp increase in electron-neutral collisions, once electron energies are lowered under those defining the Ramsauer minimum, plays a role. The observed dependence on density of the echo decay rate with τ , could be traced to the diminishing efficiency to couple to upper hybrid oscillations as the density increases.

the experiment is not possible because of the complex effects of
Coulomb and electron-neutral collisions on the echo power as τ is
varied.

4.3 Echoes Near the Cyclotron Resonance

The existence of an echo near the cyclotron resonance has
already been demonstrated when echo spectra were studied in Section
4.2.1 and also in Section 4.2.4 under the form of bumps in the upper
hybrid echo envelopes at low pressure. Although not easy to observe,
a few of its main properties were studied because of its possible
importance in a new collective effects theory. Indeed, as pointed out
by Blum (20) the cold plasma model cannot give rise to a secondary peak
of the echo near the cyclotron resonance. As can be seen from Figs.
4.3a,b and 4.5, it can only be observed when the input power is low
enough and can eventually become much larger than the upper hybrid echo
as in Fig. 4.5. Another interesting characteristic of the echo at the
cyclotron frequency is the oscillating aspect of its spectrum, see Fig.
4.3a for example; nothing of the kind was seen for the upper hybrid
echo. When the magnetic field is changed, say, from the condition for
maximum upper hybrid resonance to the cyclotron resonance, the following
behavior of the echo can be observed on an oscilloscope. The echo rises,
peaks for an (ω_c/ω) value slightly lower than that corresponding to the
maximum upper hybrid, and then decreases as the cold plasma theory
predicts. However, as the value of ω_c/ω approaches 1.0, the echo
reappears, wider, and oscillates between zero and its peak value as the
magnetic field is changed, producing beating structures in the echo

spectra. Also a marked change appears in the plasma response directly following the exciting pulses. This direct response or "linear" response of the plasma (because it can be described by a linear analysis in contrast with that of the echo) was not mentioned previously because it was impossible to observe it when the pulse's center frequency is near the maximum upper hybrid frequency. This is not surprising in view of the spectral width of the oscillators excited by one of the pulses. This width will cause a rapid dephasing of the oscillations which were coherent at the end of the pulse, inducing in turn a fast decrease in their coherent radiation. A quantitative feeling for this phenomenon is given by an experiment of Bruce, Crawford and Harp (30). With experimental conditions quite similar to ours, they were able to show that as the density is raised from $2 \times 10^6 el/cm^3$ the decay rate of the plasma response to a 10 ns pulse increases until a value of the density of $1 \times 10^9 el/cm^3$ is reached, where the direct response of the plasma cannot be distinguished from the shape of the applied pulse. This value of the density is the low limit for our experimental study. However, when the center frequency of the pulses approaches the cyclotron resonance, the plasma direct response becomes visible and gets so wide it is of comparable amplitude to the echo at the time of the echo.

Figure 4.22a shows a composite diagram of these results with input power as a parameter. The solid lines represent the radiation of the plasma at a time $t = \tau$ after the second pulse. The dashed lines display the plasma radiation at $t = \tau$ after only one pulse has hit the plasma. The two types of measurements permit us to differentiate
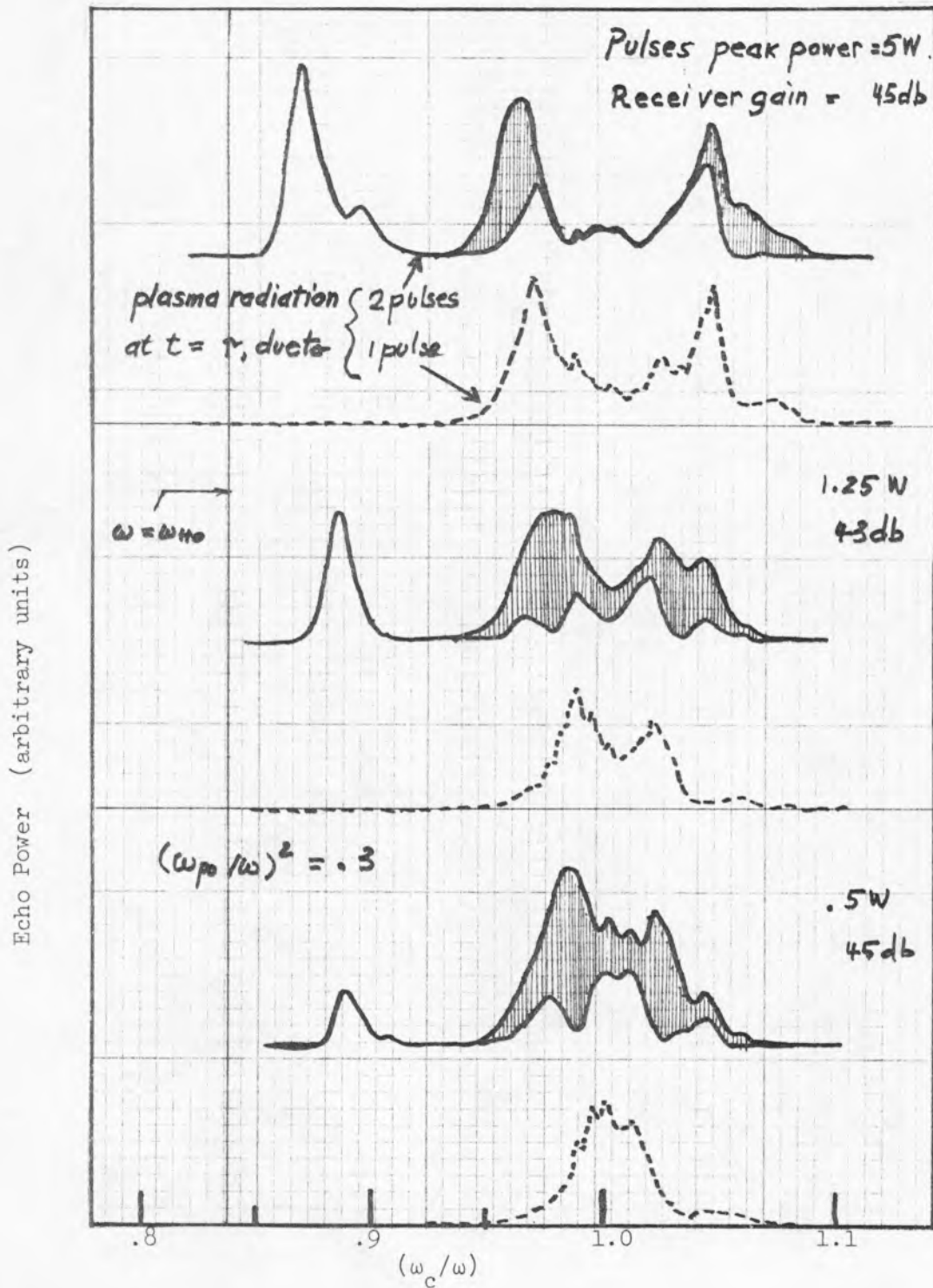
Fig. 4.22a   Plasma radiation at t = τ due to one or two pulses
vs. (ω_c/ω) with input power as a parameter.
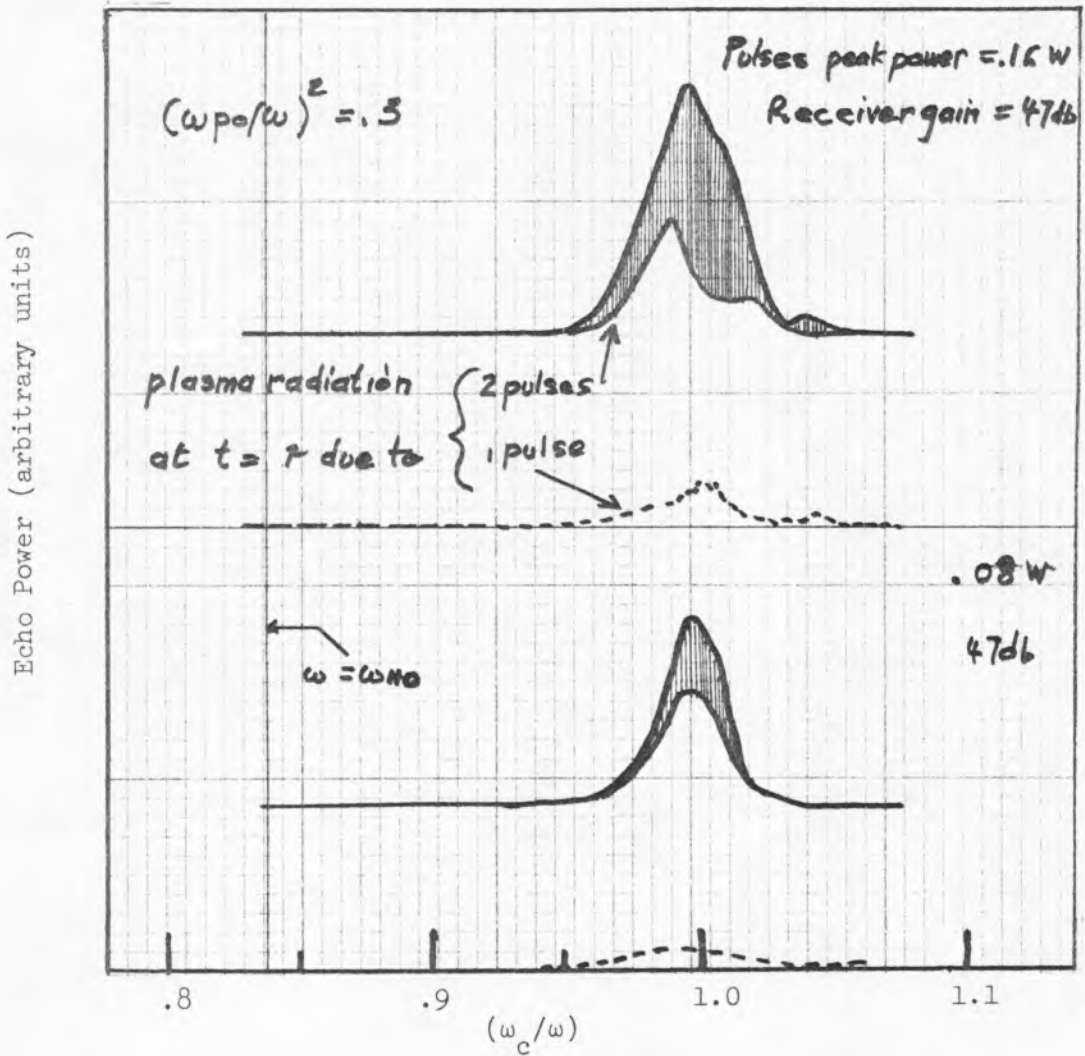Pressure = 20 microns argon, τ = 200 ns, and
pulses' center frequency = 3 GHz.

Fig. 4.22a (continued) Plasma radiation at t = τ due to one
or two pulses vs. (ω_c/ω) with input power as a
parameter.

between the contributions of the plasma linear response and echo to
the observed radiation. As pointed out earlier, no linear response
can be seen at $t = \tau$ from the upper hybrid oscillations. However,
near the cyclotron resonance, depending on the input power, the linear
response is of appreciable amplitude, double peaked or not, but always
more or less symmetrical with respect to $(\omega_c/\omega) = 1.0$. The presence
of the cyclotron echo manifests itself by a larger signal than that
contributed by the linear response alone and also by the characteristic
beating structure. To have some understanding of these facts, one
would need a new theory. Without going to that length, one can obtain
a phenomenological picture by using an independent particle approach
whose oscillators and nonlinearity will not be specified. From equa-
tion 2.15 the echo current is given by:

$$J \sim \sum_{-\infty}^{+\infty} A_n(t)\ g(t - n\tau) \tag{4.5}$$

where $A_n(t)$ is an amplitude factor and $g(t - n\tau)$ is the echo
shape factor.

$$g(t) = \int_{-\infty}^{+\infty} G(\Omega')\ e^{i\Omega't}\ d\Omega' \tag{4.6}$$

where Ω' is the frequency of one of the oscillators expressed in a
frame rotating with the pulse's center frequency ω , so that

$$\Omega' = \Omega - \omega \tag{4.7}$$

$G(\Omega')$ is the spectral density of oscillators. Now let us suppose

that this density of oscillators $G(\Omega)$ is given to us and that it is centered around the cyclotron resonance ω_c , then

$$G(\Omega) = f(\Omega - \omega_c)$$

or

$$G(\Omega') = f(\omega - \omega_c + \Omega') \tag{4.8}$$

then

$$g(t) = \int_{-\infty}^{+\infty} f(\omega - \omega_c + \Omega') \, e^{i\Omega't} \, d\Omega'$$

$$= \int_{-\infty}^{+\infty} f(\Omega'') \, e^{-i(\omega-\omega_c)t} \, e^{i\Omega''t} \, d\Omega''$$

or

$$g(t) = e^{-i(\omega-\omega_c)t} \, h(t) \tag{4.9}$$

with

$$h(t) = \int_{-\infty}^{+\infty} f(\Omega'') \, e^{i\Omega''t} \, d\Omega'' \tag{4.10}$$

and

$$\Omega'' = \omega - \omega_c + \Omega' \tag{4.11}$$

With equation 4.9 one can write the shape of the plasma "linear response" and that of the echo as:

linear response shape $\quad g_0(t) = h(t) \, e^{-i(\omega-\omega_c)t}$ \hfill (4.12)

echo shape $\quad g_1(t) = h(t-\tau)e^{-i(\omega-\omega_c)(t-\tau)}$ \hfill (4.13)

$h(t)$ is the Fourier transform of the oscillators. The variation of $h(t)$ with time will then be inversely proportional to the spectral

width of the oscillators, and if the distribution of oscillators is narrow enough, $h(t)$ will be such a slow function of time that the linear response of the plasma will still be of the same order of magnitude as the echo at the time of the echo, as is observed experimentally.

The radiation of the plasma at a time near $t = \tau$ is then the result of the addition of the linear response and of the echo. The amplitude of the plasma current will then be:

$$J(t) = A_o g_o(t) + A_1 g_1(t) \qquad (4.14)$$

$$= A_o h(t) \, e^{-i(\omega-\omega_c)t} + A_1 h(t-\tau) \, e^{-i(\omega-\omega_c)(t-\tau)} \qquad (4.15)$$

If the assumption is made that near $t = \tau$,

$$A_o h(t) \sim A_1 h(t-\tau) = A \quad , \qquad (4.16)$$

then

$$J(t) = A(e^{-i(\omega-\omega_c)t} + e^{-i(\omega-\omega_c)(t-\tau)}) \qquad (4.17)$$

and using standard trigonometric identities, taking only the real part of J :

$$Re\{J(t)\} = 2A \cos \frac{1}{2}[(\omega-\omega_c)(2t-\tau)] \cos \frac{1}{2}[(\omega-\omega_c)\tau] \qquad (4.18)$$

Through the second cosine term of equation 4.18, the real part of the current will show a beating structure with a frequency defined by $\frac{1}{2}(\omega-\omega_c)\tau = 2\pi$. The imaginary part of J shows the same beating frequency. The beating structure of the cyclotron echo in Fig. 4.22a and

the large linear response of the plasma at $t = \tau$ are then just conse-
quences of the narrowness of the oscillators' spectrum which gives rise
to the echo at the cyclotron resonance. A quantitative check of the
simple reasoning made here can be easily obtained from the experiment.
The beating frequency is seen to change with τ (see Fig. 4.3a,b and
Fig. 4.22a). Fig. 4.22b is a plot of the change of frequency necessary
to make the echo grow from zero to its peak value and back to zero
again vs. $1/\tau$. The measurements were made at different densities with
the expected results that all points fall on the line of slope 1,
meaning that $(f - f_c)\tau = 1$ or $(\omega - \omega_c)\tau = 2\pi$. The beating of the amp-
litude of the plasma current is characterized by $\frac{1}{2}(\omega - \omega_c)\tau = 2\pi$, but
experimentally one observes only power so that the beating frequency
doubles, agreeing with the experimental results. Another aspect of the
diagrams of Fig. 4.22a has not yet been explained; that is, the double
peaking of both the echo and linear response symmetrically with respect
to $(\omega_c/\omega) = 1$. This is probably a combined effect of the finite width
of the pulses' spectrum and of the electron-neutral collisions.
Analyzing, for instance, the diagram corresponding to the input power
of 5W, one can guess at the influence of the electron-neutral colli-
sions. Taking the center frequency of the pulses to be such that
 $(\omega_c/\omega) = .95$, only a weak power will excite the oscillators located at
 $(\omega_c/\omega) = 1.0$. Only a weak echo can then be observed with a corres-
ponding weak electron-neutral collision frequency. When the center
frequency is changed so that (ω_c/ω) increases, the larger power avail-
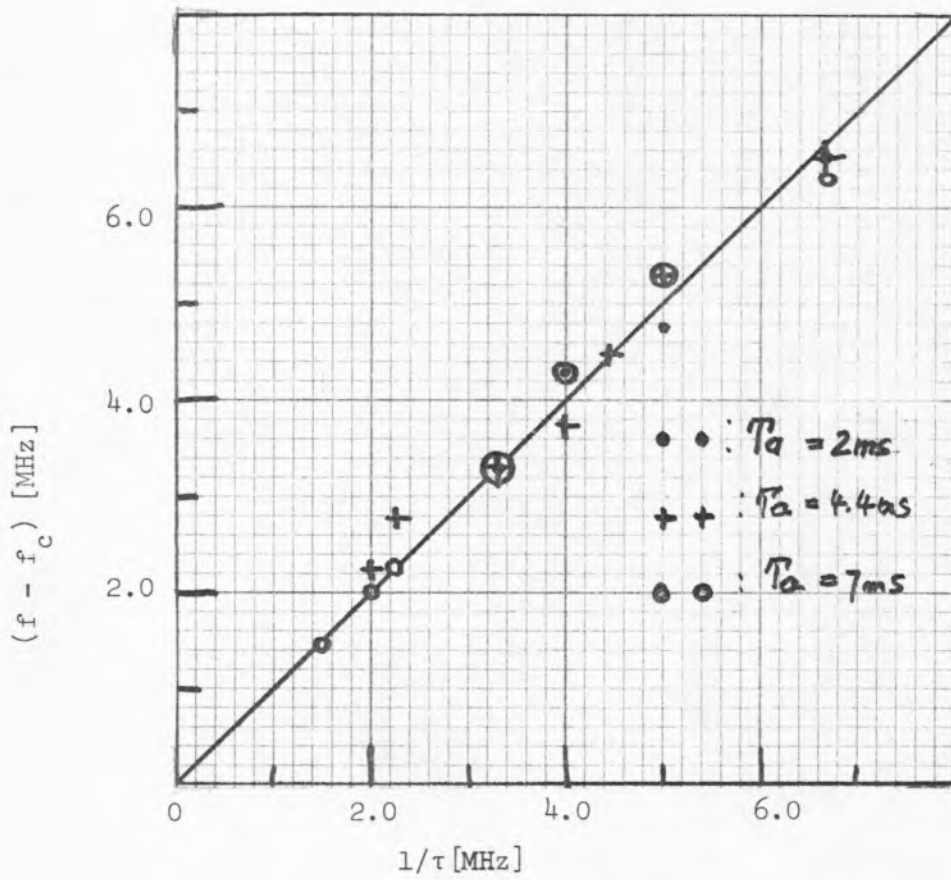able to the oscillators produces a larger echo as long as the echo

Fig. 4.22b Beating frequency of echo near cyclotron
resonance vs. 1/τ for different densities

power law more than compensates for the decrease caused by the colli-
sions. If this is not the case, the echo power will drop, accompanied
eventually by a similar decrease in the linear response, with the
minimum being reached at $(\omega_c/\omega) = 1.0$. If the pulses' center frequency
is still decreased such that $(\omega_c/\omega) \geq 1.0$, just an inverse series of
events will happen as long as the pulses' spectra are symmetrical with
respect to their center frequency, causing the symmetrical double
peaking of the echo and of the linear plasma response. A direct conse-
quence of that reasoning would be that if the input power is reduced,
the double peaking should decrease and eventually disappear. These
kinds of phenomena can be seen in Fig. 4.22a. A further argument in
favor of the strong effect of electron-neutral collisions on the echo
near the cyclotron resonance was brought out during the discussion of
echo envelopes. A factor of two change in the neutral pressure had a
clear influence on the cyclotron echo envelope (Fig. 4.19a,b).
Finally, it is interesting to note that, as the input power is lowered
sufficiently so that the spectrum of the echo near the cyclotron reson-
ance is not double-peaked any more (the power level at which presumably
the electron-neutral collisions become insignificant), the upper hybrid
echo becomes smaller than the cyclotron echo and eventually disappears,
leaving only one peak in the echo spectrum at the cyclotron resonance.

The studied plasma, as we have seen through the echo spectra,
possesses two zones where stimulated radiation can be observed. How-
ever, if the linear response of the plasma was easily detected at the
cyclotron resonance, it could not be seen at the maximum upper hybrid
resonance, because of its too rapid decay associated with the spectral

width of oscillators there. As the density is decreased, however, this
spectral width will decrease, and one can expect then to see the plasma
linear response from the maximum upper hybrid. Fig. 4.23a shows the
results of an experiment tried to check this idea. The right part of
the figure consists of composite diagrams of CW scattering and of the
pulses' spectrum. Its intention is to show what resonances can be
expected to be excited by the pulses. The left part shows the results
of echo experiments in the time domain. They are drawn from Polaroid
pictures of what was displayed on a fast oscilloscope screen. In this
experiment the density was taken as a parameter. The results showed
more than was expected. Considering, for example the case of Ta =
5.5 ms, the linear responses are easily visible and show an almost
100% modulation. The echo is modulated too. This, as can be shown
from a simple independent particle approach, is simply due to the fact
that we did. not excite just one resonance as was proposed, but two at
the same time. These resonances will have prolonged ringing due to
their narrow spectrum width, and then the sum of the ringings will
show a beating structure whose frequency should be equal to the dif-
ference frequency of the two resonances. The beating of the linear
response is then explained, but we remember that, in addition to a
phase factor (see equations 4.13, 4.12 and 4.10), the linear response
and echo shape factors are identical. The echo should, as observed,
also show a beating structure. The deformation of the top of the
early linear plasma response is just due to the receiver saturation.
The frequency beat of the linear plasma response permits an independent
determination of the plasma density if we assume that only maximum
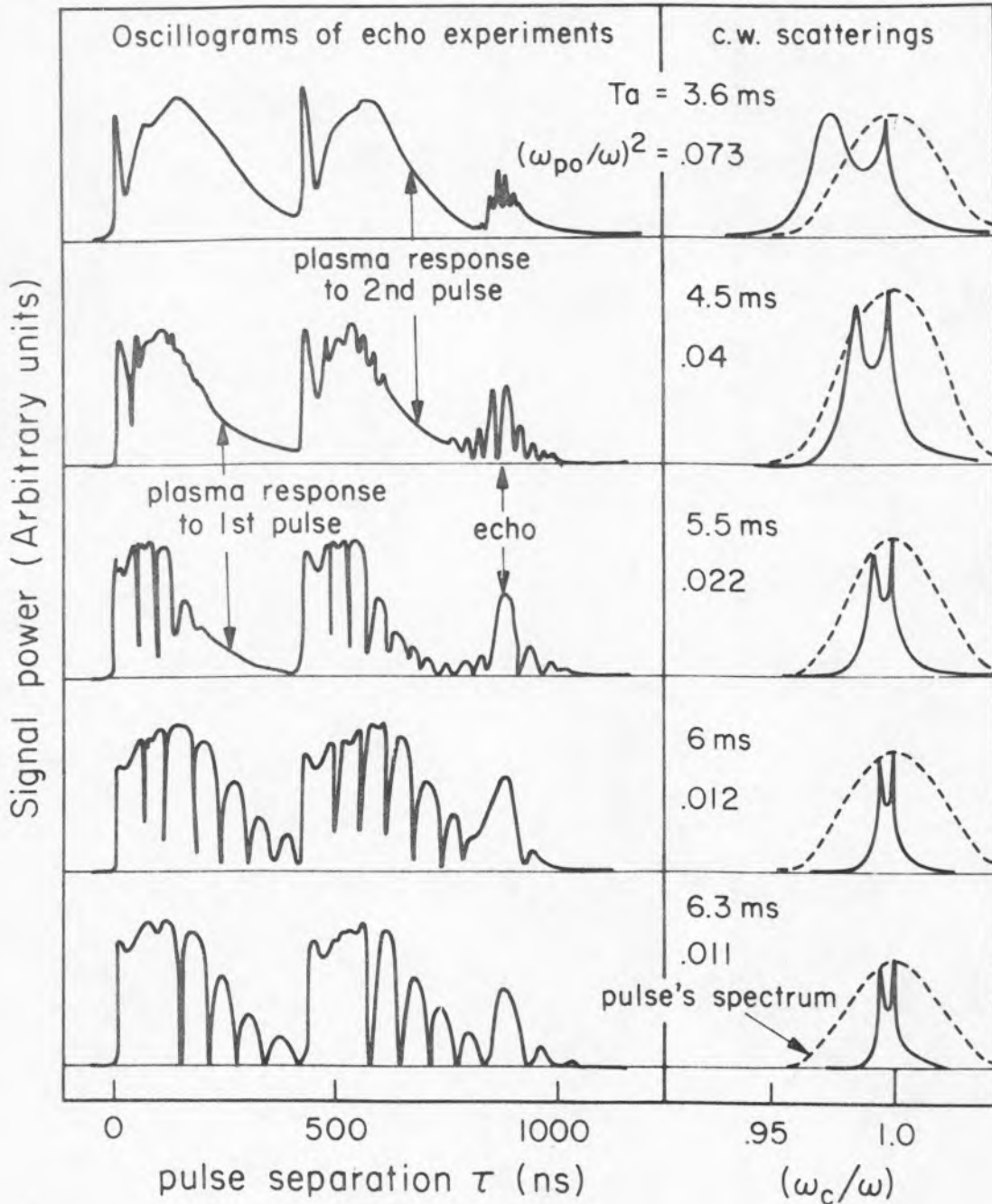
Fig. 4.23a Left: Echo and linear plasma response when both the maximum upper hybrid frequency and the cyclotron frequency are accessible to the pulses' spectrum width.

Right: CW reflection measurements vs. (ω_c/ω) compared to pulses' spectrum.

Pressure = 20 microns argon; input power = .5W.

The figure shows Electron Density [1/cm³] versus Time in Afterglow Ta (ms), with a declining straight line plot. Legend:

+ + : density as determined by c.w. scattering meas.

o o : density as determined by the beating frequency of the plasma response to 1 pulse.

△ △ : density as determined by the echo beating frequency

Fig. 4.23b   Comparison of different density measurements

upper hybrid oscillations and cyclotron oscillations are responsible

for the ringing. Fig. 4.23b shows the results of such a measurement.

Also plotted are the results given by the associated CW scattering,

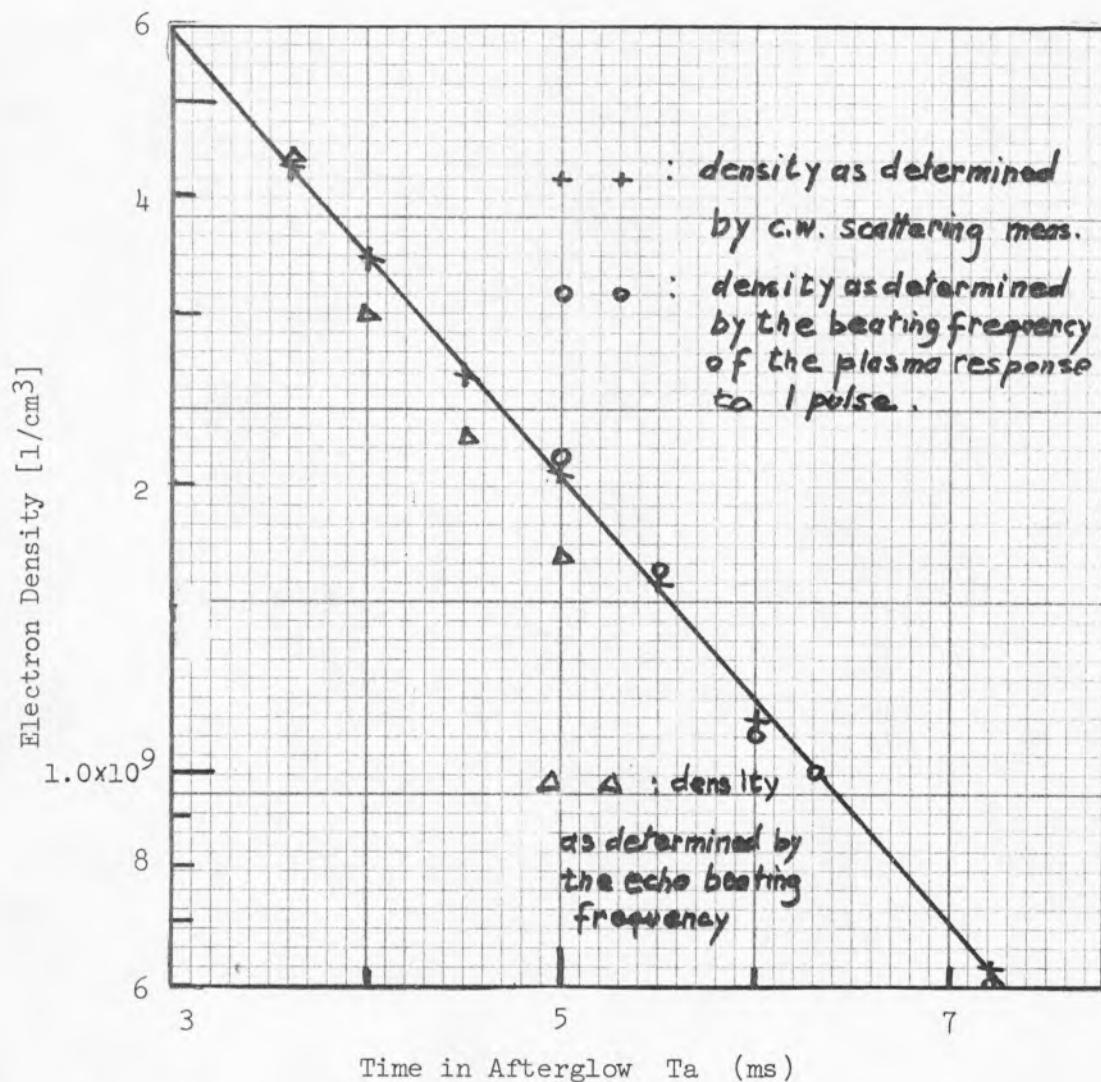assuming that the maximum upper hybrid, at these low densities, is

located at the summit of the appropriate peak in the CW scattering.

The agreement is seen to be remarkable. The beating frequency of the

echo does not seem to be the same as that of the linear response, but

with the echo arising from nonlinear processes, some small frequency

shift could be expected, and also it is more difficult to measure than

that of the linear response. This experiment is especially interest-

ing. It independently confirms some recent measurements and associated

theory of pulse-stimulated emission from plasma columns (31).

V.   SUMMARY AND CONCLUSIONS

5.1 Summary and Evaluation of Results

The original intent of this experiment was to reproduce that of Hill and Kaplan and to make some detailed comparison with the independent particle theories. The first results of early experiments in X-band frequency with the plasma vessel located in a very homogeneous magnetic field ($\Delta B/B = 10^{-4}$) displayed two-pulse echo properties not explained by these theories. Every characteristic of the echo appeared to be an unexpectedly strong function of the electron density. This, progressively, led to the idea that <u>nonlinear collective oscillations</u> excited by the microwave pulses could play an important part in the echo formation. A new experiment was designed to accentuate these effects. The center frequency of the pulses was lowered from X-band to S-band, increasing the ratio of the plasma frequency to the cyclotron frequency, thus making the observation of "plasma effects" easier. The magnetic field inhomogeneity was again kept very small. These changes brought the discovery (21) of an echo associated with the well-known upper hybrid oscillations present in a nonuniform cold plasma column. The echo spectrum peaked near what is called the maximum upper hybrid frequency of the plasma:
$\omega_{Ho}^2 = \omega_{po}^2 + \omega_c^2$ where $\omega_{po}/2\pi$ is the plasma frequency associated with the peak density on the column axis and $\omega_c/2\pi$ is the cyclotron frequency. Blum (20) developed a new echo theory in terms of a simple nonuniform unidimensional cold plasma slab. The theoretical echo spectrum also peaked near the maximum upper hybrid. Furthermore, the

theory showed that the echo properties can be described in terms of two different regimes: a "low" pulse peak power regime, and a "high" pulse peak power regime, or saturation regime. When the pulse power is low, the echo description is relatively simple. For instance, among the four most important variables $((\omega_c/\omega)$, $(\omega_{po}/\omega)^2$, pulse power P and pulse separation τ) present in an echo experiment, only the first two will have an effect on the echo width and the echo spectrum. As the pulse power is raised to reach the second regime, the four variables have a strong influence on all echo characteristics. A detailed experimental study was then made of the most important echo characteristics: echo spectrum, echo power law, echo width, and echo envelope, as a function of the previously defined variables for each of the two power regimes. An over-all remarkable qualitative agreement between the experiment and the theory was obtained. Thus it clearly confirmed the suspected importance of collective effects in the echo formation, when the distribution of cyclotron frequencies caused by magnetic field inhomogeneities was narrower than the distribution of upper hybrid frequencies due to the plasma electron density nonuniformity. The discovery of the upper hybrid echo and its qualitative understanding have provided a new insight into the difficult problem of nonlinear collective oscillations that can be excited in laboratory plasmas.

The simplicity of the model prevented a quantitative comparison of the theory with the experiment; it also caused some qualitative disagreements in some areas of the multidimensional space of the echo

parameters. We will list these areas, as they will give indications
into what directions further work could be pursued. First, the echo
spectra were seen to have a peak not predicted by the theory, at cyclo-
tron frequency. The slowness of the decay of the linear plasma
response to the exciting pulses; its interaction with the echo causing
modulation of its spectrum, were manifestations of the narrowness of
the spectrum of oscillators present there. The double peaking of the
echo spectra symmetrically with respect to $(\omega_c/\omega) = 1.0$ at large input
powers showed, it is believed, the importance of electron-neutral col-
lisions on the oscillators or modes. The mode characteristics and
their strong dependence on collisions match very well with those pre-
dicted by the hot uniform plasma theory of Bernstein near the cyclotron
frequency (32). This raises the interesting possibility that "hot"
plasma effects also play a role in the echo formation. An aspect of
the usefulness of the echo as a diagnostic tool has just been given.
Even though we do not have a theory for a collective effect echo peak-
ing at the cyclotron frequency, we know enough about the general
conditions for the existence of an echo to characterize the modes or
"oscillators" which must exist there, thus obtaining information which
perhaps could not have been obtained otherwise. For instance, the CW
reflection measurements also show a peak at $(\omega_c/\omega) = 1.0$. Following
a cold plasma approach, it was thought to be simply due to a reactive
mismatch of the plasma in the waveguide. Further emission studies by
Blum, and our experiment with the echo peaking at the cyclotron fre-
quency showed this reasoning to be erroneous.

Another discrepancy between the cold plasma echo theory and the experimental results is observed when the echo power is monitored as a function of the density. The theory predicts a monotonic increase of the echo power with the density until saturation sets in. Experimentally, as the density is raised, the echo first grows, but then drops rapidly once a certain critical density is reached. It was pointed out that at least two reasons could be found to explain the disagreement. The first is the neglect of Coulomb collisions which are linearly increasing with the density. The second could be the electrostatic approximation of the cold plasma model which discarded wavelength effects, a potential source of the difficulty in coupling to the upper hybrid resonances as the electron density increases (28). Unfortunately these effects could not be identified with enough certainty to exclude other possible factors.

5.2 Suggestions for Further Work

As far as the theory is concerned, from the difficulties encountered in dealing with some of the experimental results and their probable explanations, it seems that a quantitative description of the echo can only be given using a nonuniform hot plasma theory, with Coulomb and electron-neutral collisions, and with the full set of Maxwell equations. This is a formidable task and probably not really necessary. Not all of the complications need to be taken at once. A probably next logical step in the understanding of the echo might be an electrostatic collisionless uniform hot plasma theory in order to explain the double peaking of the echo spectra at the upper hybrid and

cyclotron resonances.

One could also consider further experimental work. First, some improvements in the instrumentation used would be profitable. For instance, the range of input power over which the echo could be studied was not wide enough. This could be remedied by the use of a traveling wave tube with a higher power output and a more sensitive receiver. Furthermore, although a good measure of electron density was obtained through the CW scattering measurements, it would be desirable to confirm it with another type of diagnostic, such as interferometry, for example. The need is especially great when different gases are studied and the location of the echo spectra peak is compared with that of the maximum upper hybrid. In our experiment we were not sure whether the slight differences in the echo spectra peak location as referred to that of the maximum upper hybrid resonance between neon and argon were a real property of the echo or just a consequence of possible changes in the shape of CW scattering spectra.

Once these improvements have been perfected, the following investigations could be performed:

a) The behavior of the two peaks in the echo spectra could be studied over the extended power and receiver range. The influences of effects such as Coulomb collisions and the upper hybrid oscillation coupling problem would become clearer.

b) The study of more, different gases in which echo properties could be affected through collision frequencies and shapes of electron density profile would be of interest, especially if the density profiles are measured experimentally.

c) Finally, the influence of magnetic field inhomogeneities on the echo could help to check, for instance, whether when the upper hybrid frequencies' spread becomes narrower than that of the electron gyrofrequencies', an independent particle theory would be more appropriate than one including collective oscillations even at the relatively high densities considered in this study.

PLASMA ECHOES AT UPPER HYBRID RESONANCE*

L. O. Bauer, F. A. Blum,† and R. W. Gould
California Institute of Technology, Pasadena, California
(Received 14 December 1967)

We report experimental observation of a new plasma echo at upper hybrid resonance
and present a simple theoretical model which exhibits some major features of the results.

Echoes from a plasma stimulated by multiple excitation pulses were first reported by Hill and Kaplan[1] in 1965 (cyclotron echoes). Their experiments involved excitation of a plasma in a strong, inhomogeneous magnetic field by pulses whose center frequency was near the electron-cyclotron frequency. Although other mechanisms have been discussed,[2] a model consisting of a collection of independent electrons gyrating in a nonuniform magnetic field subject to energy-dependent collisions[3] is believed to give an adequate description of the effect if the plasma density is low enough. More recently, Gould and Blum[4] discussed theoretically another plasma echo involving upper hybrid plasma oscillations. The upper hybrid echo[5] is associated with the macroscopic charge and current density fluctuations (at the upper hybrid frequency, $\omega_h^2 = \omega_c^2 + \omega_p^2$) of a plasma column with an inhomogeneous electron-density profile. Thus, collective effects play a dominant role in the formation of this echo. This Letter is a preliminary report on the experimental observation of this new plasma echo and a simple theoretical model which exhibits some salient features of the experimental results.

The plasmas studied experimentally were rare-gas, afterglow discharges created by an rf pulse. They were contained in a glass cylinder of 1.8 cm i.d. and about 1 m in length, aligned coaxially with the magnetic field ($\vec{B}$) of a solenoid. The glass tube was inserted through and perpendicular to the narrow walls of S-band waveguide so that the configuration for the exciting microwaves was $\vec{E} \perp \vec{k} \perp \vec{B}$, where $\vec{E}$ is the electric field and $\vec{k}$ is the propagation vector of the signal. The plasma and waveguide formed one of the side arms of a balanced microwave bridge system in which a magic tee was used. In contrast to studies of cyclotron echoes,[1,3] we studied the upper hybrid echo with $\vec{B}$ homogeneous to one part in 10^4 over the volume of plasma excited by the microwaves. All experimental data reported represent crystal rectifier detected signals.

Seeking knowledge of the normal-mode spectrum of the plasma, we were led to studies of its cw response.[6] The upper solid curves in Fig. 1 show the cw reflection from a neon plasma for three afterglow times, T_a. In these experiments the incident signal frequency $\omega/2\pi$ (3.0 Gc/sec) was held constant while the magnetic field, i.e., ω_c, the electron cyclotron frequency, was varied. The values of ω_c/ω are accurate to within ±0.2%. These data show clearly the presence of collective phenomena. The sharp peak near $\omega_c/\omega = 1$ and the broad peak at lower values are characteristic of all experiments performed. The peak in the scat-
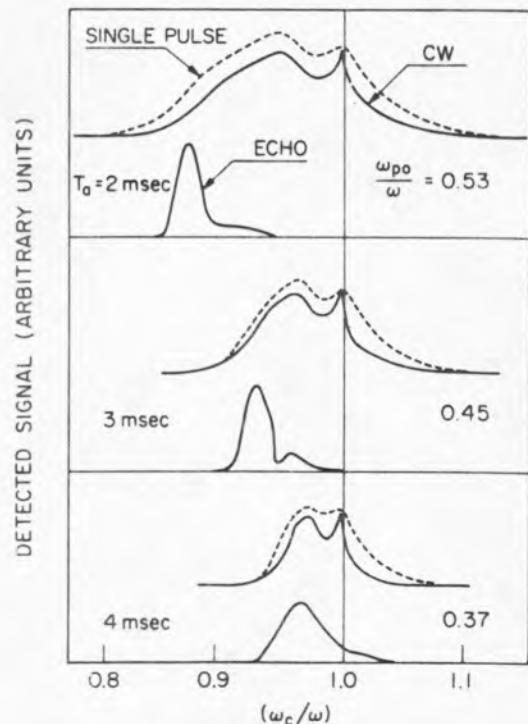

FIG. 1. Composite diagram of experimental data on cw reflection, single-pulse reflection, and echo spectra as a function of ω_c/ω for a neon afterglow plasma at a pressure of 35 μ Hg. The parameter T_a is the time after the end of the breakdown pulse, i.e., the afterglow time.

tering that significantly shifts and broadens
at high electron densities has the appearance
of a common feature of reflection, emission,
and absorption spectra of cyclotron-resonance
experiments reported by other observers.[7,8]
This feature is attributed to the upper hybrid
resonance of a cold, inhomogeneous plasma.[9]
In fact, the onset of significant scattering at
low values of ω_c/ω has proved to be a good
measure of the maximum electron density of
nonuniform plasma columns.[8] At the onset point
on the ω_c/ω axis the incident signal frequen-
cy is equal to the maximum upper hybrid fre-
quency of the plasma, i.e., $\omega^2 = \omega_{h0}^2 = \omega_c^2 + \omega_{p0}^2$,
where ω_{p0} is the maximum local plasma fre-
quency. This interpretation is the source of
the estimates of ω_{p0}/ω given in Fig. 1.

The dashed curves of Fig. 1 demonstrate that
the response of the plasma to a high power,
very short pulse such as that used in echo ex-
periments is essentially identical with the ob-
served cw scattering. These data are displays
of the maximum amplitude of the reflection
from the same neon plasma of a 20-nsec mi-
crowave pulse of 0.5-W peak power as a func-
tion of ω_c/ω. Thus the high-power pulses seem
to couple to the same normal modes of the plas-
ma that are observed in low-power cw exper-
iments.

Finally, we come to the echo and its corre-
lation with the cw and short-pulse spectra.
The echoes were stimulated by two pulses sep-
arated by a time τ. The pulses were each iden-
tical to the one used in the short-pulse reflec-
tion experiment. The echoes consist of short
bursts of radiation emitted by the plasma at
times $t = n\tau$, $n = 1, 2, \cdots$, after the second applied
pulse. The lower solid curves in Fig. 1 are
magnetic field spectra of the first echo ($n = 1$,
$\tau = 100$ nsec), i.e., the dependence of the echo
amplitude on ω_c/ω. At $T_a = 2$ msec the echo
is strongest at a point which is shifted 13%
(about five times its spectral half-width) from
the condition for free electron cyclotron res-
onance, $\omega_c/\omega = 1$. Although the data present-
ed are for neon, similar results have been ob-
tained using argon. This is the first observa-
tion of echoes under conditions far from those
for free electron cyclotron resonance and near
what the cw experiments mark as the maximum
upper hybrid frequency of the plasma.

In order to account qualitatively for the gen-
eral features of the data of Fig. 1, we consid-
er a one-dimensional inhomogeneous cold plas-

ma slab[4] of thickness $2a$ situated in a uniform
magnetic field $\vec{B}$ which is parallel to the slab
faces [see Fig. 2(a)]. The plasma is placed
between two parallel conducting plates separat-
ed by a distance $2l$. The steady-state electron
density is assumed to depend on x in such a
manner that $\omega_p^2(x) = \omega_{p0}^2(1-x^2/a^2)$. Collisions
are neglected and the ions are assumed fixed.
Simulating the conditions of the experiment,
we place a short section of this plasma slab
in a parallel-plate transmission line which has
a matched generator at one end and is termi-
nated in its characteristic impedance Z_0 at
the other end as shown in Fig. 2(a). We neglect
fringing field effects in the short section. The
dependence on ω_c/ω of the reflection coefficient
seen at the generator on this transmission line
will yield the theoretical equivalent of the ex-
perimental cw curves of Fig. 1. Since in the
experiment the lateral dimensions of the plas-
ma are small compared with the wavelength,
we replace the plasma of Fig. 2(a) which is
distributed along the transmission line by a
simple lumped-element equivalent circuit as
shown in Fig. 2(b). The circuit element C_1 is
the capacitance of the vacuum between the plas-
ma and the conducting plates, and is given by
$C_1 = \epsilon_0 A/2(l-a)$, where ϵ_0 is the permittivity
of free space and A is the lateral area of the
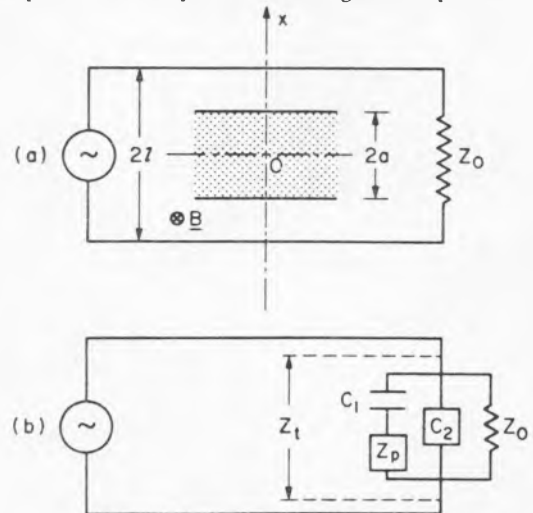capacitor-slab system. The negative capaci-

FIG. 2. (a) Diagram showing geometry of the plasma
slab and parallel-plate transmission line which com-
prise the theoretical model. (b) Lumped-element
equivalent circuit of the plasma-slab, transmission-
line model.

tance C_a results from the equivalent circuit approximation and is equal to $-\epsilon_0 A/2l$. In the linear approximation the impedance of the plasma slab is given by[10]

$$Z_p = \frac{(\omega_c^2 - \omega^2)}{i\omega\epsilon_0 A} \int_{-a}^{a} \frac{dx}{\omega_c^2 + \omega_p^2(x) - \omega^2}. \quad (1)$$

Defining Z_t to be the total impedance appearing between the two terminals of the equivalent circuit, one has the complex reflection coefficient measured at the generator, $r = (Z_t - Z_0)/(Z_t + Z_0)$.

In Fig. 3 (upper curves) we plot $|r|^2$ vs (ω_c/ω) for several values of the parameter ω_{p0}/ω. We have taken $R \equiv Z_0 l/\omega\epsilon_0 A = 5$ and $l/a = 2$ as reasonable estimates, since these parameters do not have exact experimental equivalents. Roughly, R sets the over-all scale of the amount of reflection, while l/a controls the relative height of the two peaks. The values chosen yield results which compare favorably with the experimental data; for example, the max-
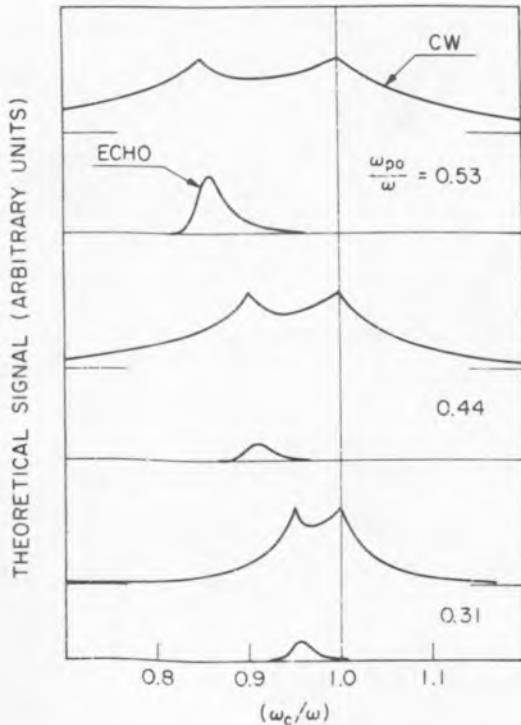

FIG. 3. Theoretical equivalent of Fig. 1. The upper curves ($|r|^2$) represent the cw reflection, while the lower curves ($|E|^2$) are the loci of the calculated echo amplitudes (ω_{p0}/ω appears as a parameter).

imum values of $|r|^2$ calculated are approximately the same as those observed experimentally (≈ 0.5). One peak in $|r|^2$ occurs at $\omega_c/\omega = 1$, while the other occurs at the maximum upper hybrid frequency of the slab, $\omega_{h0}^2 = \omega_c^2 + \omega_{p0}^2$. The two peaks are a manifestation of the fact that $|Z_p|$ is very high near $\omega = \omega_{h0}$ and very low near $\omega = \omega_c$. The quantitative difference between theory and experiment on the exact position of the upper hybrid peak is one shortcoming of the adopted model.

We have shown previously[4] that the cold-plasma-slab model has the qualitative features requisite of two-pulse echo systems: the collection of normal modes being the local upper hybrid oscillations and the nonlinearity being furnished by the spatial gradients in ω_p. The application of two short pulses results in pulsed echo responses in the voltage across the slab. In order to compute the echo magnetic field spectrum, we must modify previous plasma echo theories to include the limited spectral width of the exciting pulses. For a weak echo theory this modification results in the following expression for the relative peak voltage of the first echo:

$$E \propto \int_{-a}^{a} dx \frac{\omega_p^2}{\omega_h^4} \left\{ [\omega_p^2]'' \right.$$
$$\left. -\frac{5}{3}\left[\frac{(\omega_p^2)'}{\omega_h}\right]^2 \right\} |f(\omega - \omega_h)|^3, \quad (2)$$

where f is the Fourier transform of one of the exciting pulses and a prime denotes a derivative with respect to x. The two pulses are taken to have identical amplitudes and Gaussian shapes of width $\Delta\omega/\omega = 0.04$, a close approximation to the experimental conditions. The lower curves of Fig. 3 are plots of E^2 vs ω_c/ω computed using Eq. (2). As with the experimental results, the theoretical calculations show the echo to be strongly peaked near the maximum upper hybrid frequency of the plasma. Also, the widths of the theoretical and experimental echo spectra are comparable.

The general features of the theoretical curves in Fig. 3 are not unique to the collisionless model which yields energy-dependent normal-mode frequencies. One could include an energy-dependent phenomenological collision frequency supplying both relaxation and another nonlinear effect without qualitatively affecting the results. In either case, the echo is strong-

ly peaked near the maximum upper hybrid frequency because of the high density of normal modes there and not because of the nature of the nonlinearity.

In the low density limit $(\omega_p \ll \omega_c)$ both the upper hybrid echo and the cyclotron echo occur near $\omega = \omega_c$. Therefore, the independent-particle theories which have been used rather universally in the interpretation of cyclotron echo experiments[2,3] cannot be valid in general unless the spread in upper hybrid frequencies due to the spatial dependence of ω_p is considerably less than the spread due to the magnetic field inhomogeneity.[11] That is, the experiments must satisfy the condition $\omega_{p0}^2/2\omega_{c0}^2 \ll \Delta\omega_c/\omega_{c0}$, where $\Delta\omega_c$ is the spread in cyclotron frequencies and ω_{c0} is the value of the local cyclotron frequency at the position where the plasma density is the greatest, i.e., where $\omega_p = \omega_{p0}$. For typical laboratory experiments[1,3] this condition places a significant limitation on the maximum electron density $(\approx 10^9\text{-}10^{10}$ cm$^{-3})$ for which the echo can be correctly understood on the basis of independent particle theories. The competition between these two sources for the spread in upper hybrid frequencies has been studied.[11]

Although the simple plasma model presented gives results strikingly similar to the experimental observations, it should be taken as a first approximation. An appropriate hot plasma theory[12] would also be expected to yield a set of normal modes whose frequencies are intimately related to the nonuniform electron density profile and the associated upper hybrid frequencies. However, a hot plasma theory, particularly a nonlinear one, would prove considerably more difficult. Also, our theory ignores the problem of coupling to the upper hybrid oscillations.[13] Kaplan, Hill, and Wong[14] failed to find echoes near upper hybrid resonance in a high-density cesium plasma. As they discussed, from the point of view of cold-plasma theory, this fact may be the result of a failure to couple effectively (due to an evanescent layer) to the region of high normal-mode density near the maximum upper hybrid frequency. Other experiments[15] have produced echoes that are strongest at frequencies between the electron cyclotron frequency and the maximum upper hybrid frequency. Again, this is perhaps a manifestation of the efficiency of coupling to the upper hybrid oscillations. The experiments discussed in this paper would be expected to couple more efficiently to the upper hybrid oscillations, since the wavelength is longer compared with the scale length of the plasma density gradients than that in the other experiments.

The authors are indebted to R. S. Harp, R. M. Hill, D. E. Kaplan, and A. Y. Wong for interesting discussions and communication of their work during the course of this research. In addition, we benefited from stimulating conversations with F. L. Hinton.

*Research supported by the U. S. Office of Naval Research under Contract No. Nonr 220(50).

†Howard Hughes Predoctoral Fellow.

[1]R. M. Hill and D. E. Kaplan, Phys. Rev. Letters 14, 1062 (1965).

[2]R. W. Gould, Phys. Letters 19, 477 (1965); W. H. Kegel and R. W. Gould, Phys. Letters 19, 531 (1965); G. F. Herrmann and R. F. Whitmer, Phys. Rev. 143, 122 (1966); W. H. Kegel, Phys. Letters 23, 317 (1966), and Plasma Phys. 9, 23, 339 (1967); L. O. Bauer, R. W. Gould, and W. H. Kegel, Bull. Am. Phys. Soc. 12, 756 (1967).

[3]D. E. Kaplan and R. M. Hill, Bull. Am. Phys. Soc. 11, 496, 538 (1966); G. F. Herrmann, R. M. Hill, and D. E. Kaplan, Phys. Rev. 156, 118 (1967); F. W. Crawford and R. S. Harp, Phys. Letters 21, 292 (1966), and J. Appl. Phys. 37, 4405 (1966); D. E. Kaplan, R. M. Hill, and A. Y. Wong, Phys. Letters 22, 585 (1966); R. S. Harp, R. L. Bruce, and F. W. Crawford, J. Appl. Phys. 38, 3385 (1967).

[4]R. W. Gould and F. A. Blum, in Proceedings of the Eighth International Conference on Phenomena in Ionized Gases (Springer-Verlag, Vienna, Austria, 1967), p. 405.

[5]The possibility of plasma echoes due to effects of upper hybrid resonance was first suggested by G. F. Herrmann and R. F. Whittmer [Phys. Rev. 143, 122 (1966)].

[6]Since relatively low-power cw microwaves were found to heat the plasma, experiments on the magnetic field dependence of the reflections from the plasma using a wide (≈ 1 μsec), low-power (-30 dBm) pulse were performed in the bridge system. These wide-pulse experiments yield results essentially identical with those of a low-power cw experiment, if the spectral width of the pulse is narrow compared with the normal mode spectrum width of the plasma.

[7]G. Bekefi, J. D. Coccoli, E. B. Hooper, and S. J. Buchsbaum, Phys. Rev. Letters 9, 6 (1962); S. J. Buchsbaum and A. Hasegawa, Phys. Rev. Letters 12, 685 (1964), and Phys. Rev. 143, 303 (1966); S. Tanaka, H. Kubo, and K. Mitani, J. Phys. Soc. Japan 20, 462 (1965).

[8]H. J. Schmitt, G. Meltz, and P. J. Freyheit, Phys. Rev. 139, A1432 (1965); C. D. Lustig, Phys. Rev. 139, A63 (1965); S. Tanaka, J. Phys. Soc. Japan 21, 1804 (1966).

[9]S. J. Buchsbaum, Bull. Am. Phys. Soc. 7, 151 (1962); S. J. Buchsbaum, L. Mower, and S. C. Brown, Phys. Fluids 3, 806 (1960).

[10]When ω lies in the band of upper hybrid frequencies, the integrand of Eq. (1) has a simple pole for some value of x ($|x| \leq a$). The inclusion of electron collisions removes this singularity from the path of integration. Taking the limit of zero collision frequency tells one how to integrate around the pole. This limit is equivalent to the Dirac formulation of such integrals and is responsible for giving Z_p a real part.

[11]R. S. Harp, R. L. Bruce, and F. W. Crawford, J. Appl. Phys. 38, 3385 (1967).

[12]See, for example, G. A. Pearson, Phys. Fluids 9, 2454 (1966); H. L. Frisch and G. A. Pearson, Phys. Fluids 9, 2464 (1966).

[13]For a discussion of this problem, see G. Bekefi, Radiation Processes in Plasmas (John Wiley & Sons, Inc., New York, 1966), p. 223.

[14]D. E. Kaplan, R. M. Hill, and A. Y. Wong, Phys. Letters 22, 585 (1966).

[15]L. O. Bauer, F. A. Blum, and R. W. Gould, in the Ninth Annual Meeting of the Division of Plasma Physics of the American Physical Society, Austin, Texas, 8-11 November 1967 (unpublished); R. M. Hill and D. E. Kaplan, private communication.

APPENDIX B

Electron collisions have been observed to affect many echo properties. In this appendix some data on electron-neutral and electron-ion collision frequencies will be presented.

B.1 Electron-Neutral Collision Frequency

Figure B.1 displays, in a slightly different way, some data found in S. C. Brown's Basic Data of Plasma Physics (11). One can read directly from Fig. B.1 the electron neutral collision frequency in neon and argon as a function of the electron energy. The data presented were calculated for a pressure of 10 microns, so for a pressure of 20 microns, one simply has to multiply all values of the collision frequency by a factor two. The thin line defines the maximum energy the electrons are believed to acquire from a microwave pulse typical of an echo experiment.

B.2 Electron-Ion or Coulomb Collision Frequency

Figure B.2 presents data obtained from Heald and Wharton (33) regarding the Coulomb collision frequency. The term log Λ is a weak function of the electron energy. It is equal to 12 for 3eV electrons and drops monotonically to 6 for .01 eV electrons. The rectangle drawn in thin lines delineates the extreme values of the electron energy and density in our experiment.
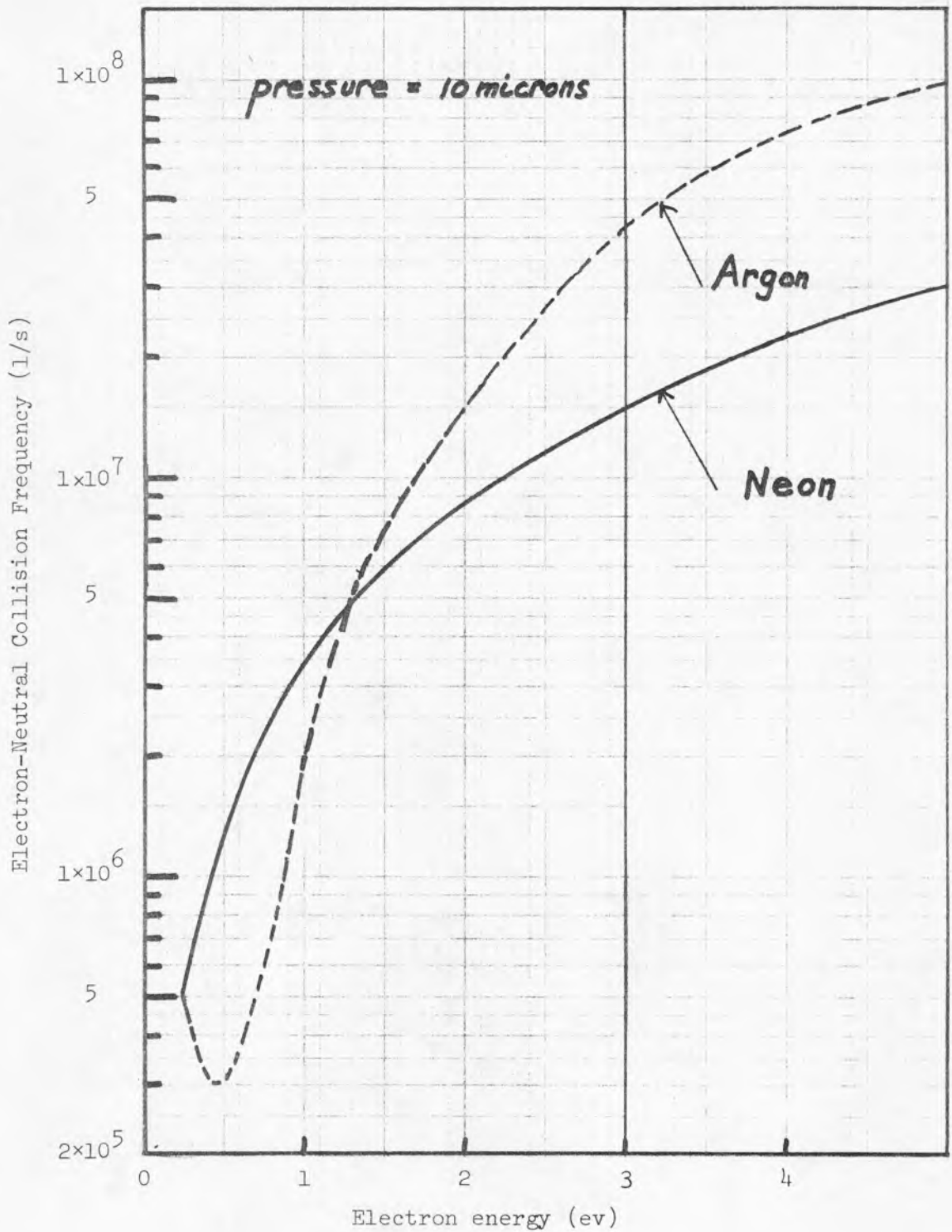
Fig. B.1 Electron-neutral atom collision frequency in neon
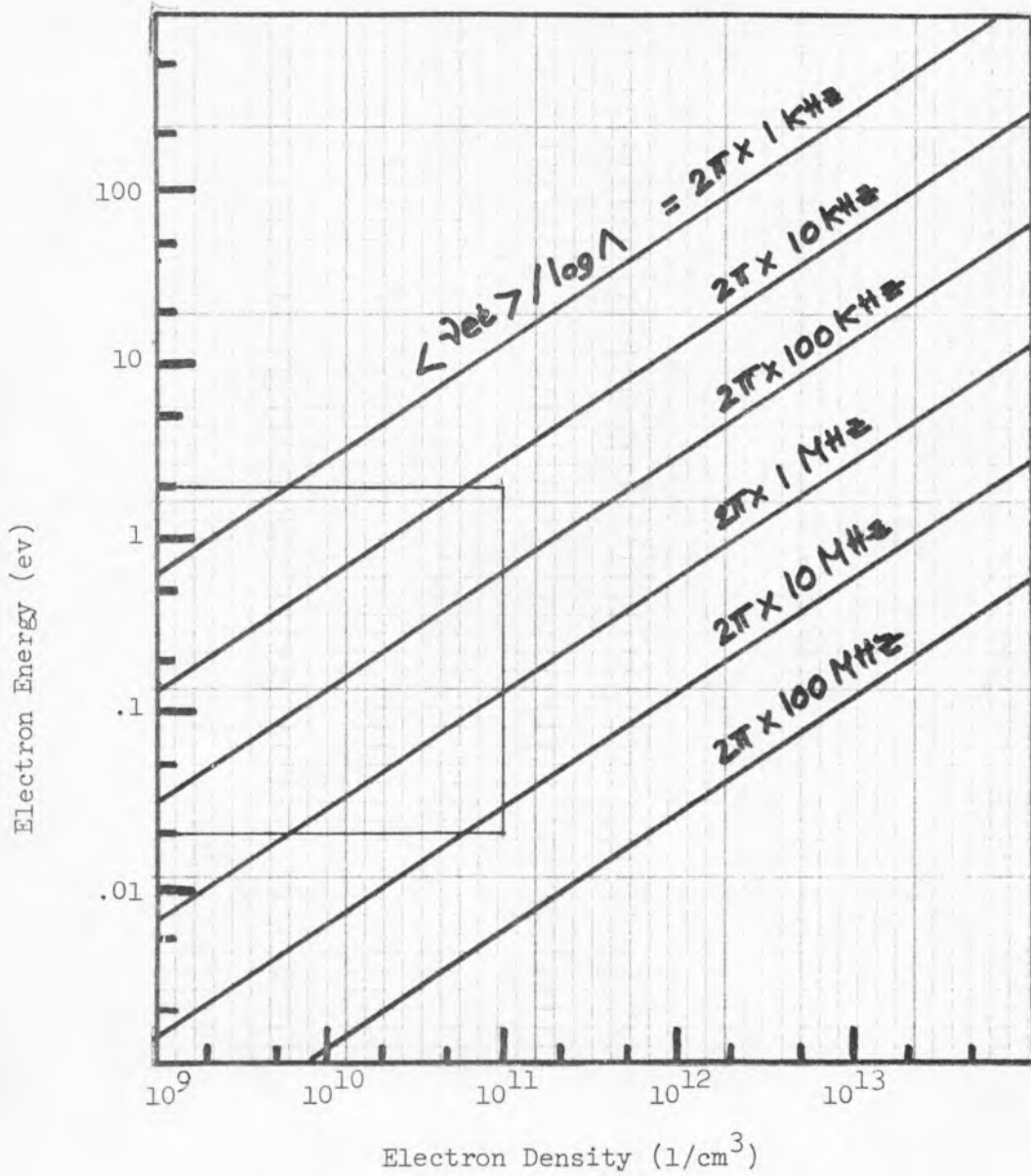and argon as a function of electron energy for a
pressure of 10 microns.

Fig. B.2 Electron-ion collision frequency for singly ionized
ions as a function of the electron energy and density.
(log Λ is a very weak function of the electron
energy and is equal to 12 for 3 eV electrons. It
drops monotonically to 6 for .01eV electrons.)

REFERENCES

1. See, for instance, J. C. Nickel, J. V. Parker, R. W. Gould, Phys. Rev. Letters 11, 183 (1963).

2. S. J. Buchsbaum and A. Hasegawa, Phys. Rev. Letters 12, 685 (1964) and Phys. Rev. 143, 303 (1966).

3. I. B. Bernstein, Phys. Rev. 109, 10 (1958).

4. R. M. Hill and D. E. Kaplan, Phys. Rev. Letters 14, 1062 (1965).

5. E. L. Hahn, Phys. Rev. 80, 580 (1950).

6. See, for instance, H. Y. Carr and E. M. Purcell, Phys. Rev. 94, 630 (1954); R. J. Blume, Phys. Rev. 109, 1867 (1958); J. P. Gordon and K. D. Bowers, Phys. Rev. Letters 1, 368 (1958); D. E. Kaplan, Phys. Rev. Letters 14, 254 (1965); N. A. Kurnit, I. B. Abella, and S. R. Hartmann, Phys. Rev. Letters 13, 567 (1964).

7. R. P. Feynman, F. L. Vernon and R. L. Hellwarth, J. Appl. Phys. 28, 49 (1957).

8. R. W. Gould, CIT Technical Report No. 28, December 1965; and R. W. Gould, Phys. Letters 19, 477 (1965).

9. W. H. Kegel and R. W. Gould, Phys. Letters 19, 531 (1965).

10. D. E. Kaplan and R. M. Hill, Bull. Am. Phys. Soc. 11, 496, 538 (1966); G. F. Herrmann, R. M. Hill and D. E. Kaplan, Phys. Rev. 156, 118 (1967); F. W. Crawford and R. S. Harp, Phys. Letters 21, 292 (1966), and J. Appl. Phys. 37, 4405 (1966); D. E. Kaplan, R. M. Hill and A. Y. Wong, Phys. Letters 22, 585 (1966); R. S. Harp, R. L. Bruce and F. W. Crawford, J. Appl. Phys. 38, 3385 (1967).

11. S. C. Brown, Basic Data of Plasma Physics, 1966, 2nd edition revised (MIT Press, 1967).

12. W. H. Kegel and R. W. Gould, Phys. Letters 19, 531 (1965); W. H. Kegel, Plasma Phys. 9, 23, 339 (1967).

13. See, for example, G. F. Herrmann, R. M. Hill and D. E. Kaplan, Phys. Rev. 156, 118 (1967).

14. A. Y. Wong and O. Judd, Bull. Am. Phys. Soc. 12, 758 (1967)

15. L. O. Bauer, R. W. Gould and W. H. Kegel, Bull. Am. Phys. Soc. 12, 756 (1967).

16. J. V. Parker, Phys. Fluids 6, 1657 (1963).

17. G. F. Herrmann and R. F. Whittmer, Phys. Rev. 143, 122 (1966).

18. R. W. Gould and F. A. Blum, in Proceedings of the Eighth International Conference on Phenomena in Ionized Gases (Springer-Verlag, Vienna, Austria, 1967), p. 405.

19. A. Y. Wong, O. Judd, Plasma Physics Group UCLA, Technical Report No. 11 (1967).

20. F. A. Blum, PhD Thesis, California Institute of Technology, May 1968.

21. L. O. Bauer, F. A. Blum and R. W. Gould, Phys. Rev. Letters 20, 435 (1968). (See Appendix A.)

22. J. J. Stoker, Nonlinear Vibrations in Mechanical and Electrical Systems (Interscience Publishers, New York, 2nd printing 1966).

23. L. B. Young, Technique of Microwave Measurements, MIT Radiation Laboratory Series, Vol. 11, edited by G. Montgomery, p. 515.

24. R. Stenzel (Private communication).

25. G. Bekefi, J. D. Coccoli, E. B. Hooper and S. J. Buchsbaum, Phys.
     Rev. Letters $\underline{9}$, 6 (1962); S. J. Buchsbaum and A. Hasegawa, Phys.
     Rev. Letters $\underline{12}$, 685 (1964), and Phys. Rev. $\underline{143}$, 303 (1966);
     S. Tanaka, H. Kubo and K. Mitani, J. Phys. Soc. Japan $\underline{20}$, 462
     (1965).

26. H. J. Schmitt, G. Meltz and P. J. Freyheit, Phys. Rev. $\underline{139}$,
     A1432 (1965); C. D. Lustig, Phys. Rev. $\underline{139}$, A63 (1965); S. Tanaka,
     J. Phys. Soc. Japan $\underline{21}$, 1804 (1966).

27. S. J. Buchsbaum, Bull. Am. Phys. Soc. $\underline{7}$, 151 (1962); S. J.
     Buchsbaum, L. Mower, and S. C. Brown, Phys. Fluids $\underline{3}$, 806 (1960).

28. For a discussion of this problem see G. Bekefi, Radiation
     Processes in Plasmas (John Wiley and Sons, Inc., New York, 1966)
     p. 223.

29. Our estimate is based on echo envelopes and pulse transient
     studies made at densities below 1×10^9 el/cm^3 by G. F. Herrmann
     R. M. Hill, and D. E. Kaplan, Phys. Rev. $\underline{156}$, 118 (1967); and
     R. L. Bruce, F. W. Crawford and R. S. Harp, SU-IPR Report No. 186
     July 1967.

30. R. L. Bruce, F. W. Crawford and R. S. Harp, SU-IPR Report No. 186
     July 1967.

31. R. M. Hill, D. E. Kaplan and S. K. Ichiki, Phys. Rev. Letters $\underline{19}$,
     154 (1967); D. E. Baldwin, D. M. Henderson and J. L. Hirschfield,
     Phys. Rev. Letters $\underline{20}$, 314 (1968).

32. See, for example: F. W. Crawford, Nuclear Fusion $\underline{5}$, 73 (1965);
     J. A. Tataronis and F. W. Crawford in Proceedings of the VIIth
     International Conference on Phenomena in Ionized Gases, Belgrade,
     Yugoslavia, August 1965, $\underline{II}$, p. 244-247.

33. Heald and Wharton, Plasma Diagnostics with Microwaves, (John Wiley
     and Sons, Inc., New York, 1965), p. 82.